THE POTENTIAL ROLE OF CONSCIOUSNESS IN THE COLLAPSE OF RANDOM PHYSICAL SYSTEMS: A QUANTITATIVE BIOPHYSICAL INVESTIGATION OF COGNITIVE INTENTION

by

Joseph M. Caswell

A thesis submitted in partial fulfillment
of the requirements for the degree of
Master of Arts (MA) in Human Development

The School of Graduate Studies
Laurentian University
Sudbury, Ontario, Canada

THESIS DEFENCE COMMITTEE/COMITÉ DE SOUTENANCE DE THÈSE

Laurentian Université/Université Laurentienne
School of Graduate Studies/École des études supérieures

Title of Thesis Titre de la thèse	THE POTENTIAL ROLE OF CONSCIOUSNESS IN THE COLLAPSE OF RANDOM PHYSICAL SYSTEMS: A QUANTITATIVE BIOPHYSICAL INVESTIGATION OF COGNITIVE INTENTION
Name of Candidate Nom du candidat	Caswell, Joseph M.
Degree Diplôme	Master of Arts

Department/Program Département/Programme	Human Development	Date of Defence Date de la soutenance	May 05, 2014

APPROVED/APPROUVÉ

Thesis Examiners/Examinateurs de thèse:

Dr. Michael A. Persinger
(Supervisor/Directeur de thèse)

Dr. Cynthia Whissell
(Committee member/Membre du comité)

Dr. John Lewko
(Committee member/Membre du comité)

Dr. Robert G. Jahn
(External Examiner/Examinateur externe)

Approved for the School of Graduate Studies
Approuvé pour l'École des études supérieures
Dr. David Lesbarrères
M. David Lesbarrères
Director, School of Graduate Studies
Directeur, École des études supérieures

ACCESSIBILITY CLAUSE AND PERMISSION TO USE

ABSTRACT

Decades of research into the anomalous phenomenon of consciousness-correlated collapse of random systems has supported the contention that human intention appears capable of eliciting significant deviations within these external systems. The following series of experiments was conducted in order to identify potential physical factors which might play a role in the consciousness-correlated effects on a random event generator device. Transcerebral application of a specific physiologically-patterned electromagnetic field was found to enhance the occurrence of this consciousness-mediated interaction. Furthermore, immersing the test area in electromagnetic 'noise' appears to interfere with the apparent effects of intention. Subsequent analyses were conducted in order to examine the potential contributions of gravitational sources on this phenomenon. Cerebral biophoton emission was also examined which determined that biophotons are related to the output of a proximal random event generator within both time and frequency domains. This initial series of experiments revealed a seemingly integral temporal component in this form of experiment which occurs at approximately 2 minutes into the test phase. Finally, space weather factors were examined for potential associations with the random event generator phenomenon which revealed a number of significant relationships that may contribute to this process. An artificial neural network was then constructed in order to predict values of geomagnetic activity for future experiments. These results may be among the first to quantitatively identify the probable energies and physical parameters associated with successful consciousness-mediated non-local interaction with an external system.

Keywords

Consciousness, Biophotons, Apogee-Perigee, Geomagnetic Activity, Space Weather, Electromagnetic Fields, Physical Anomalies, Random Event Generator, Dimensional Analysis, Psi, Artificial Neural Network, NARX, Solar Activity, Non-locality

ACKNOWLEDGEMENTS

I would like to thank Dr. Michael Persinger for believing in me. He has served as a tremendous reservoir of knowledge on all things, and aided me in achieving my goals. I will be eternally grateful for the support and guidance.

I would also like to thank Dr. John Lewko for taking a chance on me and affording me endless opportunities in the Interdisciplinary Human Development M.A. program. Furthermore, I would like to thank Dr. Cynthia Whissell for her valuable insight involved in the completion of this document.

Thank you to my parents; without the help of my mom and dad I never would have gotten where I am. Your endless emotional and financial support will be forever appreciated. You have let me fulfill my dreams.

Thank you to the Neuroscience Research Group (NRG). Your collegial support, suggestions, assistance, and collaboration were integral to completing this project. I would like to give special thanks to Dr. Blake Dotta, Lyndon Juden-Kelly, David Vares, Mark Collins, and Kevin Saroka for technical assistance and collaboration in this research.

Finally, I would like to thank Psyleron (www.psyleron.com) and Herb Mertz in particular for additional technical assistance and REG hardware supply.

TABLE OF CONTENTS

LIST OF FIGURES

LIST OF TABLES

Chapter 1 – Introduction

1.1 Probability and the Concept of Random

Randomness and Probability

In all sciences, the concept of "random" typically refers to a lack of predictability and/or determinism. However, given appropriate statistical likelihoods, certain phenomena can become associated with various *probable* outcomes. As a typical example, a sum of 7 will tend to occur more often by chance than a sum of 4 when rolling two six-sided dice. Therefore, randomness may be better described in terms of probabilities. This is the basis of all empirical investigation as all experimental results are statistically examined with regard to their likely *probabilities* against chance expectancy when considering typical distributions of data (e.g., the Gaussian or normal distribution). Despite the vital role this concept plays in all scientific endeavours, there is a tendency to misconstrue the true meaning of the term. For example, the standard mathematical software package, Matlab, contains an internal "random" number generator function. However, when this function is initially executed using default settings the same number appears on any system (Moler, 2004). This is not truly random by definition but it is expected given that computer systems are deterministic and function based on algorithmic processing. Because an algorithm is employed to produce "random" digit-strings in any given software package, this process is actually referred to as *pseudo*-random. Truly random, non-deterministic behaviour is observed in natural processes such as the decay of a radioactive isotope, Brownian motion, or atmospheric noise. Random number generator hardware devices have been developed which measure these natural phenomena in order to produce true-random sequences (e.g., Jahn et al., 1997).

Bernoulli Process

A Bernoulli process is a statistical concept in probability theory consisting of x_n random trials, each of which is independent from previous results. The Bernoulli trials which this process consists of possess two potential outcomes, 0 or 1, and as such are also referred to as binomial trials. Given that each value obtained is independent of previous values (e.g., a "memoryless" system) the outcome for each event in a Bernoulli process typically has an identical probability. However, given the probability of obtaining a "success" (1), the probability of a "failure" (0) can be obtained by subtracting the probability of success from 1 ($p_{failure} = 1 - p_{success}$). Using a fair coin flip as an example, the probability of success (heads, 1) is $p = 0.5$. Subsequently, the probability of failure (tails, 0) is $1–p = 0.5$. This type of binomial stochastic process is often employed in random number generator systems, which are discussed in greater detail elsewhere. Random number systems tend to employ binary measures such as bidirectional electron tunneling within a transistor. Over the course of n trials under normal circumstances a finite (or infinite) number of binary events, assuming a truly random system, should approximate a normal (Gaussian) distribution. However, the results of a Bernoulli process can be examined with regard to significant deviations from the expected distribution through statistical standardization procedures such as z-scores. Assume a session consisting of n = 400 coin flips, with each outcome having a probability of 50%. If an individual obtains 230 heads ("success", 1), then the associated z-score can be computed by subtracting $n_{successes}$ (230) from n/2 (200), and dividing the result by the square root of n/4 (100). In this example, the standardized value would be $z = (230/200)-\sqrt{100} = 3$. The probability of this score is derived by integrating a Gaussian distribution function (normal distribution) with a lower limit of the z-score and an upper limit theoretically extending towards infinity, using the following integral equation:

$$p_z = {}_z\int^{\infty} f(t)\, dt$$

where $f(t) = (2\pi)^{-1/2} \exp(-t^2 / 2)$

In this case, $z = 3 = p = .001$ (one-tailed) = .002 (two-tailed). Therefore, the results of this particular Bernoulli process (combining all separate Bernoulli trials) would be considered significantly different from chance expectations.

1.2 Consciousness

Theoretical Perspectives on Consciousness

The problem of consciousness has plagued natural philosophers for centuries and remains a dividing point between many scientists and other thinkers. Being that we are all conscious beings we often feel we understand what it means to be conscious. However, empirically defining this peculiar property rarely moves beyond mere speculation. It is generally understood that consciousness encompasses the sense of self and awareness, although how and why this occurs is a point of contention. This is the initial, physical problem of consciousness. However, the 'hard problem' as explained by Chalmers (1995) is why we have phenomenal experience at all. This is, of course, the *philosophical* issue of consciousness. Although other theorists have adopted opposing viewpoints on the existence of a 'hard problem' (e.g., Dennett, 1996), recent theories regarding this phenomenon have emerged which suggest the relevance of the issue; although previously considered in a purely organic-materialist context, contemporary physical theory suggests that consciousness enters into empirical processes (e.g., Schwartz et al., 2005), and therefore should be understood as a phenomenology independent of purely biological processes in the brain. Indeed, the true nature of consciousness must be understood if we are to adequately explain concepts like free will or mental experience as a causal agent (e.g., Giroldini, 1991).

Although many scientists disregard consciousness as irreducible to physical quantization, a number of modern physicists have begun attempting to provide physical theories regarding both the biophysical bases and phenomenology of conscious awareness. Some of these theories also suggest that by addressing the issue of consciousness other problems in physics may be solved (Drageset, 2013). Numerous biophysical properties have been hypothesized to underlie this phenomenon including quantum computations occurring within neuronal microtubules (Hameroff & Penrose, 1996; Hameroff et al., 2002), and also associated electroencephalographic (EEG) gamma synchrony (Hameroff, 2010). Although determining the neural substrates of consciousness is a relevant endeavour, other theorists have suggested that this line of questioning is an error in the philosophy of mind (e.g., Amoroso, 1999). In a cosmological framework, the mind or consciousness should be a physically quantifiable independent process which *interacts* with the brain (Amoroso, 1999). There is some experimental evidence for this given the apparent empirical relationships observed between conscious processes, such as intentionality and cognition, and associated activity of cerebral biophoton emission (e.g., Dotta & Persinger, 2011). Furthermore, photons have been specifically identified as a potential basis for consciousness in other theoretical frameworks. In this sense conscious awareness may be best represented in the context of holographic information (Bokkon, 2005). This perspective would also be consistent with evidence suggesting apparently non-local characteristics of consciousness (Persinger & Lavallee, 2010; Persinger et al., 2010a). The electromagnetic properties of conscious phenomenology similarly provide an alternate context for understanding consciousness outside of basic neuroanatomical correlates (Lehmann et al., 1998; Persinger & Koren, 2007).

Other theories regarding this phenomenon further suggest that consciousness may be an intimate property of reality itself (e.g., Jahn & Dunne, 1986). For example, although the area of

neurotheology has tended to reduce seemingly anomalous or mystical subjective experiences to basic neural properties, the emerging field of neuroquantology has suggested that these beliefs and experiences may reflect the inherent nature of consciousness as part of the very fabric of space and time (Persinger et al., 2010b). Further convergence between fundamental properties of the universe and consciousness has been derived through neuroquantological analyses (Persinger & Koren, 2007). However, quantum equations may simply apply to the contents of space and this is insufficient to account for associated sensations of space (Baer, 2010). Therefore, it may be useful to conceive of the universe itself as a consciousness within which the properties of nature are reflected (Baer, 2010). In this context, action of mind itself may be a physical function of space. Although this notion may clash with contemporary mainstream scientific viewpoints, there have been both theoretical frameworks (Jahn & Dunne, 1986) and convergent quantifications (Persinger et al., 2008) which suggest that consciousness interacts with and potentially affects the physical universe.

Intention and Random Physical Systems

Various forms of anomalous physical phenomena associated with consciousness, collectively referred to as 'psi', have been noted in many experiments over the course of decades of empirical investigation. Furthermore, many prominent early psychologists, including William James, were involved in examining these seemingly paranormal events. Subsequent researchers, such as J. B. Rhine, would contribute to the field of parapsychology by introducing more stringent methodologies and statistical procedures. Fortunately a number of investigators persisted in their efforts and a number of new technologies were developed which have allowed more precise measurement of the various factors that have been hypothesized to play a role in these anomalous interactions.

Psi processes refer to seemingly non-local interactions between consciousness and an external system. However, the specific phenomenon focused on in the following series of experiments is the apparent process of consciousness-correlated collapse (3C). This type of psi interaction involves a conscious operator attempting to exert some form of mental influence on an external system with the aim being to obtain a specifically intended outcome within the system. This process has been referred to by a number of labels including mind-matter interaction and psychokinetic interaction. However, the more appropriate title of 3C has recently been proposed and will be the standard term employed throughout the following experiments.

As previously stated, a number of new technologies have been designed in order to empirically test various psi hypotheses. The study of 3C was historically focused on affecting the outcome of simple macro-events, such as dice rolls (e.g., Rhine & Rhine, 1943). However, prominent psi researcher Helmut Schmidt developed early models of electronic random number generators, or random event generators, based on statistical noise within a microelectronic system (Schmidt, 1970). It was determined through subsequent experiments that human participants appear capable of affecting the outcome within these devices which significantly deviate from chance expectations, and that this effect does not differ between various device models (Schmidt, 1974). Furthermore, Schmidt (1987) hypothesized that this effect would only occur in relation to a non-deterministic, true random system. These points were later confirmed through subsequent experiments (Nelson et al., 2000). Although many detractors derided these claims, a number of experiments have been conducted in association with other external investigators, and the apparent effect remains (e.g., Schmidt, 1993). This effect has also been noted to occur despite either geographical or temporal dislocation, suggesting properties of entanglement and retrocausation respectively (Schmidt, 1987; Dunne & Jahn, 1992). Although this phenomenon

may appear at odds with classical intuition, analysis of contemporary physical theory has suggested that these anomalous occurrences could be allowed by nature (e.g., Moddel, 2004; 2006). Furthermore, the development of quantum mechanics has provided a potential basis for 3C to occur. For example, Schmidt (1982) has suggested that collapse of a systems wave-function as a result of observation may underlie the apparent 3C effect. This is directly related to the quantum measurement problem and the role of the observer in any measurement (Radin et al., 2012). However, it may also be that statistical noise itself is the signal involved in regulating 3C. According to Landauer (1998), a correlation in noise between two paths should occur given an appropriate magnetic flux overlapping these two points. If consciousness is derived from a complex electromagnetic configuration then the action of mind may simply be an outward extension of consciousness which subsequently orders the random noise within an external system. This concept regarding the action of mind has previously been extended to the molecular realm (Burns, 2002). Regardless of issues involving the strange world of quantum theory, this anomalous phenomenon has been largely supported by a number of laboratories and independent investigators (Radin & Nelson, 2003). While other researchers have suggested these results could simply be due to a selective reporting bias, these claims have also been refuted through careful statistical examination of the available data (Radin et al., 2006). Although the observed interactions appear to have very small effect sizes, the results are consistently highly significant and may suggest some fundamental property not yet considered in modern physics (Nelson et al., 2000). Finally, although the apparent actions of intention appear to operate solely on non-deterministic processes, the effect of 3C remains generalizable to a number of different types of random systems. This includes microelectronic noise typically employed (Nelson et al., 2000), behaviour of photons in a double-slit experiment (Radin et al., 2012), and background levels of ionizing radiation (Radin, 1993). Furthermore, there are no observed differences in 3C

occurrence between trials where participants received feedback and those where no feedback was provided, trial position within an experimental series, or the length of testing (Nelson et al., 2000). Although performance differences have been revealed between males and females, the exact nature of this difference remains relatively elusive (e.g., Gissurarson, 1992; Dunne, 1998). Determining the potential role of environmental factors has proven similarly difficult (e.g., Gissurarson, 1992; Radin, 1993). Finally, despite the fact that consciousness and brain activity are directly related, and consciousness appears to correlate with results from studies of this phenomenon, there have been surprisingly few studies which have examined potential biological correlates of successful 3C (e.g., Giroldini, 1991; Radin et al., 2012).

Altered States and Cross-Cultural Perspectives on Consciousness Anomalies

A number of investigators have begun to examine the claims of exceptional subjective experiences found in non-Western cultures from the perspective of consciousness anomalies in general (e.g., Krippner, 1991). The emerging discipline of paranthropology specifically seeks to unite the study of anthropology and physical anomalies by further investigating the claims of cross-cultural practitioners, particularly shamans, regarding exceptional subjective experience or ability (Miller, 2012). Shamanism itself is a universal feature in developing cultures and may underlie an important biological or evolutionary function (Winkelman, 2002). The field of neuroquantology has begun to unite philosophical notions of spirituality and empiricism in the context of physical principles, and this area may provide quantitative support for cross-cultural anomalous subjective experience (Persinger et al., 2010b).

One of the defining features of shamans and other cultural healers is their apparent ability to affect or access information that others in their society are unable to (Krippner, 2000). Although a

portion of this information has been hypothesized to occur due to unconscious information temporarily surfacing to conscious attention (Hubbard, 2003), there is also experimental evidence which suggests some individuals possess fundamentally altered or enhanced propensities toward anomalous non-local interactions. For example, personalities who are high on openness to experience, among other personality measures, have been found to possess a greater capacity for psi experiences (Zingrone et al., 1998-99). An apparent innate disposition towards anomalous physical interactions in some individuals has also been supported in experiments examining other forms of psi in the context of neural activity (e.g., Persinger & Saroka, 2012). Furthermore, shamans have specifically been studied for a propensity to exert mental influence on external systems. One case found an individual seemingly capable of affecting plant germination and mitigating saline damage on plant seeds through mental intention (Saklani, 1988).

The effects of other traditionally spiritual practices have also been examined in the context of random physical systems. For example, one study investigating the outcome of a random system during a shaman healing ceremony found statistically significant deviations in random event generator (REG) data while the ritual was taking place, whereas the device output conformed to statistical expectations during a sham procedure involving the same individual (Nelson et al., 1998). A similar series of experiments investigated various forms of meditation in close proximity to a REG and found highly statistically significant deviations in the device output during large group meditations (Mason et al., 2007). Given the fact that enhanced electroencephalograph (EEG) activity in the alpha band has been associated with successful 3C (Giroldini, 1991), and meditation has been shown to enhance alpha activity (Kerr et al., 2011), this latter study may also provide indirect support for a bioelectric correlate of successful psi phenomena which might become enhanced in spiritual practitioners.

Experimentally induced shamanic states have been shown to be significantly psi-conducive within a normal population, even when compared to traditional parapsychological paradigms (Rock & Storm, 2010). Shamans and other healers have historically engaged in altered states of consciousness (ASC) in order to facilitate their mystical feats (Krippner, 2000). However, this tends to be accomplished through the ingestion of hallucinogenic substances. Although this biochemical intervention is difficult to affect within the laboratory, a number of recent studies have shown that physiologically-patterned electromagnetic fields (EMF) applied transcerebrally can also elicit altered states (e.g., Cook & Persinger, 1997; Tsang et al., 2004; Collins & Persinger, 2013). It is with these relationships in mind that the following hypothesis was formulated: Given the association between shamanic ASCs and the capacity for non-local influence, the application of EMFs associated with altered states during a test of the 3C phenomenon should show an enhanced occurrence or magnitude of anomalous deviations within a REG device compared to trials where no EMF application is employed.

1.3 Photons and Biological Systems

Biophoton Emission

Photons are essentially the quanta of electromagnetic radiation, or discrete packets of light. The famous physicist Albert Einstein developed the theoretical concept of these particles through his work on the photoelectric effect. The existence of photons was later determined experimentally, with particularly important research conducted by Arthur Compton. Although photons were historically considered to have a rest mass of zero, it has recently been demonstrated that they may actually possess a non-zero rest mass (Tu et al., 2005). Despite the fact that the potential mass is incredibly small ($\sim 10^{-52}$ kg), this discovery has massive implications regarding variations in the velocity of light and the role light quanta may play within the context of potential

information transfer. Because light exists within different wavelengths photons possess different energies within each wavelength. However, the average energy value of an individual photon can be estimated given a range of λ = 495-570 nm (green, the center of the visible spectrum), assuming a median wavelength of ~533 nm and the relationship $E = h \cdot c \cdot \lambda^{-1}$, where h = Planck's constant ($6.626 \cdot 10^{-34}$ J·s^{-1}), c = the speed of light ($2.99792 \cdot 10^{8}$ m·s^{-1}), and λ = wavelength (e.g., $5.33 \cdot 10^{-7}$). Therefore, the average energy value of an individual photon can be defined as approximately $3.73 \cdot 10^{-19}$ J, with all other nm wavelengths falling within the same range, from ultraviolet (~$7.95 \cdot 10^{-19}$ J) to infrared (~$2.34 \cdot 10^{-19}$ J). Using the same values, the average photon frequency can be estimated given the relationship $f = c \cdot \lambda^{-1}$ for electromagnetic waves. Therefore, the average frequency of photons in the visible spectrum would be approximately $5.62 \cdot 10^{14}$ Hz, with $1.2 \cdot 10^{15}$ Hz in the ultraviolet range, and $3.53 \cdot 10^{14}$ Hz in the infrared range.

Aside from their integral relevance to both modern computing and communications systems, photon emission has also been studied in biological systems (e.g., Isojima et al., 1995; Cohen & Popp, 1997). Bioluminescence, or biophoton emission (BPE), is typically produced in relation to reactive oxygen species which are generally formed through cellular metabolism (Apel & Hirt, 2004). However, recent experiments have identified novel molecular approaches exploiting the mechanism of BPE, including the identification and classification of cancerous cells (Gourley et al., 2005; Dotta et al., 2011a). A potential role in cellular communication has also been examined (Sun et al., 2010). Aside from more general uses of photon measurement in biological contexts, there have also been a number of relatively exotic applications of this phenomenon.

Biophotons and Physical Anomalies

Bokkon (2005; 2009) has suggested that biophotons play a role in thermoregulation, visual imagery, and even dream-imagery. The latter hypothesis has been implicated as an explanation for anomalous cognition associated with the perception of future events (Dotta & Persinger, 2009). There is also some experimental support for the role of BPE in both visual perception (Wang et al., 2011) and visual imagery (Dotta et al., 2012). Related to Bokkon's hypothesis, the phenomenon of ultraweak BPE has been suggested as a correlate of consciousness itself (Dotta & Persinger, 2011), with some theorists describing specific types of photons which could mediate conscious phenomenology (e.g., Amoroso, 1999). However, specific psi-processes have also been examined in relation to BPE. For example, an exceptional individual was shown to produce an increase of about $1.5 \cdot 10^{-11}$ $J \cdot s^{-1}$ from the right side of the head when engaging in an 'intuitive' state compared to baseline condition (Hunter et al., 2010). Applying concepts from quantum mechanics, researchers have found experimental evidence that cerebral biophoton emission is capable of entanglement between subjects in distant locations (e.g., Persinger & Lavallee, 2010; Dotta et al., 2011b). Given the association between photons, consciousness, and visual imagery, as well as that between BPE and both psi and quantum interactions, this suggests that cerebral biophoton emission may be a good candidate for some form of mediator in the occurrence of consciousness-correlated collapse (3C). It is therefore hypothesized that specific increases in cerebral photon emission will accompany significant deviations in the output of a proximal random event generator (REG). It is also suggested that specific ranges of BPE should occur in relation to particular ranges in REG output.

1.4 Solar Activity

General Features of the Sun

The sun, a main-sequence star, is an enormous sphere of plasma. This star at the center of our solar system is a massive aggregate of thermonuclear fusion fuelled by enormous quantities of hydrogen, and provides the energy required to support a large proportion of life on Earth. There are a number of specific measurements associated with various types of solar activity. One particular measure used is the sunspot number. Sunspots are seemingly isolated regions of the sun caused by tremendous magnetic activity within the solar photosphere, observations of which have been recorded since before the Common Era (Schove, 1955). Although they appear visibly as dark regions, this is simply due to the fact that sunspots have relatively lower temperatures (3000-4500 K) compared to the surrounding areas (~5780 K). One reason for examining this phenomenon in the context of solar radiation is because many coronal mass ejections (CMEs) originate from areas surrounding sunspots (e.g., Hundhausen et al., 1984). One of the major measurements of sunspots is the Wolf number (R). This is a daily value used to denote the number of sunspots observed in a given day, and has been in use since 1848 (Clette et al., 2007). The formula used to obtain R is $k(10g + s)$, where k = the personal reduction coefficient, g = number of sunspot groups, and s = number of sunspots. Another measure associated with overall solar activity is the solar radio flux. This refers to radio emissions often produced when plasma within highly active regions of the sun becomes trapped beneath magnetic fields (Donnelly et al., 1983), and as such are also related to sunspots. These emissions are measured around 2800 MHz at the 10.7 cm wavelength (Tapping, 1987). The background x-ray flux is another similar measure often used which is also related to the occurrence of solar flares (e.g., Sheeley et al., 1983). Emissions in the x-ray wavelength are measured as background flux within the ionosphere

(e.g., Thomson et al., 2004). This variable is typically denoted in coefficients of flux ($W \cdot m^{-2}$) ranging from low background ($< 10^{-8}$) to extreme flares ($> 10^{-3}$).

Heliobiology

The integration of biological sciences with solar physics was originally examined through a host of research conducted by Russian biophysicist Alexander Chizhevsky. His insightful work revealed potential relationships between solar activity and human behaviour (e.g., Chizhevsky, 1936). Subsequent research has expanded this idea a great deal and has since shown that solar activity may be related to epidemiological factors as well (e.g., Cherry, 2003, Dimitrova et al., 2009). Because solar winds and coronal mass ejections (CME) from the sun influence the local planetary geomagnetic field (Richardson et al., 2001), this has potential implications for identifying significant relationships between solar-mediated perturbations of geomagnetic activity and the range of physiological effects that have been demonstrated to occur in association with the geomagnetic field, including brain activity (Saroka et al., 2014) and cardiac functioning (Dimitrova et al., 2009). Given the associations observed between these phenomena, it was hypothesized that variations in solar activity should be correlated with the output of a REG device which has been intended upon by human participants.

1.6 References

Amoroso, R. L. (1999). An introduction to noetic field theory: The quantization of mind. *Noetic Journal*, *2*(1), 28-37.

Apel, K., & Hirt, H. (2004). Reactive oxygen species: Metabolism, oxidative stress, and signal transduction. *Annual Review of Plant Biology*, *55*, 373-399.

Baer, W. (2010). Introduction to the physics of consciousness. *Journal of Consciousness Studies*, *17*(3-4), 165-191.

Bókkon, I. (2005). Dreams and neuroholography: An interdisciplinary interpretation of development of homeotherm state in evolution. *Sleep and Hypnosis, 7*(2), 61-76.

Bokkon, I. (2009). Visual perception and imagery: A new molecular hypothesis. *Biosystems, 96*, 178-184.

Burns, J. E. (2002). Quantum fluctuations and the action of mind. *Noetic Journal*, *3*(4), 312-317.

Chalmers, D. J. (1995). Facing up to the problem of consciousness. *Journal of Consciousness Studies*, *2*(3), 200-219.

Cherry, N. J. (2003). Sudden infant death syndrome (SIDS) related to solar activity through the Schumann resonance mechanism. Lincoln University Research Archive.

Chizhevsky, A. (1936). *The Terrestrial Echo of Solar Storms*. Mysl'Press, Moscow.

Clette, F., Berghmans, D., Vanlommel, P., Van der Linden, R. A. M., Koeckelenbergh, A., &

Wauters, L. (2007). From the Wolf number to the International Sunspot Index: 25 years of SIDC. *Advances in Space Research, 40*(7), 919-928.

Cohen, S., & Popp, F. A. (1997). Biophoton emission of the human. *Journal of Photochemistry and Photobiology, 40,* 187-189.

Collins, M. W. G., & Persinger, M. A. (2013). Changing velocity circumcerebral magnetic fields produce altered state experiences and lowered delta-theta power over the temporal lobes. *Frontiers in Psychological and Behavioral Science, 2*(2), 26-29.

Cook, C. M., & Persinger, M. A. (1997). Experimental induction of the 'sensed presence' in normal subjects and an exceptional subject. *Perceptual and Motor Skills, 85,* 683-693.

Dennett, D. C. (1996). Facing backwards on the problem of consciousness. *Journal of Consciousness Studies, 3*(1), 4-6.

Dimitrova, S., Mustafa, F. R., Stoilova, I., Babayev, E. S., & Kazimov, E. A. (2009). Possible influence of solar extreme events and related geomagnetic disturbances on human cardio-vascular state: Results of collaborative Bulgarian-Azerbaijani studies. *Advances in Space Research, 43*(4), 641-648.

Donnelly, R. F., Heath, D. F., Lean, J. L., & Rottman, G. J. (1983). Differences in the temporal variations of solar UV flux, 10.7-cm solar radio flux, sunspot number, and Ca-K plage

data caused by solar rotation and active region evolution. *Journal of Geophysical Research: Space Physics*, *88*(A12), 9883-9888.

Dotta, B. T., & Persinger, M. A. (2009). Dreams, time distortion, and the experience of future events: A relativistic, neuroquantal perspective. *Sleep and Hypnosis*, *11*(2), 29-39.

Dotta, B. T., & Persinger, M. A. (2011). Increased photon emissions from the right but not the left hemisphere while imagining white light in the dark: The potential connection between consciousness and cerebral light. *Journal of Consciousness Exploration & Research*, *2*(10), 1463-1473.

Dotta, B. T., Buckner, C. A., Cameron, D., Lafrenie, R. F., & Persinger, M. A. (2011a). Biophoton emissions from cell cultures: Biochemical evidence for the plasma membrane as the primary source. *General Physiology and Biophysics*, *30*(3), 301-309.

Dotta, B. T., Buckner, C. A., Lafrenie, R. M., & Persinger, M. A. (2011b). Photon emissions from human brain and cell culture exposed to distally rotating magnetic fields shared by separate light-stimulated brains and cells. *Brain Research*, *1388*, 77-88.

Dotta, B. T., Saroka, K. S., & Persinger, M. A. (2012). Increased photon emission from the head while imagining light in the dark is correlated with changes in electroencephalographic power: Support for Bokkon's biophoton hypothesis. *Neuroscience Letters*, *513*, 151-154.

Drageset, O. (2013). How physics could explain the mind. *Physics Essays*, *26*(1), 7-14.

Dunne, B. J. (1998). Gender differences in human/machine anomalies. *Journal of Scientific Exploration*, *12*(1), 3-55.

Dunne, B. J., & Jahn, R. G. (1992). Experiments in remote human/machine interaction. *Journal of Scientific Exploration*, *6*(4), 311-332.

Giroldini, W. (1991). Eccles's model of mind-brain interaction and psychokinesis: A preliminary study. *Journal of Scientific Exploration*, *5*(2), 145-161.

Gissurarson, L. R. (1992). The psychokinesis effect: Geomagnetic influence, age and sex differences. *Journal of Scientific Exploration*, *6*(2), 157-165.

Gourley, P. L., Hendricks, J. K., McDonald, A. E., Copeland, R. G., Barrett, K. E., Gourley, C. R., et al. (2005). Mitochondrial correlation microscopy and nanolaser spectroscopy : New tools for biophotonic detection of cancer in single cells. *Technology in Cancer Research & Treatment*, *4*(6), 585-592.

Hameroff, S. (2010). The "conscious pilot": Dendritic synchrony moves through the brain to mediate consciousness. *Journal of Biological Physics*, *36*(1), 71-93.

Hameroff, S., & Penrose, R. (1996). Orchestrated reduction of quantum coherence in brain microtubules: A model for consciousness. *Mathematics and Computer Simulation, 40*,

453-480.

Hameroff, S., Nip, A., Porter, M., & Tuszynski, J. (2002). Conduction pathways in microtubules, biological quantum computation, and consciousness. *BioSystems*, *64*, 149-168.

Hubbard, T. L. (2003). Further correspondences and similarities of shamanism and cognitive science: Mental representation, implicit processing, and cognitive structures. *Anthropology of Consciousness*, *14*(1), 40-74.

Hundhausen, A. J., Sawyer, C. B., House, L., Illing, R. M. E., & Wagner, W. J. (1984). Coronal mass ejections observed during the Solar Maximum Mission: Latitude distribution and rate of occurrence. *Journal of Geophysical Research: Space Physics*, *89*(A5), 2639-2646.

Hunter, M. D., Mulligan, B. P., Dotta, B. T., Saroka, K. S., Lavallee, C. F., Koren, S. A., & Persinger, M. A. (2010). Cerebral dynamics and discrete energy changes in the personal environment during intuitive-like states and perceptions. *Journal of Consciousness Exploration & Research*, *1*(9), 1179-1197.

Isojima, Y., Isoshima, T., Negai, K., Kikuchi, K., & Nakagawa, H. (1995). Ultraweak biochemiluminescence detected from rat hippocampal slices. *NeuroReport*, *6*, 658-660.

Jahn, R. G., & Dunne, B. J. (1986). On the quantum mechanics of consciousness, with application to anomalous phenomena. *Foundations of Physics*, *16*(8), 721-772.

Jahn, R. G., Dunne, B. J., Nelson, R. D., Dobyns, Y. H., & Bradish, G. J. (1997). Correlations of random binary sequences with pre-stated operator intention: A review of a 12-year program. *Journal of Scientific Exploration, 11*(3), 345-367.

Kerr, C. E., Jones, S. R., Wan, Q., Pritchett, D. L., Wasserman, R. H., Wexler, A., et al. (2011). Effects of mindfulness meditation training on anticipatory alpha modulation in primary somatosensory cortex. *Brain Research Bulletin, 85*, 96-103.

Krippner, S. (1991). Research strategies in the study of shamanism and anomalous experience. *Anthropology of Consciousness*, *2*(1-2), 13-19.

Krippner, S. (2000). The epistemology and technologies of shamanic states of consciousness. *Journal of Consciousness Studies*, *7*(11-12), 93-118.

Landauer, R. (1998). The noise is the signal. *Nature*, *392*, 658-659.

Lehmann, D., Strik, W. K., Henggeler, B., Koenig, T., & Koukkou, M. (1998). Brain electric microstates and momentary conscious mind states as building blocks of spontaneous thinking: I. Visual imagery and abstract thoughts. *International Journal of Psychophysiology*, *29*, 1-11.

Mason, L. I., Patterson, R. P., & Radin, D. I. (2007). Exploratory study: The random number generator and group meditation. *Journal of Scientific Exploration, 21*(2), 295-317.

Miller, I. (2012). A transdisciplinary look at paranthropology: An emerging field of exploration. *Journal of Consciousness Exploration & Research, 3*(8), 1018-1031.

Moddel, G. (2004). Entropy and subtle interactions. *Journal of Scientific Exploration, 18*(2), 293-306.

Moddel, G. (2006). Entropy and information transmission in causation and retrocausation. In D. Sheehan (Ed.), *Frontiers of Time, Retrocausation: Experiment and Theory* (pp. 62-74). Melville, NY: American Institute of Physics.

Moler, C. (2004). Random numbers. In *Numerical computing with Matlab*. Society for Industrial and Applied Mathematics.

Nelson, R. D., Jahn, R. G., Dunne, B. J., Dobyns, Y. H., & Bradish, G. J. (1998). FieldREG II: Consciousness field effects. *Journal of Scientific Exploration, 12*(3), 425-454.

Nelson, R. D., Jahn, R. G., Dobyns, Y. H., & Dunne, B. J. (2000). Contributions to variance in REG experiments: ANOVA models and specialized subsidiary analyses. *Journal of Scientific Exploration, 14*(1), 73-89.

Persinger, M. A., & Koren, S. A. (2007). A theory of neurophysics and quantum neuroscience: Implications for brain function and the limits of consciousness. *International Journal of Neuroscience*, *117*, 157-175.

Persinger, M. A., Koren, S. A., & Lafreniere, G. F. (2008). A neuroquantologic approach to how human thought might affect the universe. *NeuroQuantology, 6*(3), 262-271.

Persinger, M. A., & Lavallee, C. F. (2010). Theoretical and experimental evidence of macroscopic entanglement between human brain activity and photon emissions: Implications for quantum consciousness and future applications. *Journal of Consciousness Exploration & Research, 1*(7), 785-807.

Persinger, M. A., & Saroka, K. S. (2012). Protracted parahippocampal activity associated with Sean Harribance. *International Journal of Yoga, 5,* 145-150.

Persinger, M. A., Saroka, K. S., Lavallee, C. F., Booth, J. N., Hunter, M. D., Mulligan, B. P., et al. (2010a). Correlated cerebral events between physically and sensory isolated pairs of subjects exposed to yoked circumcerebral magnetic fields. *Neuroscience Letters, 486,* 231-234.

Persinger, M. A., Corradini, P. L., Clement, A. L., Keaney, C. C., MacDonald, M. L., Meltz, L. I., et al. (2010b). Neurotheology and its convergence with neuroquantology. *NeuroQuantology, 8*(4), 432-443.

Radin, D. I. (1993). Environmental modulation and statistical equilibrium in mind-matter interaction. *Subtle Energies, 4*(1), 1-30.

Radin, D. I., & Nelson, R. D. (2003). Meta-analysis of mind-matter interaction experiments: 1959-2000. In *Healing, Intention, and Energy Medicine* (pp. 39-48). London: Harcourt Health Sciences.

Radin, D., Nelson, R., Dobyns, Y., & Houtkooper, J. (2006). Reexamining psychokinesis: Comment on Bosch, Steinkamp, and Boller (2006). *Psychological Bulletin*, *132*(4), 529-532.

Radin, D., Michel, L., Galdamez, K., Wendland, P., Rickenbach, R., & Delorme, A. (2012). Consciousness and the double-slit interference pattern: Six experiments. *Physics Essays*, *25*(2), 157-171.

Rhine, L. E., & Rhine, J. B. (1943). The psychokinetic effect: I. The first experiment. *Journal of Parapsychology*, *7*, 20-43.

Richardson, I. G., Cliver, E. W., & Cane, H. V. (2001). Sources of geomagnetic storms for solar minimum and maximum conditions during 1972-2000. *Geophysical Research Letters*, *28*(13), 2569-2572.

Rock, A. J., & Storm, L. (2010). Shamanic-like journeying and psi: II. Mental boundaries, phenomenology, and the picture-identification task. *Australian Journal of Parapsychology*, *10*(1), 41-68.

Saklani, A. (1988). Preliminary tests for psi-ability in shamans of Garhwal Himalaya. *Journal of the Society for Psychical Research*, *55*(811), 60-70.

Saroka, K. S., Caswell, J. M., Lapointe, A., & Persinger, M. A. (2014). Greater electroencephalographic coherence between left and right temporal lobe structures during increased geomagnetic activity. Neuroscience Letters, in press.

Schmidt, H. (1970). A PK test with electronic equipment. *Journal of Parapsychology*, *34*(3), 175-181.

Schmidt, H. (1974). Comparison of PK action on two different random number generators. *Journal of Parapsychology*, *38*(1), 47-55.

Schmidt, H. (1982). Collapse of the state vector and psychokinetic effect. *Foundations of Physics*, *12*(6), 565-581.

Schmidt, H. (1987). The strange properties of psychokinesis. *Journal of Scientific Exploration*, *1*(2).

Schmidt, H. (1993). Observation of a psychokinetic effect under highly controlled conditions. *Journal of Parapsychology*, *57*.

Schove, D. J. (1955). The sunspot cycle, 649 B.C. to A.D. 2000. *Journal of Geophysical Research*, *60*(2), 127-146.

Schwartz, J. M., Stapp, H. P., & Beauregard, M. (2005). Quantum physics in neuroscience and psychology: A neurophysical model of mind-brain interaction. *Philosophical Transactions for the Royal Society B, 360*, 1309-1327.

Sheeley, N. R., Howard, R. A., Koomen, M. J., & Michels, D. J. (1983). Associations between coronal mass ejections and soft x-ray events. *The Astrophysical Journal, 272*, 349-354.

Sun, Y., Wang, C., & Dai, J. (2010). Biophotons as neural communication signals demonstrated *in situ* biophoton autography. *Photochemical & Photobiological Sciences, 9*(3), 315-322.

Tapping, K. F. (1987). Recent solar radio astronomy at centimeter wavelengths: The temporal variability of the 10.7-cm flux. *Journal of Geophysical Research: Atmospheres*, *92*(D1), 829-838.

Thomson, N. R., Rodger, C. J., & Dowden, R. L. (2004). Ionosphere gives size of greatest solar flare. *Geophysical Research Letters, 31*(6).

Tsang, E.W., Koren, S.A., & Persinger, M.A. (2004). Electrophysiological and quantitative electroencephalographic measurements after treatment by transcerebral magnetic fields generated by compact disc through a computer sound card: The Shakti treatment. *International Journal of Neuroscience, 114*(8), 1013-1024.

Tu, L. C., Luo, J., & Gillies, G. T. (2005). The mass of the photon. *Reports on Progress in*

Physics, *68*(1).

Wang, C., Bokkon, I., Dai, J., & Antal, I. (2011). Spontaneous and visible light-induced ultraweak photon emission from rat eyes. *Brain Research*, *1369*, 1-9.

Winkelman, M. (2002). Shamanism as neurotheology and evolutionary psychology. *American Behavioral Scientist*, *45*(12), 1875-1887.

Zingrone, N. L., Alvarado, C. S., & Dalton, K. (1998-99). Psi experiences and the "Big Five": Relating the NEO-PI-R to the experience claims of experimental subjects. *European Journal of Parapsychology, 14*, 31-51.

Chapter 2 – Gravitational and Experimental Electromagnetic Contributions to Cerebral Effects upon Deviations from Random Number Variations Generated by Electron Tunneling

Published in *International Letters of Chemistry, Physics and Astronomy*

2.1 Abstract

New theoretical and traditional quantitative solutions involving a pervasive unit quantum of ~10^{-20} J within biological and large-scale physical systems predicted that the mass of the human subject, subtle changes in gravitational phenomena, and the energy available within the cerebral volume should affect proximal random number variations produced by electron tunneling. In a series of experiments application of a specific, physiologically-patterned weak magnetic field over the right temporal lobe significantly enhanced the effects of intention upon deviations from random variations created by electron tunneling devices at a distance of 1 m. These variations were strongly (r = ~0.80) correlated with the coupling between the forces from the background free oscillations of the earth and the energy differences across the cell width between lunar perigee and apogee. The results support the approach that complex cognitive processes including "intention" can be described by physicochemical parameters and their magnitude of energies are within the range by which interactions or modulations from subtle gravitational forces applied across the cellular membrane and width might occur.

2.2 Introduction

Experimental demonstrations of the quantitative interaction between living masses, gravitational phenomena and electromagnetic variations have the capacity to reveal the intricate relationships between all three of these classes of phenomena within a universal context (Borowski, 2012). A fundamental quantum of energy associated with living systems, as manifested by the plasma membrane, is $\sim 10^{-20}$ J (Persinger, 2010), which is the increment energy associated with the separation of K^+ ions correlated with the resting membrane potential, the action potential ($\Delta v = 1.4 \cdot 10^{-1}$ V $\cdot$ $1.6 \cdot 10^{-19}$ A·s = $2.2 \cdot 10^{-20}$ J), and the value associated with hinge motions subsequent to the sequestering of the agonist to the receptor. It is the same effective value for second shell hydrogen bonds that are implicitly involved with proton mobility in water (Decoursey, 2003). Approximately 10^{-20} J, when solved for its frequency (by dividing Planck's constant), results in a wavelength that is the average width of a cell (~10 μm) which is remarkably congruent with the expected peak wavelength of a 37 °C (310 K) black body according to Wien's law.

What is less known is that the gravitational energy from the earth across the membrane of a typical cell (10 μm) is also $\sim 10^{-20}$ J. Assuming an average mass of a cell is $5 \cdot 10^{-13}$ kg and the earth's mass is $5.976 \cdot 10^{24}$ kg, the force at the inverse square of the distance from the earth's center (radius, $6.378 \cdot 10^6$ m) multiplied by G ($6.672 \cdot 10^{-11}$ m^3 kg^{-1} s^{-2}) is about 10^{-12} N. When applied across the width of a plasma membrane (10^{-8} m) that separates the ions contributing to the voltage of the resting membrane potential, the energy is 10^{-20} J. Persinger et al. (2008) calculated that the average force available within the known universe per Planck's voxel (the cube of Planck's length) when spread across the neutral hydrogen line results in a value of $\sim 10^{-20}$ J.

That changes in geomagnetic activity, as one source of electromagnetic perturbations, could interact with gravitational process has been shown theoretically by Minakov et al. (1992). Their equations indicated that the conversion of plane gravity waves into electromagnetic radiation would occur optimally with the primary harmonic of the Schumann resonance which is generated within the earth-ionospheric cavity. Vladmirski (1995) measured discrete enhancements of about 10^{-3} of the value of G, the gravitational constant, during lower geomagnetic activity. Indicators of equivalence between gravitational and electromagnetic properties appear to be more related to discrete quantitative solutions than to a singular equation (Persinger, 2012a).

That human mass could interact with fluctuations in gravitational forces through resonance processes and be coupled with adjacent physical chemical reactions has potential. Fundamental spheroidal modes or background free oscillations within the earth occupy a relatively wide band between 2 mHz and 7 mHz. Their peak-to-peak amplitudes are in the order of $0.5 \cdot 10^{-11}$ $m \cdot s^{-2}$. According to Nishida et al (2000) the excitation source emerges at the boundary between the earth's surface and atmosphere. For a 70 kg person or the 1.5 kg human cerebrum this would result in forces of $3.5 \cdot 10^{-10}$ N and $7 \cdot 10^{-12}$ N, respectively. For the latter, if applied across the width of neuronal membrane (10^{-8} m) the energy would be within the range of 10^{-20} J.

However, assuming a cross sectional length of $2.2 \cdot 10^{-1}$ m for the whole body and $1.1 \cdot 10^{-1}$ m (11 cm) for the cerebrum the equivalent energies for the 10^{-10} and $7 \cdot 10^{-12}$ N forces are $7.7 \cdot 10^{-11}$ J and 10^{-13} J, respectively. For comparison the magnetic energy within the cerebral volume associated with the physiologically-patterned magnetic fields we have found to be most effective for altering subjective states with correlative measurable changes within the cerebral volume (Saroka & Persinger, 2013) involve a range between ~40 nT and 400 nT amplitudes. From the formula:

$$J = [B^2 (2 \cdot 4\pi\mu)^{-1}] \cdot v,$$

where B is the strength of the field, μ is magnetic permeability, and v is volume (~$1.3 \cdot 10^{-3}$ m^3) of the cerebrum, the resultant magnetic energy is within the range of ~10^{-13} to 10^{-12} J. In other words the magnetic energies from the experimentally applied fields have the capacity to enhance the processes that reveal the coupling between cerebral activity and subtle gravitational-like energies from the earth.

These calculated values (~10^{-13} J) are relevant because the energies associated with the activity of only 10^6 neurons within the cerebral cortices each discharging around 7 to 8 Hz (the intrinsic resonance of the cerebrum) assuming 10^{-20} J per action potential, is within this range (Persinger & Lavallee, 2012). Considering there are in the order of $20 \cdot 10^9$ neurons in the cortices, this means that a fraction of a percent of the total neuronal capacity would match the energy associated with a coupling between earth oscillations and the cerebrum. The numbers of neurons are within the range of the critical mass that, depending upon the amount of recruitment of other neurons, could be below the threshold of "awareness" for the participant (Berns et al., 1997).

Annual oscillations in the amplitude of these slow waves have been reported around 230 s (4.3 mHz) and 270 s (3.7 mHz). Annual variations of background photon emissions of ~10^{-11} $W \cdot m^{-2}$ within the 3 mHz range have also been measured (Persinger, 2012b). The power associated with these energies at the fastest component of the 3 to 5.5 mHz band ($5.5 \cdot 10^{-3}$ s^{-1}) would be $4.1 \cdot 10^{-12}$ and 10^{-14} W for the 70 kg body and the 1.5 kg cerebrum, respectively. Assuming 1 m^2 cross-sectional area for the body and 10^{-2} m^2 cross sectional area for the cerebrum, the flux densities would be ~10^{-12} $W \cdot m^{-2}$.

Flux densities in the order of 10^{-11} $W \cdot m^{-2}$ are similar to photon densities that have been reliably measured from the right hemisphere of people sitting in complete darkness when they imagine light. The effect requires about 10 to 12 s to maximize and is reversible. The strength of the association between electroencephalographic power and the energy associated with photon emissions (Dotta et al., 2012) from the brain is strong (*r*s = ~0.9) and exhibits strong contributions from regions (the left prefrontal cortices). This functional association is consistent with the possibility that intentions or thoughts have clear physical bases with energies that are similar in magnitude to fundamental forces.

We reasoned that if gravitational and electromagnetic processes were coordinated within brain space these subtle changes could be coupled with proximal discrete physical chemical changes, specifically those involving electron tunneling across gaps that meet the criteria for the potential inclusion of Casimir forces. One device that utilizes this process is the Random Number Generator which has been employed for several decades to measure the effects of "intention" on random variation. The effects were so consistent over years, as shown by Jahn and Dunne (1987), that they have been included as examples of classical subtle cerebral-environment effects within the *Encyclopedia of Neuroscience* (Adelman, 1987).

If the operating mode is within the range of ~10^{-20} J, then any source of energy within this range, including electromagnetic energy (~10^{-19} J) either phase- or frequency-modulated within the dimensions of a plasma cell membrane (10 nm) would have the capacity to interact with these phenomena. Lunar distance ranges between ~$3.567 \cdot 10^{8}$ m (perigee) to ~$4.063 \cdot 10^{8}$ m (apogee). The gravitational effect from the moon ($7.33 \cdot 10^{24}$ kg) on a cell mass of $5.24 \cdot 10^{-13}$ kg would range from 15.52 to $20.14 \cdot 10^{-16}$ N and when applied across the width of a cell (10^{-5} m) would range from 1.55 to $2.01 \cdot 10^{-20}$ J. Considering the closer proximity of the latter to the energy associated

with neuronal action potentials, ~$1.9 \cdot 10^{-20}$ J (Persinger, 2010), we predicted that perigee would be particularly effective.

Here we present for the first time that the quantitative displacement from random of a dynamic process is strongly associated with the mass of the proximal person, strong modulations by changes in gravitational energies, and the capacity to modify this effect by applying experimentally generated weak magnetic fields over the temporal lobes. The most effective pattern which was designed to simulate long-term potentiation (LTP), the central process involved with consolidation of memory through the hippocampal formation, was within the 5 to 8 Hz range. These values are also within the range of the resonance frequency of the average cerebrum and the earth's circumference. The former is calculated by assuming a bulk velocity of about 4.5 $m \cdot s^{-1}$ (Nunez, 1995) for the rostral-caudal waves generating the 20 to 25 ms intervals of consciousness and a circumference of about 60 cm. The latter is the traditional solution where the velocity of light is divided by $4 \cdot 10^{7}$ m.

2.3 Methods

Subjects

Participant age ranged from 22-52 years for N = 15 (N = 7 females, N = 8 males). All were recruited from Laurentian University campus or the local community.

Equipment

Four solenoids (telephone pickup coils obtained from Radio Shack or The Source, Model: 44-533) were arranged over the approximate location of the temporal lobe of each hemisphere in a '+' pattern. Vertical solenoids were separated by 5 cm, while the horizontal solenoids were separated by 8 cm. The 4 solenoids were maintained in position on each side of a cap by Velcro.

Shiva Technology software version 1G was designed by Professor Todd Murphy as part of the Shiva Neural Stimulation system (www.shaktitechnology.com/shiva/), and was employed to generate the fields.

This technology employs signals based on patterns used in previous studies (Persinger et al., 2010). Patterned waveforms are converted into audio files, which were delivered from 4 USB soundcards to the solenoids attached to the cap. Each audio device sends its signal to two of the solenoids, splitting the left audio channel to one solenoid and the right channel to the other (e.g., audio device 1 controls solenoids 1 and 2, while device 2 controls solenoids 3 and 4). The resultant activation of the solenoid creates a weak-intensity magnetic field within the .04 to .4 μT range as verified by milligauss meters (AC Milligauss Meter Model UHS2, AlphaLab, Inc; www.trifield.com).

Random data was produced using a Psyleron REG-1 random event generator (www.psyleron.com). The device produced a random output which was generated by electron tunnelling effects within two field effect transistors. The varying voltage levels which result from this process were converted into digital data through a gated sampling procedure which allows for regularly spaced bit sequences.

The output of both transistors was internally compared through an XOR masking process (using an alternating 1/0 pattern to maintain complete randomness from chance expectation) in order to reduce any potential influence of physical artefacts or other external environmental variables.

The device itself was further protected from static electromagnetic factors by an aluminum outer shielding and a Permalloy mu-metal inner shield. Furthermore, the device was rigorously calibrated prior to shipment in order to ensure output conformed to statistical expectations. The

random event generator (REG) was also tested in control experiments within our laboratory to confirm these expectations.

The resulting data stream was collected through USB-port using Psyleron FieldREG and Reflector software packages on a laptop computer. Data were produced at a rate of 1 event (200 0,1 bits/event) per second, with each event referring to the number of 1's out of 200 bits with binary probabilities, represented by a value of 0-200.

The theoretical (chance) mean for each event is 100 with a standard deviation of √50. Statistical analyses were conducted using SPSS software v.17.

Procedure

Prior to testing, participants viewed a short demonstration with the REG software in order to understand how they would be focusing their intention. No feedback was provided during testing. They were then seated in a comfortable chair in a dark acoustic chamber which was also a Faraday cage. During the experiment each subject wore the hat containing the 4 pairs of solenoids situated over the regions of the temporal lobes. The REG was placed approximately 1 m away at ground level on the *right* side of the participant approximately 45° from the plane of the forward line of sight.

Participants were first asked to intend for the REG data output to deviate either up or down for ~5 minutes. Following this, a 40 Hz 'chirp' signal was applied bilaterally through the Shiva software for 20 minutes as a 'primer' field. A physiologically-patterned 'target' field was then applied for 15 minutes before the participant was asked to again focus intention on the REG for 5 minutes while the field continued running. During this period N = 9 participants received an EMF patterned after LTP (long-term potentiation) in the hippocampus over the right hemisphere.

The other N = 6 received an EMF patterned after burst-firing in the amygdala over the left hemisphere. Field assignment was randomized. REG data collection was hidden from the experimenter until testing had completed. The selection of these two patterns was based upon their efficacy revealed by previous research. In addition, there is evidence of differential responsivity of the two hemispheres. The right hemisphere appears to be particularly sensitive to small changes in global geomagnetic activity (Mulligan et al., 2010).

Data Transformation

Random Event Generator (REG) data was obtained for N = 15 participants during three conditions (pre-field, baseline, and field). For pre-field and field conditions (e.g., those involving conscious intention) all individual REG event scores were reversed where necessary in order to produce positive overall session deviations when output was shifted in the intended direction, and negative deviations for sessions which shifted in the direction opposite of intention.

This was accomplished by obtaining the deviation from the hypothetical mean (in bits) for each event score (x-100) and multiplying by -1, then adding 100 to the subsequent values, effectively reversing the overall trend to represent the direction of intention. All individual events were subsequently z-scored according to .5 chance expectations ([x-100] / √50). Overall session z-scores were derived using Stouffer's method (Σz / √n), where z = individual event z-scores, and n = the number of events. Event sample sizes varied slightly between sessions, and therefore overall z-scores for each condition (z_c) were obtained by first combining all individual event scores for all participants within a given condition (raw event values ranging from 0-200).

The overall deviation from the natural mean (100) was computed (δ_μ), along with the measurement uncertainty associated with the actual condition mean ($\sigma_\mu = \sigma$ / √N, where N = total

number of events, and σ = the natural standard deviation of $\sqrt{50}$). These two values were then divided ($z_c = \delta_\mu / \sigma_\mu$) in order to produce the z-scores and subsequent probabilities associated with each overall condition.

One-tailed probabilities are reported where z-scores are used for overall sessions or conditions involving participant intention (e.g., testing for intended direction). Comparisons between conditions were examined by obtaining the absolute difference between condition means (e.g., $\mu_{field} - \mu_{baseline}$), as well as the measurement uncertainty associated with this value given the specific event samples (e.g., $\sigma \cdot \sqrt{([1 / N_{field}] + [1 / N_{baseline}])}$, where N = number of events, and $\sigma = \sqrt{50}$). These values were then divided ($z_c = \delta_\mu / \sigma_\mu$) in order to produce a z-score used to determine the magnitude of the difference between conditions.

2.4 Results

Overall Condition Results

During the baseline (no intention) condition the REG data conformed to statistical expectations (z_c = -.6, p = .548). Results from the pre-field condition also did not significantly differ from chance (z_c = 1.406, p = .08).

However, the REG data from the field condition showed a significant deviation in the direction the participants had intended (z_c = 2.876, p = .002). The overall results for each condition are represented in *Figure 1* as cumulating deviations. More detailed descriptive parameters for each condition are presented in *Table 1*.

These values account for slight variations in event sample sizes between participants and subsequently for overall conditions. As shown in *Table 2* the only significant overall difference

between conditions revealed through this more precise process was between field and baseline conditions (z_c = 2.45, p = .007).

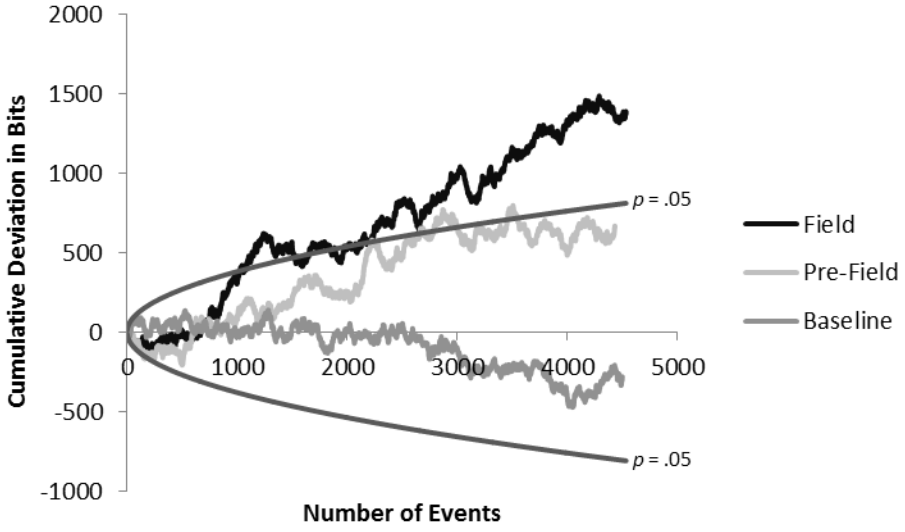

Figure 1 - Combined cumulative deviations in REG output 1 m away for each condition; parabolas indicate threshold of statistical significance (p = .05, one-tailed). The magnetic fields were applied over the temporal lobes of the participants.

Parameter	Baseline (BL)	Pre-Field	Field
N	4500	4433	4533
μ	99.937	100.149	100.302
sd	7.042	7.1	7.183
σ_{sd}	.001	.001	.001
δ_{μ}	-.063	.149	.302
σ_{μ}	.105	.106	.105
z_c	-.6	1.406	**2.876**
p	.548 **	.08 *	**.002** *
%ID	.467 †	.667	.733

Table 1 - Detailed REG results for overall conditions (Baseline, Pre-Field Intention, Intention with EMF application), data converted to directional measures (e.g., accounting for intended direction of deviations).

Parameter Key:

N: Number of events (200 bits/event)

$\boldsymbol{\mu}$: Mean event score (0-200)

sd: Standard deviation of REG event scores

$\boldsymbol{\sigma_{sd}}$: Measurement uncertainty in value of *sd*; $\sigma_{sd} = \sigma / \sqrt{2N}$, where $\sigma = \sqrt{50}$

$\boldsymbol{\delta_{\mu}}$: Absolute deviation from theoretical chance expectations (μ-100)

$\boldsymbol{\sigma_{\mu}}$: Measurement uncertainty in value of δ_{μ}; $\sigma_{\mu} = \sigma / \sqrt{N}$, where $\sigma = \sqrt{50}$

$\boldsymbol{z_c}$: Overall condition z-score adjusted for measurement uncertainty; $z_c = \delta_{\mu} / \sigma_{\mu}$

p: Probability of z_c * & **

%ID: Proportion of sessions with deviation in the intended direction; %ID = $Ns_{\text{ with intention}}$ / Ns, where Ns = number of test sessions †

†For directionality of baseline sessions, positive values are considered to be with intention.

*One-tailed probability (e.g., intention involved).

**Two-tailed probability (e.g., no intention).

Parameter	PreField-BL	Field-BL	Field-PreField
N	8933	9033	8966
$\boldsymbol{\delta_{\mu}}$	.212	.365	.153
$\boldsymbol{\sigma_{\mu}}$	.15	.149	.149
$\boldsymbol{z_c}$	1.413	**2.45**	1.027
p	.079 *	**.007** *	.152 *

Table 2 - Detailed REG results comparing overall conditions, data converted to directional measures (e.g., accounting for intended direction of deviations).

Parameter Key:

N: Combined number of events (200 bits/event)

$\boldsymbol{\delta_{\mu}}$: Absolute deviation; e.g., = $\mu_{\text{ field}} - \mu_{\text{ baseline}}$

$\boldsymbol{\sigma_\mu}$: Measurement uncertainty in δ_μ; e.g., = $\sigma \cdot \sqrt{([1 / N_{field}] + [1 / N_{baseline}])}$, where $\sigma = \sqrt{50}$

$\boldsymbol{z_c}$: z-score of overall difference adjusted for measurement uncertainty; $z_c = \delta_\mu / \sigma_\mu$

$\boldsymbol{p}$: Probability of z_c (one-tailed)

REG Differences between Field Treatments

The overall deviation from chance for the nine subjects exposed to the hippocampal field condition was statistically significant (*Figure 2*; $z_c = 3.067$, $p = .001$), with three independently significant sessions. All sessions in this condition deviated in the direction intended. However, results from the amygdaloid pattern condition were within chance expectations (*Figure 2*; $z_c = .79$, $p = .215$). Although there were two independently significant sessions within this condition, there were also two sessions which deviated in the direction opposite of intention.

Following further analyses (*Table 3*) it was discerned that the hippocampal field treatment significantly differed from the associated baseline results ($z_c = 2.656$, $p = .004$), while the amygdala treatment did not significantly differ from control measures ($z_c = .61$, $p = .271$).

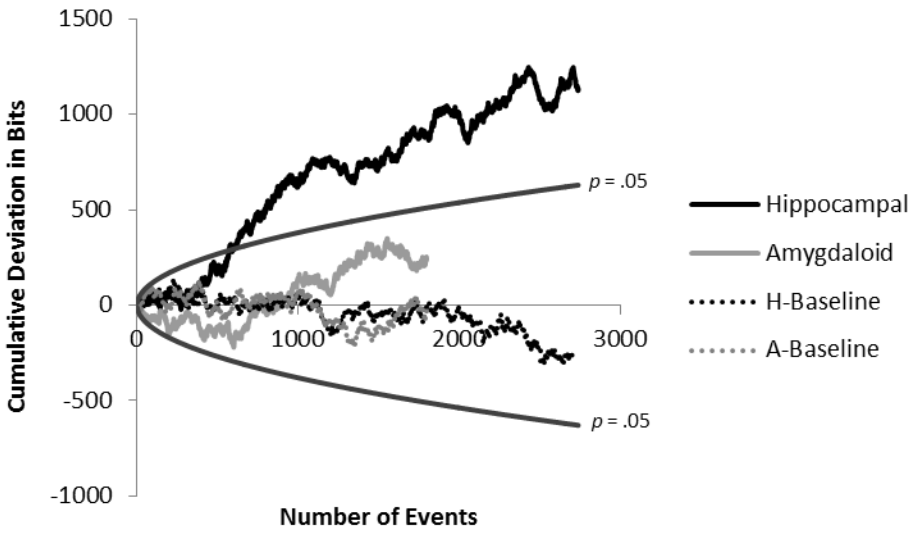

Figure 2 - Combined cumulative deviations of REG output for each field condition and associated baseline measures; parabolas indicate threshold of statistical significance (p = .05, one-tailed). The "hippocampal" patterned magnetic field applied over the right temporal lobe during intention produced significant deviations.

Means, absolute means, and standard deviations were obtained for each minute (5) of REG output using data prior to directional transformation; sessions were not converted with respect to direction while z-scores were obtained from the raw data. An independent t-test revealed a statistically significant difference between field treatments (hippocampal and amygdaloid, respectively μ = .132, *sd* = .066 and μ = .046, *sd* = .013) for the absolute mean REG score during minute 3.

Parameter	Hippocampus(Hi)	Amygdala(Am)	BL(Hi)	BL(Am)
N	2737	1796	2700	1800
$\boldsymbol{\mu}$	100.414	100.132	99.904	99.988
sd	7.253	7.075	7.031	7.06
$\boldsymbol{\sigma_{sd}}$	.096	.118	.096	.118
$\boldsymbol{\delta_{\mu}}$	.414	.132	-.096	-.012
$\boldsymbol{\sigma_{\mu}}$	.135	.167	.136	.167
$\boldsymbol{z_c}$	**3.067**	.79	-.706	-.072
p	**.001** *	.215 *	.76 **	.529 **
%ID	.889	.5	.333 †	.667 †

Table 3 - Detailed REG results for each field condition (hippocampal and amygdaloid) with associated baseline measures; data converted to directional measures (e.g., accounting for intended direction of deviations).

Analysis of Potential Gravity Contributors

To examine any potential influence of subtle changes in gravity on REG output during human intention paired with the additional energy from transcerebral EMF application, the weight of each participant (kg) was obtained. The participant database was subsequently split by the year they were tested (2012 and 2013). Pearson and Spearman analyses indicated that participant weights in the test block from 2012 (N = 7) were significantly correlated with average REG scores during minute 1 of testing (*Figure 3*; *rho* = -.805, *p* = .029). Within the second block of testing (N = 8), Spearman correlations revealed a significant relationship between weight and average REG output during minute 3 (*Figure 4*; *rho* = -.857, *p* = .014). Assuming the maximum value for a period, this would be equivalent to 16 mHz to 5.5 mHz (3 min) which is well within the range predicted if there is a coupling between the earth's free oscillations, the person's mass, and the forces and energies available locally for the effect.

Although body weight of the participants was clearly associated with the deviations we pursued the hypothesis the interaction between the mass of the cell and the most obvious proximal

changing source of small gravitational force, the moon, could contribute to the interaction between the cerebral activity associated with intention and a proximal (within 1 m) random physical process. Subsequently, the numbers of days since the most recent lunar apogee and perigee were obtained for each session. Lunar data was derived from the Lunar Extremes database. Both parametric and non-parametric correlation analyses (*Figure 5*) revealed a significant relationship between perigee and the average REG score during minute 2 (r = -.718, p = .003; *rho* = -.774, p = .001).

In order to determine if this effect was further influenced by the mass, and therefore gravity, of the participant a partial correlation was completed between perigee and average REG score during minute 2 while controlling for participant weight. The significant correlation (*Figure 6*) was maintained and, furthermore, there was an increase in the strength of this relationship (r = -.77, p = .001; *rho* = -.818, p < .001) when controlling for individual weight differences. Both perigee and average REG score were entered into separate linear regressions with weight to obtain the standardized residual values plotted in order to demonstrate the partial correlation. Subsequent correlation analyses revealed a significant relationship between the average REG score during minute 2 and the overall final session score (r = .671, p = .006; *rho* = .70, p = .004). This would be consistent with the approach that the forces and energies associated with the second minute, the duration overlapping with the periodicity of Earth oscillations, was central to affecting the overall outcome of the deviations from chance.

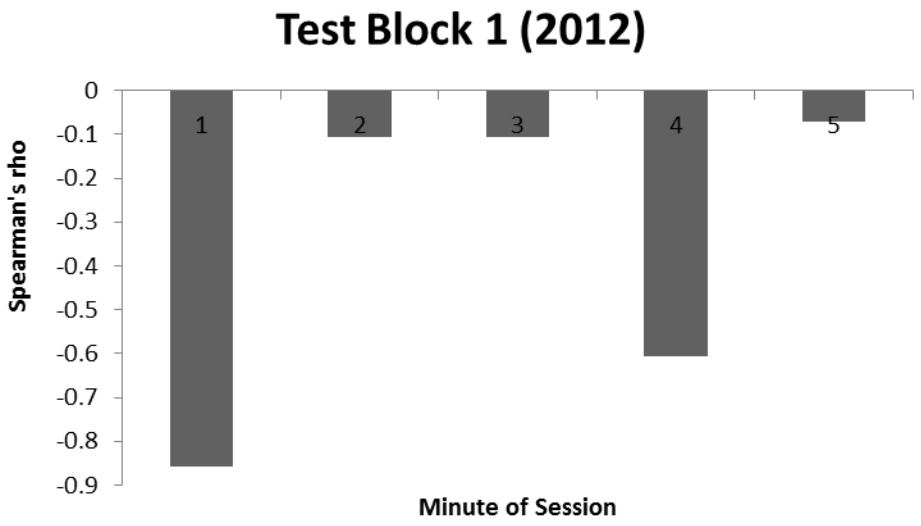

Figure 3 - Spearman correlation values for participant weight and mean REG score in each minute of testing (2012).

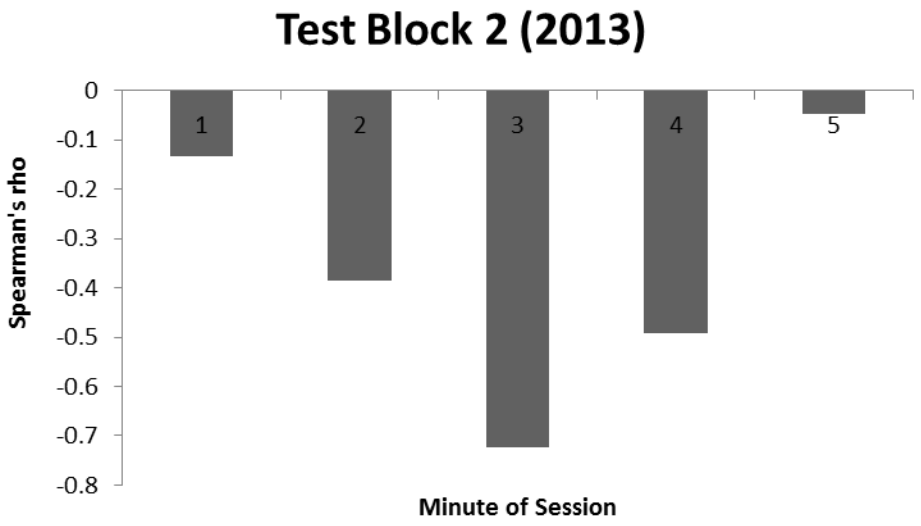

Figure 4 - Spearman correlation values for participant weight and mean REG score in each minute of testing (2013).

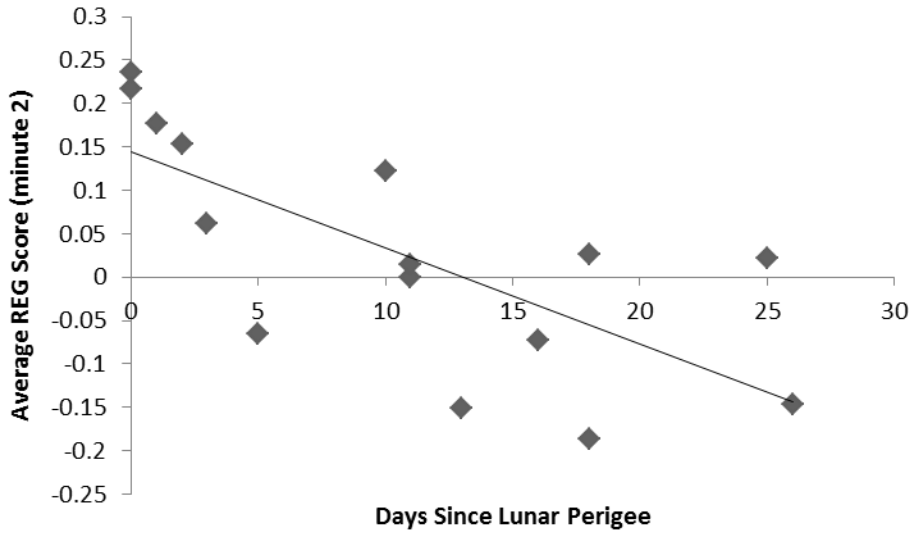

Figure 5 - Correlation between perigee values and average REG score during minute 2.

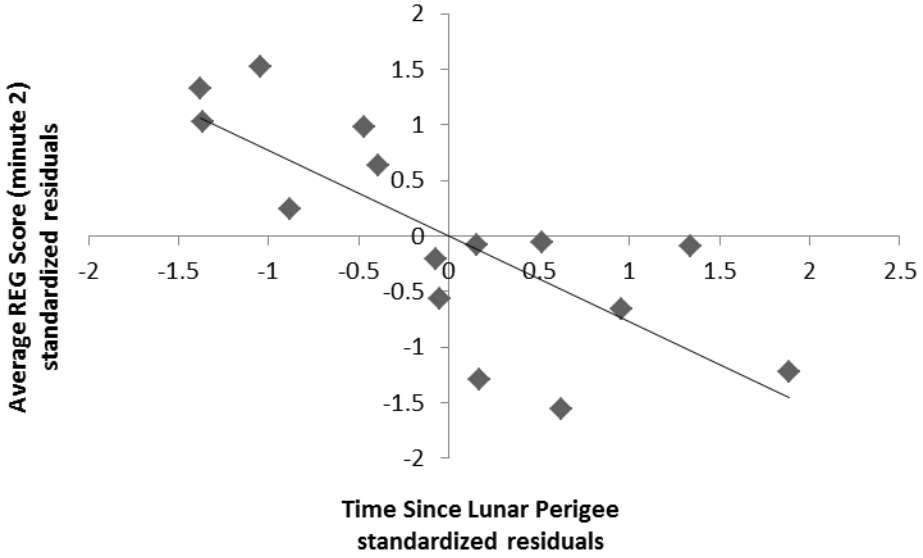

Figure 6 - Partial correlation between perigee values and average REG score during minute 2, controlling for participant weight; standardized residual values.

2.5 Discussion and Conclusions

The results of this study may reflect one of the first interdisciplinary and integrative experiments that relate the quantitative values from theoretical relationships between the electromagnetic energies generated by cells and aggregates of cells with those associated with inferred or direct effects of gravity and gravitational-like forces. The consistency and convergence of the results emphasize the importance of multidisciplinary approaches to critical physical phenomena that include concepts and problems that relate astronomy, chemistry, and physics as well as their reflection within the biological sciences.

The concept of "random" is essential to all sciences and is the implicit assumption that drives the central limit theorem, that is, if an infinite number of means from random populations of numbers were plotted, they would display the normal distribution. The possibility that proximity to electronic devices that control electron tunneling in a "random" fashion can influence the outcome of the "random" occurrence of events as a function of the mass of the person suggests that local gravitational effects may be more relevant than previously assumed. The modulation of this effect by lunar distance, particularly when perigee was employed as the reference, supports this type of process.

The effect of an applied magnetic field upon the effectiveness by which the intent of the participant displaced the random variations from chance indicates that the phenomena are physically-based and can be easily affected by experimental methods. The magnetic field pattern (Mach & Persinger, 2009) is known to affect the representation of experience (memory) within brain space which is expressed as specific changes in spine growth and dendritic patterns. In essence the 40 to 400 nT intensity patterned magnetic fields that were generated primarily over

the right temporal lobes of the participants markedly enhanced the effects of their intention upon the deviation from random variation of proximal (1 m) electron tunneling in a commercial device.

We suggest that the increment of energy or quantum that mediates this effect is ~$2 \cdot 10^{-20}$ J. This is the energy upon a unit charge ($1.6 \cdot 10^{-19}$ A·s) from a typical change in voltage during an action potential from a neuron. The unit of energy is also the implicit energy from the gravitational force from the earth upon a typical cell mass when applied across the plasma membrane and the functional energy from lunar gravitational effects around the time of perigee across the width of the typical neuronal soma. Such convergence allows the condition for the potential interaction, amplification, and dampening of these energies during dynamic processes.

The primary temporal component for the energy within the cerebral volume and the general body mass is likely to originate from the natural free oscillations from the earth-atmospheric interface during seismic-free conditions (Nishida et al., 2000). The energy within the volume of the human cerebrum or average body mass would be in the order of 10^{-13} J to 10^{-11} J, respectively. From this perspective the fact that our most effective changes from applied magnetic fields across the temporal lobes is usually between 40 nT and 400 nT is expected because comparable magnetic energies would be available within the cerebral volume from this range of intensities. In the present study this was sufficient, when the appropriate pattern was applied, to produce large deviations within the random number generators.

Why the presence of and intention by a human being should affect electron tunneling may be related to shared spatial features of the functional unit of the brain (the synapse) and the two surfaces across which electrons tunnel. The typical surface area of a synapse is in the order of 0.5 to 2 μm^2 and in the balance of probabilities this is the approximate width surface area from which

the electrons tunnel within the REG. The two "plates" of the synapse are separated by about 10 nm which is within an order of magnitude of the separation likely for the random number generators.

If this feature is relevant then a type of resonance could occur whereby energies are exchanged. The Casimir force within the brief period of neutrality for the geometry of a typical synapse is $\sim 0.52 \cdot 10^{-6}$ N and when applied over the distance of this separation (10^{-8} m) is $\sim 0.52 \cdot 10^{-14}$ J. When divided by Planck's constant to obtain the frequency the equivalent electromagnetic wavelength, assuming the velocity of light, is 38 pm. This is within measurement error of the radius of the hydrogen atom (Persinger & Lavallee, 2010). We think it may be relevant that a classic Cosic (Cosic, 1994) velocity of an electron, $\sim 2 \cdot 10^{5}$ $m \cdot s^{-1}$ would be associated with mass-energy equivalence of $\sim 1.8 \cdot 10^{-20}$ J. Hence the congruence between the energetic boundaries could allow for the conditions for non-locality. We (Dotta & Persinger, 2012) have shown previously that non-local effects, that is "entanglement" or "excess correlation" between two loci can occur for periods of about 8 min when they share similar shaped magnetic fields with specific rates of change in angular velocities.

2.6 References

Adelman, G. (Ed.), (1987). *Encyclopedia of neuroscience*. Birkhauser.

Berns, G. S., Cohen, J. D., & Mintun, M. A. (1997). Brain regions responsive to novelty in the absence of awareness. *Science*, *276*(5316), 1272-1275.

Borowski, T. (2012). The new theory of gravitation representing the movement of planets. *International Letters of Chemistry, Physics and Astronomy*, *1*(2012), 1-5.

Cosic, I. (1994). Macromolecular bioactivity: Is it resonant interaction between macromolecules?. Theory and applications. *IEEE Transactions on Biomedical Engineering*, *41*(12), 1101-1114.

Decoursey, T. E. (2003). Voltage-gated proton channels and other proton transfer pathways. *Physiological Reviews*, *83*(2), 475-579.

Dotta, B. T., & Persinger, M. A. (2012). "Doubling" of local photon emissions when two simultaneous, spatially-separated, chemiluminescent reactions share the same magnetic field configurations. *Journal of Biophysical Chemistry*, *3*(1), 72-80.

Dotta, B. T., Saroka, K. S., & Persinger, M. A. (2012). Increased photon emission from the head while imagining light in the dark is correlated with changes in electroencephalographic power: Support for Bokkon's biophoton hypothesis. *Neuroscience Letters*, *513*(2), 151-154.

Jahn, R. G., & Dunne, B. J. (1987). *Margins of reality: The role of consciousness in the physical world*. Harcourt Brace Javanovich.

Mach, Q. H., & Persinger, M. A. (2009). Behavioral changes with brief exposures to weak magnetic fields patterned to simulate long-term potentiation. *Brain Research, 1261*, 45-53.

Minakov, A. A., Nikolaenko, A. P., & Rabinovich, L. M. (1992). Gravitational-to-electromagnetic wave conversion in electrostatic field of earth-ionosphere resonator. *Radiophysics and Quantum Electronics*, *35*(6-7), 318-323.

Mulligan, B. P., Hunter, M. D., & Persinger, M. A. (2010). Effects of geomagnetic activity and atmospheric power variations on quantitative measures of brain activity: Replication of the Azerbaijani studies. *Advances in Space Research*, *45*(7), 940-948.

Nishida, K., Kobayashi, N., & Fukao, Y. (2000). Resonant oscillations between the solid earth and the atmosphere. *Science*, *287*(5461), 2244-2246.

Nunez, P. L. (1995). *Neocortical dynamics and human EEG rhythms*. Oxford University Press.

Persinger, M. A. (2010). 10^{-20} joules as a neuromolecular quantum in medicinal chemistry: An alternative approach to myriad molecular pathways?. *Current Medicinal Chemistry*, *17*(27), 3094-3098.

Persinger, M. A. (2012a). Potential origins of a quantitative equivalence between gravity and light. *The Open Astronomy Journal*, *5*, 41-43.

Persinger, M. A. (2012b). Annual variation of local photon emissions' spectral power within the mHz range overlaps with seismic-atmospheric acoustic oscillations. *International Journal of Geosciences*, *3*, 192-194.

Persinger, M. A., & Lavallee, C. F. (2010). Theoretical and experimental evidence of macroscopic entanglement between human brain activity and photon emissions: Implications for quantum consciousness and future applications. *Journal of Consciousness Exploration & Research*, *1*(7), 785-807.

Persinger, M. A., & Lavallee, C. (2012). The sum of n = n concept and the quantitative support for the cerebral-holographic and electromagnetic configuration of consciousness. *Journal of Consciousness Studies*, *19*, 128-153.

Persinger, M. A., Koren, S. A., & Lafreniere, G. F. (2008). A neuroquantologic approach to how human thought might affect the universe. *NeuroQuantology*, *6*(3), 262-271.

Persinger, M. A., Saroka, K., Koren, S. A., & St-Pierre, L. S. (2010). The electromagnetic induction of mystical and altered states within the laboratory. *Journal of Consciousness Exploration & Research*, *1*(7), 803-830.

Saroka, K. S., & Persinger, M. A. (2013). Potential production of Hughlings Jackson's "parasitic consciousness" by physiologically-patterned weak transcerebral magnetic fields: QEEG and source localization. *Epilepsy and Behavior*, *28*, 395-407.

Vladmirskii, B. M. (1995). Measurements of gravitational constant and heliogeophysical electromagnetic perturbations. *Biophysics, 40*, 915-923.

Chapter 3 – Cerebral Biophoton Emission as a Potential Factor in Non-Local Human-Machine Interaction

Published in *NeuroQuantology*

3.1 Abstract

Subjects were instructed to employ intention to affect the direction of random number generation from a device located on their right side at 1 m distance. Biophoton emissions from the right hemisphere were recorded simultaneously. Significant increases (~$3.5 \cdot 10^{-12}$ $W \cdot m^{-2}$) in photon radiant flux density occurred when there were marked deviations from random variations suggesting that the correlative variable for intent was coupled to cerebral photon emission. Cross-spectral analyses indicated a significant coupling between photon density and deviation from random variation within the 6 mHz range. The estimated raw power over the most likely area of influence (10^{-10} m^2) over the peak duration would be within the order of 10^{-20} J. This quantum is associated with single action potentials and the difference in energy equivalents after Lorentz contraction between the electron's Compton wavelength and traditional particle width. The resulting ~1.5 μm wavelength for this energy, which matches Bohr's solution, is also within the width of the synapse. The moderately strong correlation between the strength of the coherence between the deviations during intention and the photon emission and the entropy within the temporal distribution of the "random" number variations in the mHz range suggests that a shared source with the earth's free background oscillations may be involved. Our results strongly indicate that photon-electron interactions between cerebral function and electronic devices that

reflect "random" electron tunnelling may be more powerful than accommodated by classical physics and indicate the powerful role of a neuroquantological process.

3.2 Introduction

Photons are the quanta of electromagnetic radiation, essentially particles of light. Their average energies, according to the relationship $E = h \cdot c \cdot \lambda^{-1}$, are typically within the range of 10^{-19} J for the ultraviolet to infrared portions of the electromagnetic spectrum. Although traditionally thought to possess no mass, recent evidence has suggested a non-zero rest mass for the photon (upper limit ~10^{-52} kg; Tu et al., 2005). The phenomenon of biophoton emission (BPE) refers to the occurrence of ultraweak light emission from biological matter, typically in association with reactive oxygen species formation and cellular metabolism (Apel & Hirt, 2004). Biophotons have been a major focus in the area of biophysics for a number of years (e.g., Li et al., 1983), and novel approaches to molecular biology have been revealed through the study of this mechanism (e.g., Isojima et al., 1995; Gourley et al., 2005). Subsequent experiments have suggested the plasma membrane of the cell as the most likely source (Dotta et al., 2011). BPE has also been examined in the context of the human body (e.g., Kobayashi et al., 2009). Furthermore, this phenomenon has been suggested as a potential mechanism in cellular communication (Sun et al., 2010). A number of more exotic applications have been proposed in this area.

Bokkon's innovative theories (2005; 2009) have implicated biophotons in visual imagery. In order to test this hypothesis, recent experiments examined the relationship between BPE, visualization, as well as intention, which suggest that imagining white light consistently produces an increase in photon emission from the right side of the head compared to both mundane thoughts and baseline conditions (Dotta & Persinger, 2011). The radiant flux density associated with BPE increases was measured to be approximately $5 \cdot 10^{-11}$ $W \cdot m^{-2}$ and was estimated to be

associated with ~10^7 cortical neurons (Dotta et al., 2012). It was subsequently revealed that BPE was significantly and strongly correlated with electroencephalographic (EEG) power during this task. Aside from the more obvious relationship with visual imagery revealed by these studies, cerebral biophotons have also been suggested as a potential mechanism in consciousness (Amoroso, 1999; Dotta et al., 2013). Furthering Bokkon's hypotheses, studies have revealed properties of photon entanglement (e.g., Persinger & Lavallee, 2010) and the potential transfer of non-local information (Dotta & Persinger, 2009) in the context of human brain activity and cerebral biophotons. Given the apparent associations between consciousness, intention, biophotons, and non-locality, it is suggested that cerebral BPE may play a role in mediating non-local physical anomalies associated with consciousness. Although evidence supporting this contention has been examined in the context of incoming non-local information (Persinger & Saroka, 2012), BPE has not been studied during processes associated with outgoing non-local information. The phenomenon of consciousness-correlated collapse (3C) has suggested that a human operator is capable of influencing the outcome of a non-deterministic external system through mental intention alone (e.g., Jahn et al., 1997; Radin & Nelson, 2003). Although brain activity has been examined to some degree during this apparent interaction (Gissurarson, 1992), the non-local qualities of photon emissions and their intimate link to consciousness provide a reasonable measure of potential influence within 3C processes. The following experiment tested the hypothesis that BPE may be a factor involved in the apparent influence of cognitive "intention" on an external random physical system. We measured BPE from the right side of participants' heads while they focused their intention on a random event generator (REG) device in order to produce a desired outcome in the data. It was hypothesized that specific ranges of photon emission would be associated with various levels of overall performance, determined by the overall magnitude of deviation within the REG data, as well as specific ranges of individual

events. It was further speculated that any relationship between photon emission and REG device output would likely become apparent upon examination of both spectral characteristics of the data and statistical signal complexity.

Given the apparent associations between consciousness, intention, biophotons, and non-locality, it is suggested that cerebral BPE may play a role in mediating non-local physical anomalies associated with consciousness. Although evidence supporting this contention has been examined in the context of incoming non-local information (Persinger & Saroka, 2012), BPE has not been studied during processes associated with outgoing non-local information. The phenomenon of consciousness-correlated collapse (3C) has suggested that a human operator is capable of influencing the outcome of a non-deterministic external system through mental intention alone (e.g., Jahn et al., 1997; Radin & Nelson, 2003). Although brain activity has been examined to some degree during this apparent interaction (Gissurarson, 1992), the non-local qualities of photon emissions and their intimate link to consciousness provide a reasonable measure of potential influence within 3C processes. The following experiment tested the hypothesis that BPE may be a factor involved in the apparent influence of cognitive "intention" on an external random physical system. We measured BPE from the right side of participants' heads while they focused their intention on a random event generator (REG) device in order to produce a desired outcome in the data. It was hypothesized that specific ranges of photon emission would be associated with various levels of overall performance, determined by the overall magnitude of deviation within the REG data, as well as specific ranges of individual events. It was further speculated that any relationship between photon emission and REG device output would likely become apparent upon examination of both spectral characteristics of the data and statistical signal complexity.

3.3 Methods

Subjects

Participant age ranged from 22-42 years for N = 11 (N = 8 females, N = 3 males). All were recruited from Laurentian University campus.

Equipment

Biophoton emission (BPE) for the first N = 8 participants was measured using a Model 15 Photometer from SRI Instruments (Pacific Photometric Instruments), which contained a unit scale ranging in single units from 1 to 100. Calibration indicated a single unit was equal to $\sim 5 \cdot 10^{-11}$ $W \cdot m^{-2}$. The photomultiplier tube (PMT) housing (BCA IP21) for the RCA electron tube was placed at a distance of approximately 15 cm from the right side of the participant's head. Data output was sent to a laptop computer with a sampling rate of 3 samples per second. Participants in this test segment contributed n = 23 individual sessions. BPE for the latter N = 3 participants was obtained using a digital photometer Model DM009C (Senstech Ltd.), also placed ~15 cm from the right side of the head, with a sample rate of 50 samples per second. This measured the numbers of individual photons in each sample as opposed to an absolute measure of power. Values from all trials were subsequently averaged and standardized accordingly. Data obtained from both PMT models were compared in previous experiments which revealed congruence between the devices (e.g., Persinger et al., 2013). Participants in this segment contributed n = 4 individual sessions.

Random data was produced using a Psyleron REG-1 random event generator (*Figure 7*; www.psyleron.com). The device produces a random output which is generated by electron tunneling effects within two field effect transistors. The varying voltage levels which result from

this process are converted into digital data through a gated sampling procedure which allows for regularly spaced bit sequences. The output of both transistors is internally compared through an alternating (0, 1) XOR masking process in order to maintain true randomness and reduce any potential influence of physical artefacts or other external environmental variables (Jahn et al., 2000). The device itself is further protected from static electromagnetic factors by an aluminum outer shielding and a Permalloy mu-metal inner shield. Furthermore, the device was rigorously calibrated prior to shipment in order to ensure output conformed to statistical expectations. The random event generator (REG) was also tested in control experiments within our laboratory to confirm these expectations. The resulting data stream is collected through USB-port using Psyleron FieldREG and Reflector software packages on a laptop computer. Data was produced at a rate of 2 events (200 0,1 bits/event) per second, with each event referring to the number of 1's out of 200 bits with binary probabilities, represented by a value of 0-200. The theoretical (chance) mean for each event is 100 with a standard deviation of $\sqrt{50}$.

Measures of entropy (HX) were computed using Matlab 2011a software. All other statistical procedures, including spectral analyses, were conducted using SPSS software v.17.

Figure 7 - Random event generator (REG); Psyleron REG-1 device used throughout the following experiment

Procedure

Prior to testing, participants viewed a short demonstration with the REG software (e.g., *Figure 8*) in order to understand upon what they would be focusing their intention. No feedback was provided during testing. They were seated in a dark, comfortable environment, approximately 1 m away from the REG (right side). The PMT was located 15 cm from the right side of the head (*Figure 9*). They were then asked to intend for the data output of the REG to deviate either up or down for one to three periods of ~8 minutes each while the PMT measured photon emission. REG software data collection was hidden from the experimenters during this process.

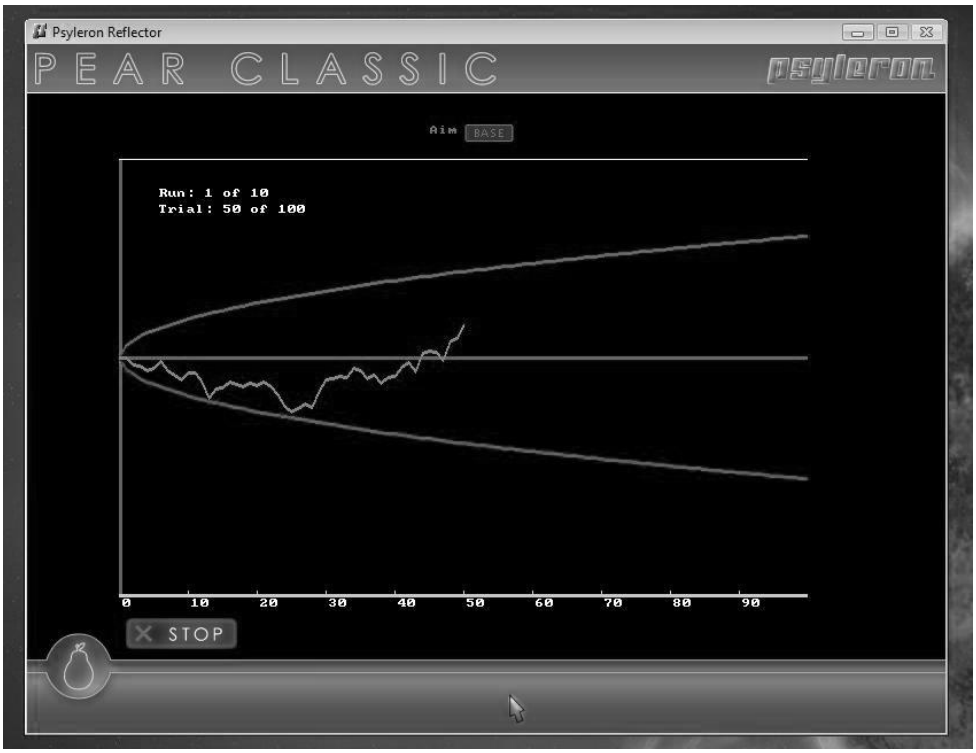

Figure 8 - Screenshot of Reflector software collecting data from REG device; jagged center line is the moving cumulative deviation

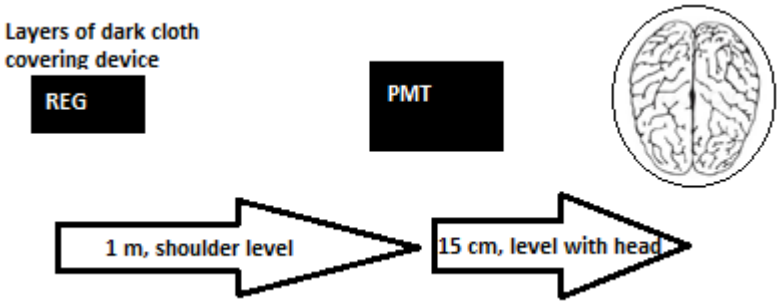

Figure 9 - Schematic of experiment; relative positions of REG, PMT, and human operator

3.4 Results

Data Transformation

Random Event Generator (REG) data was collected for a total of 27 test sessions from N = 11 participants. Individual REG event scores were standardized according to .5 chance expectations using z-scores ([*x*-100] / √50). Overall session scores were obtained using Stouffer's method ($\sum z$ / √n), where *z* = individual event z-scores, with n = the number of events. While participants intended for a specific outcome in the REG data biophoton emission was recorded from the right side of the head with a photomultiplier tube (PMT). One model of PMT was used for N = 8 participants (23 sessions), while a second model was used for N = 3 participants (4 sessions). In order to accommodate varied sampling across PMTs, as well as individual differences, all photon data was standardized independently within each session using z-scores. Prior to transformation each session was de-trended by entering PMT data into a linear regression with time as the independent variable and obtaining the residual values for subsequent standardization and analyses. Mean values and standard deviations were computed for each minute (8) of both REG and PMT data. All sessions were used as separate trials (N = 27).

Investigating Session Serial Position

Out of the N = 11 participants involved in this experiment there were N = 8 who each completed three consecutive sessions. Each session consisted of an identical number of individual events (n = 1000), and therefore unweighted Stouffer's z-scores were adequate for comparing results between sessions. Overall session z-scores were converted to directional measures with regard to operator intention (e.g., output deviated in intended direction = positive value). One-way analysis of variance (ANOVA) indicated that there were no statistically significant differences between

sessions 1, 2 or 3 ($p > .05$). The two largest individual deviations ($z > 2$), both in the intended direction, were obtained within sessions 1 and 3 (*Figure 10*).

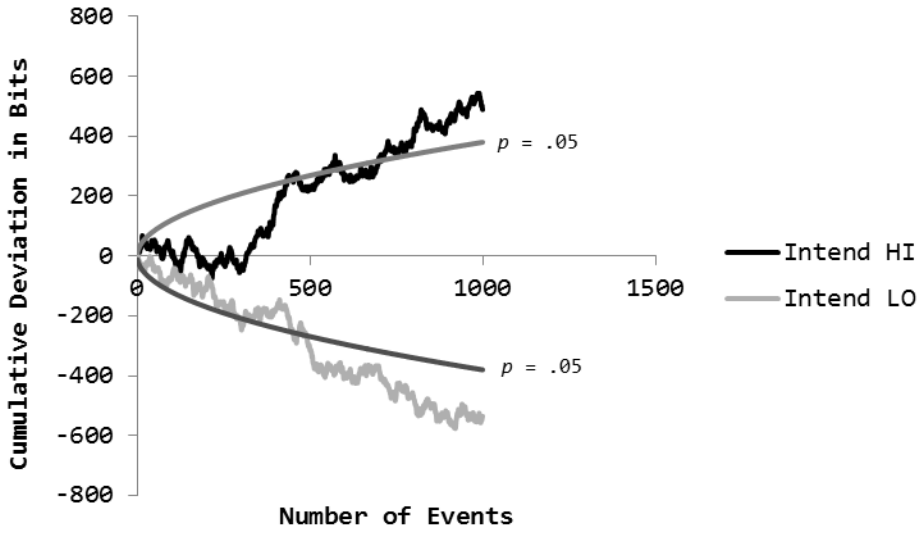

Figure 10 - Cumulative deviations for two sessions with the greatest overall deviations, both in the intended direction (actual directionality of data maintained); parabolas indicate threshold for statistical significance (p = .05, one-tailed)

Differences in Photon Emission between REG Session Scores

Data was entered into a cluster analysis which grouped trials by overall session REG score. Three clusters emerged that represented positive deviations, negative deviations, and deviations which closely approximated chance expectation results. A one-way analysis of variance (ANOVA) was then performed to determine potential differences in photon emission between REG score using three clusters (*Table 4* & *Table 5*). There was a significant difference revealed between clusters for the mean photon emission during minute 2 (*Figure 11*; $F_{(2, 26)} = 4.18$, $p = .03$, $\eta^2 = .26$). *Post-hoc* tests (Tukey) found a significant difference between clusters 1 and 3 ($p = .022$), but not clusters 1 and 2 ($p = .82$), or 2 and 3 ($p = .08$). This timeframe (2 minutes) is precisely what we

had previously found (Caswell et al., 2013) for potential gravitational, electromagnetic, and cerebral effects involved in this phenomenon. Furthermore, when data were examined using a temporal resolution of seconds (*Figure 12*), there were significant increases in PMT units associated with individual REG events at both high and low extremes of ordered deviation (F = 8.41, p = .005, η^2 = .13). The mean and standard deviations for the analog PMT units were 40 and 1.03, respectively. For a z-score increase of 0.07 the net increases in flux density would have been $3.5 \cdot 10^{-12}$ $W \cdot m^{-2}$.

Cluster	**N**	***μ* (REG)**	***sd* (REG)**
1	14	-.038	.523
2	9	1.505	.401
3	4	-1.79	.407

Table 4 - N, μ (mean) and sd (standard deviation) values of actual REG session scores for each cluster

Cluster	**N**	***μ* (PMT)**	***sd* (PMT)**
1	14	-.098	.255
2	9	-.03	.283
3	4	.329	.229

Table 5 - N, μ (mean) and sd (standard deviation) values of average (minute 2) PMT z-scores for each cluster

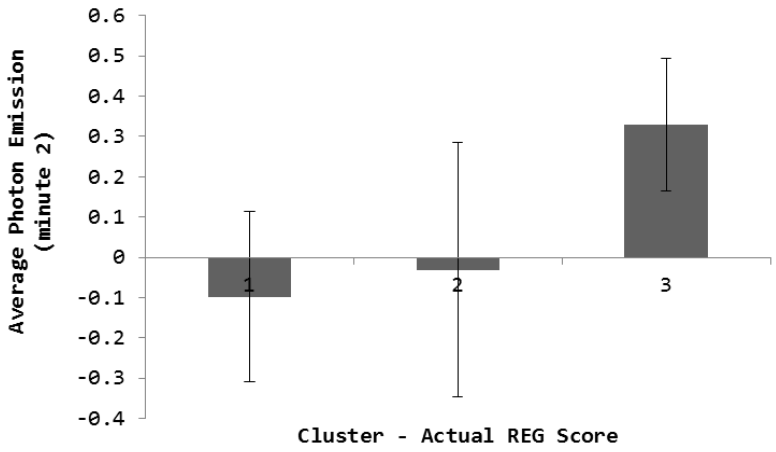

Figure 11 - Difference in average photon emission during minute 2 between actual REG session score clusters; vertical bars are standard deviations (sd)

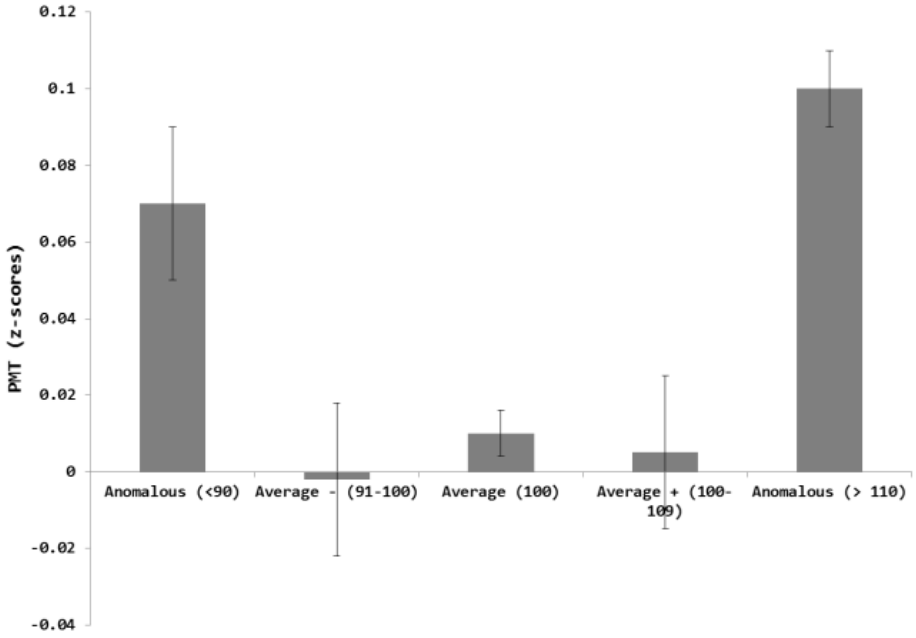

Figure 12 - Difference in standardized PMT units associated with specific ranges of REG event scores (each event = sum of 200 0, 1 bits); Anomalous (< 90), Average - (91-100), Average (100), Average + (100-109), Anomalous (> 110); vertical bars represent standard error of the mean (SEM)

Spectral Characteristics

Spectral analysis is a statistical method used in signal processing which allows examination of a random time-series with respect to the frequency domain as opposed to time. This process is used to decompose a particular signal into simpler components, and is particularly useful given that many signals or processes may be described as the summation of a number of individual frequencies. Spectral power density is obtained for a number of frequencies up to the Nyquist limit (n/2) for a time series. Spectral density itself is a measure of power within a signal after it has been decomposed into separate frequencies following Fourier transform (e.g., *Figure 13*).

In this example, there is an apparent spike in PMT spectral power density during significant REG operations compared to non-significant events which occurs at a frequency of .272 Hz (3.68 s). Although subtle, the effect was consistent within individual records. The difference in PMT spectral power density between a significant and non-significant REG session for a single participant is shown in *Figure 14*. A number of quantifiable processes associated with each spectral frequency of a given signal can be obtained through this process, including phase, amplitude, and power. We have found that z-scores of the raw data from which a spectral power density is derived will minimize the inflation effects from the absolute values of the numbers that compose the scale.

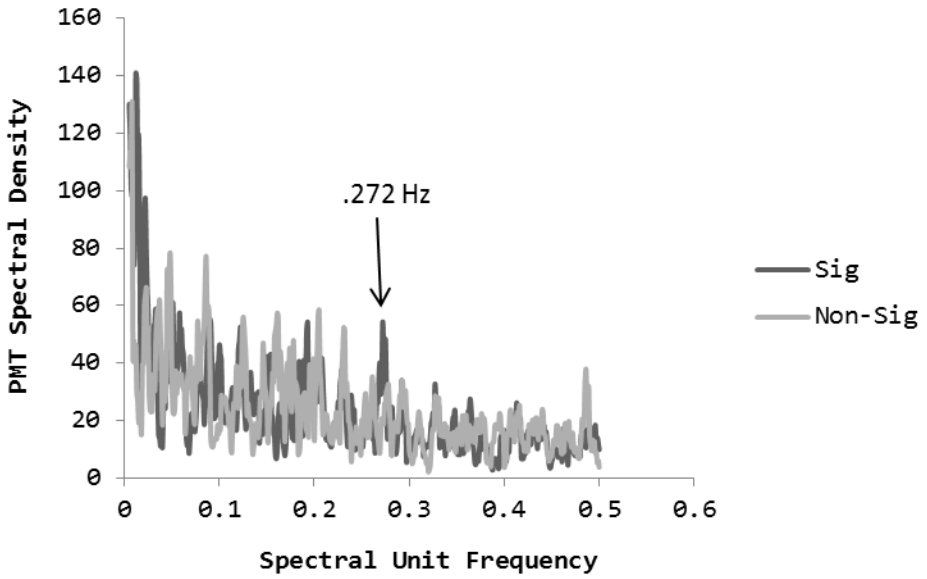

Figure 13 - Power spectrum of photon emission during significant (Sig) and non-significant (Non-Sig) REG output for a single participant using complete samples (n = 1000). The results are derived from 1 s sampling increments. This pattern was also noted in other participants during the course of the study.

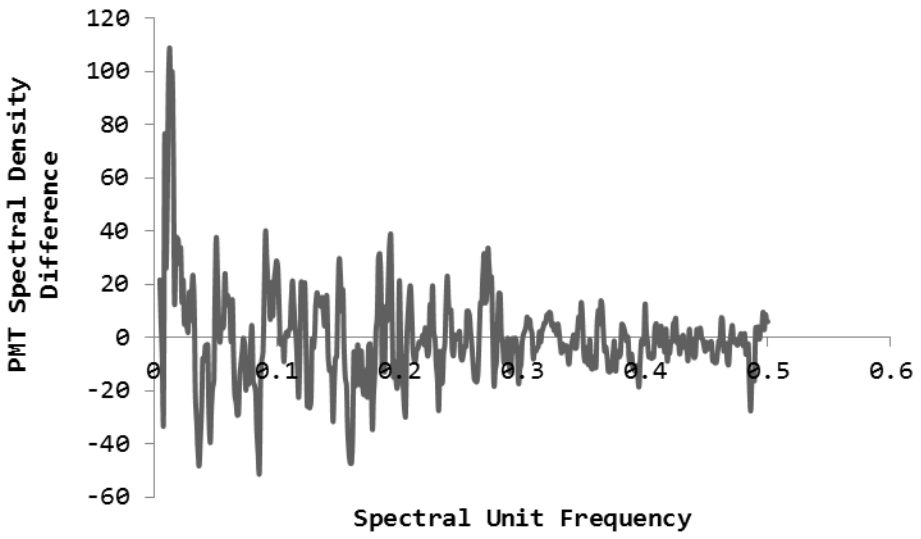

Figure 14 - Difference in PMT spectral power density between a significant and non-significant REG session for a single participant (Spectral density $_{significant}$ – Spectral density $_{non\text{-}significant}$), 1 s increments

A bivariate or cross-spectral analysis can be employed to obtain a number of statistics associated with the spectral densities of two random variables, including the amplitude of their cross-spectral densities (e.g., *Figure 15*), which is a measure of the difference between the extreme values of the variables examined. The cross-spectral coherence is also typically used. This value refers to the covariance observed between the spectral power densities of two variables within each frequency (e.g., *Figure 16*). REG and PMT data were each transformed to 10 second averages for each test session and entered into a series of separate cross-spectral analyses.

Averages of 10 seconds were employed in order to diminish any temporal "mismatching" between the devices; because both devices were manually controlled it is possible that the output of REG and PMT data could have been discrepant by ~1-2 seconds. The averaging procedure was used in order to better align the output between devices. Furthermore, this reduction in

individual data points also resulted in fewer frequency bands for subsequent analyses. This amounted to n = 50 points for REG and PMT data from each session, which subsequently resulted in 25 frequency bands. Data was transposed in order to examine relevant values of each frequency in isolation. Actual frequencies were computed by dividing 1 by the spectral unit frequency multiplied by the unit of time (e.g., spectral unit frequency of .28 = (1 /.28) · 10 s = 35.7 s). Dividing 1 by the real frequency in seconds yields a value in Hz (.28 = 1 / 35.7 = 28 mHz). For comparison this is within the range of slow electrical processes ("infraslow" potentials) within the brain (Aladjalova, 1964).

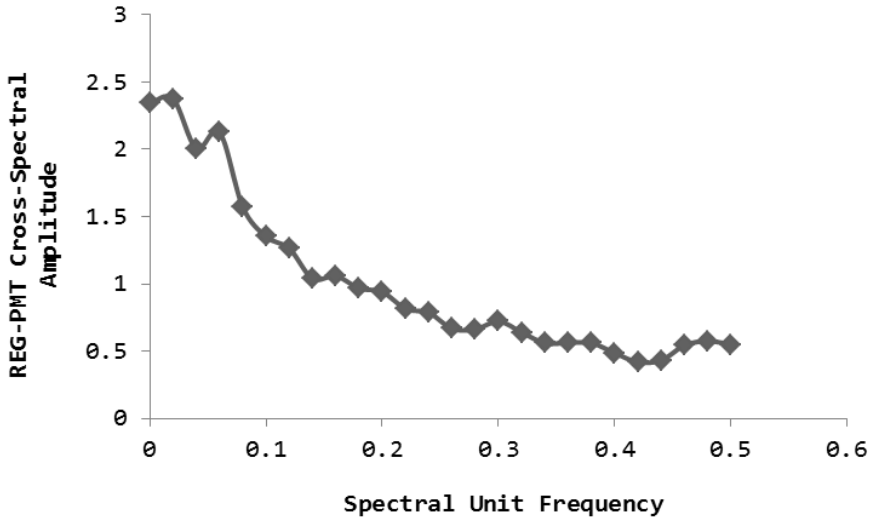

Figure 15 - Amplitude of REG and PMT cross-spectra averaged across all sessions for each frequency, 10 s averages

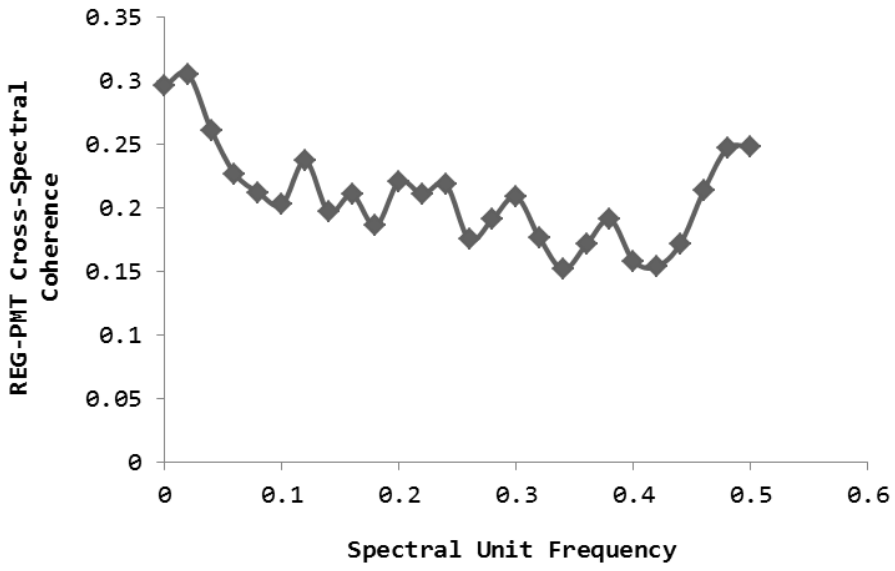

Figure 16 - Cross-spectral coherence (covariance) observed between REG and PMT spectral densities averaged across all sessions for each frequency, 10 s averages

Cross-spectral amplitude between REG output and PMT measures was entered into a number of parametric and non-parametric correlational analyses with overall REG session scores. Only those of $p < .05$ and $r \geq .5$ are reported. It was determined that the values for cross-spectral amplitude corresponding to a frequency of 28 mHz were significantly correlated with the actual value of REG session scores (*Figure 17*; $r = -.58$, $p = .002$; *rho* = -.505, $p = .007$). This suggests that the magnitude of the difference between the extreme values of REG output and PMT measures were statistically related to the final overall value obtained by the REG device. More specifically, as the photon flux density from the brain diminished the REG effect increased.

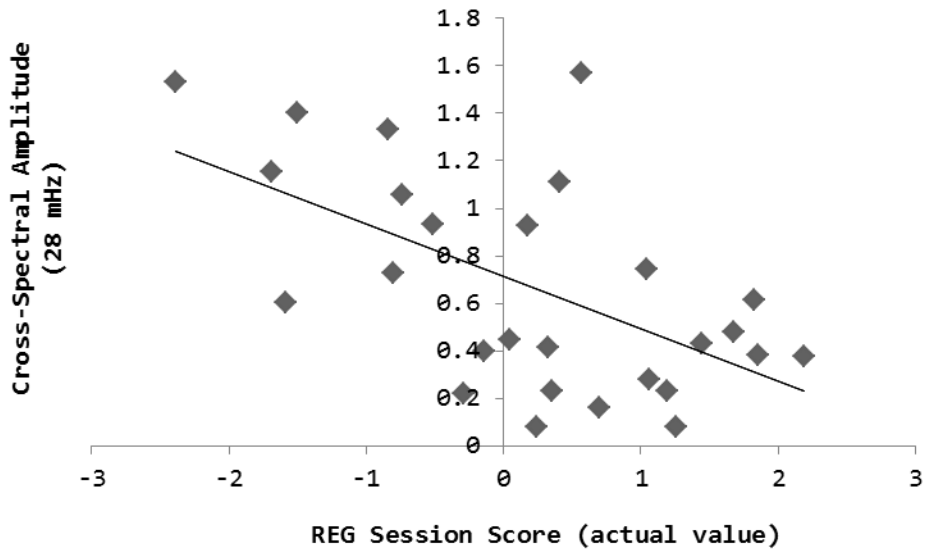

Figure 17 - Correlation between cross-spectral amplitude (28 mHz) and overall REG session score (actual value)

Signal Complexity

Entropy as applied to information theory is generally used to describe the measure of uncertainty or predictability within a random variable (Jaynes, 1957). The application of entropy to statistical prediction was originally formulated by Shannon (1948), and follows the basic equation for Shannon entropy $H(X) = -\sum x\ P(x)\log_2 P(x)$, where x = the random variable, X = the number of possible values within x, and P = the probability mass function. The entropy function in the Matlab software package was used to obtain a value similar to the Shannon entropy for a time series using an internal algorithm. A base 2 logarithm was employed in order to produce values in units of bits. Variables with a greater number of distinct values, as well as those within which these values are more evenly distributed possess greater statistical entropy. Therefore, higher values for entropy (HX) indicate greater complexity, while low values represent greater predictability within the signal.

Using the entropy function, HX values were computed for all individual REG sessions and examined for correlations with cross-spectral properties obtained in the previous analysis. Pearson and Spearman analyses revealed a significant correlation between HX values of REG data (e.g., the overall complexity) and the cross-spectral coherence corresponding to a frequency of 6 mHz (*Figure 18*; r = -.543, *rho* = -.55, p = .003). This suggests that the overall statistical complexity of REG results is related to the covariance observed between spectral power density of REG and PMT measures within the 6 mHz frequency. More specifically, as the coherence between the REG and photon emission data within this discrete band of the Earth's continuous free oscillations (Nishida et al, 2000) decreased the complexity of the information increased.

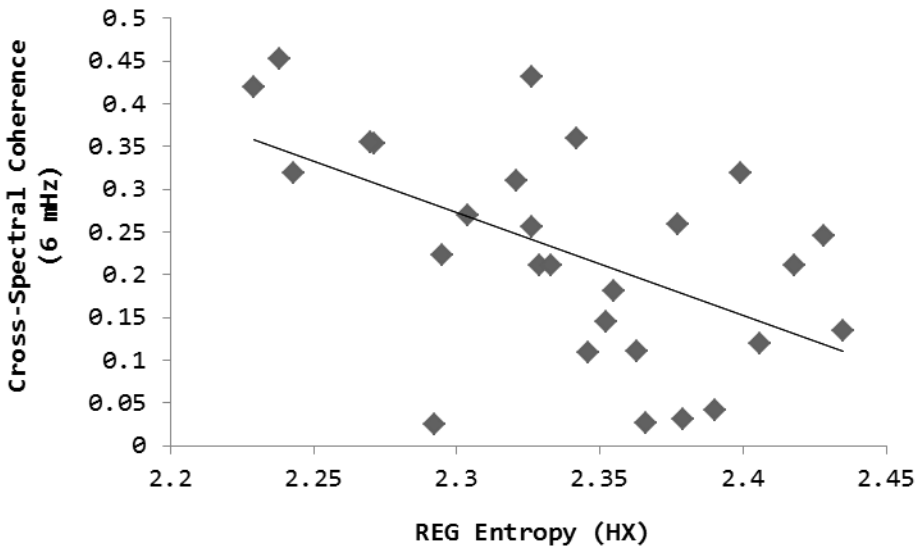

Figure 18 - Correlation between REG entropy values (HX) and cross-spectral coherence (6 mHz)

A cluster analysis was performed using HX values of each sample. Three clusters were chosen for further analysis of variance (*Table 6* & *Table 7*) based on previous results using three groups of REG z-scores. This method revealed statistically significant differences in the PMT standard deviation during minute 3 of testing (*Figure 19*; $F_{(2, 26)}$ = 4.051, p = .03, η^2 = .253). *Post-hoc*

tests (Tukey) indicated a significant difference between clusters 1 and 2 (p = .028), but not 1 and 3 (p = .197) or 2 and 3 (p = .637). This would suggest that the average departure from the mean of photon emission in minute 3 significantly differed between participant clusters based on overall complexity of REG output.

Cluster	**N**	***μ* (HX)**	***sd* (HX)**
1	11	2.342	.016
2	8	2.404	.022
3	8	2.268	.028

Table 6 - N, μ (mean) and sd (standard deviation) values of REG entropy scores for each cluster

Cluster	**N**	***μ* (PMT)**	***sd* (PMT)**
1	11	.752	.264
2	8	1.02	.14
3	8	.925	.173

Table 7 - N, μ (mean) and sd (standard deviation) values of minute 3 PMT standard deviations (z-scores) for each cluster

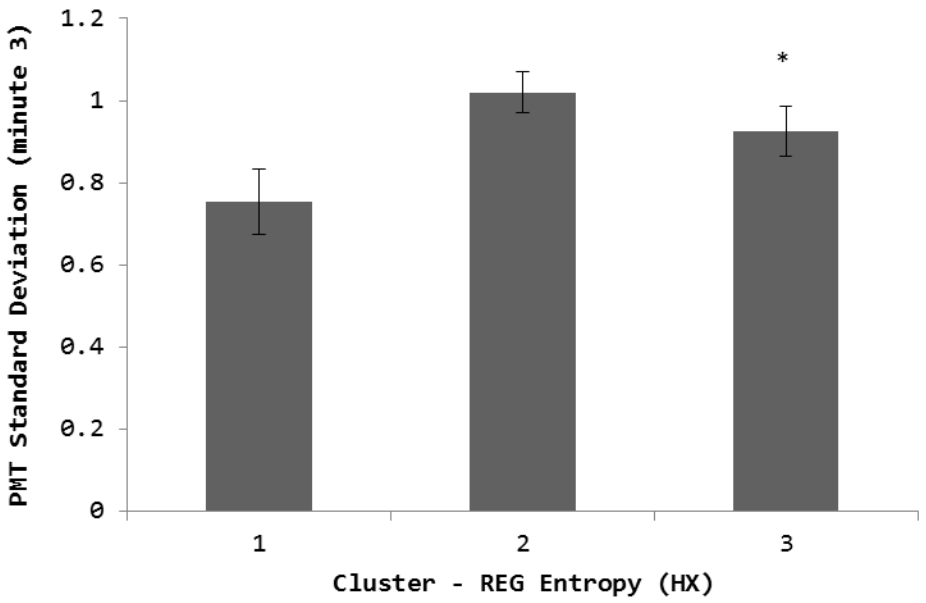

Figure 19 - Difference in PMT standard deviation during minute 3 between REG entropy clusters; vertical bars represent standard error of the mean (SEM);

** indicates a non-significant difference from cluster 1 (p > .05)*

3.5 Discussion

There has been a long history of experimentation and speculation that the physical presence of a human being or the engagement in cognitive activity near dynamic processes can affect their consequences. For decades research and casual observation have indicated that "intention" can affect objects in motion. More specifically these objects display a transient acceleration (Jahn et al, 2000). With the growing presence of electronic devices within the human environment, the contribution of the physical bases of "intention" to their operations has become evident. Although the energy levels, as Bohr anticipated, would be very small, they would be within the order of magnitude associated with the bifurcation in events where one direction or another occurs. The increment of energy associated with a single shift from one electron shell to another could result in a cascade that ultimately influences the current structure of matter at macrolevels.

The results of the present study replicated the multiple experimental observations that normal people who are proximal to random number generators can significantly affect the deviations of the intrinsic dynamic processes within these devices. In addition, we have shown that the deviations are associated with measurable, physical changes within the brains of the participants. These changes involved the emissions of biophotons from the cerebral volume as measured by photomultiplier tubes. Comparable effects were measured from both digital and analogue equipment; hence, the phenomena were not likely to be a consequence of idiosyncratic instrumentation.

The primary relationship between the increased quantitative measures (radiant flux density) of photon emissions from the right cerebrums of the participants and deviations of random number generation from "chance variation" occurred for both extremes. Periods of enhanced photon flux density from the right hemisphere were associated with both positive and negative extremes of the REG score. The observation was more reflective of a scalar process analogous to the long history of "psi hitting" and "psi missing" that has confounded paranormal researchers for decades.

The reliable increase in a specific power density associated with the extreme deviations from chance variation in REG scores could indicate the source. The increase in power density increase was ~$3.5 \cdot 10^{-12}$ $W \cdot m^{-2}$. If we assume the likely focus of the effect would involve the approximate width of an average (10 µm) neuronal soma (which is within range of p-n junctions) the power is $3.5 \cdot 10^{-22}$ $J \cdot s^{-1}$ (W) and when distributed over the duration of 6 mHz, which showed the strongest coherence between the extreme REG deviations and photon power densities, the energy is within the order of 10^{-20} J.

A neuroquantum unit of $\sim 2 \cdot 10^{-20}$ J (Persinger, 2010) is the energy associated with influence of an action potential ($\Delta v = 1.1 \cdot 10^{-1}$ V) upon a unit charge ($1.6 \cdot 10^{-19}$ A·s). The action potential is considered the primary correlate of the fundamental dynamic process within the human cerebrum that mediates intention and cognition. If thought is to be coupled to influence upon random number generation then the congruence between the energy associated with the physical substrate of intention and the photon emissions that could affect electron tunnelling within the REG devices would be expected. From a more popular perspective, the energy associated with thought and intention would be transferred into a particular range of probabilities for electron tunnelling.

The two solutions for the length of an electron, the Compton λ ($2.42 \cdot 10^{-12}$ m) and the classical ($2.1 \cdot 10^{-15}$ m) values, would require a specific value to be accommodated by the Lorentz contraction. The difference in velocities approaching *c,* the velocity of light in a vacuum, that would be required to produce this discrepancy in distance that defines the wave vs the particle properties of an electron results in a discrete quantum. This value is $\sim 10^{-20}$ J. This could be the quantity of energy associated with the frequently hypothesized "collapse of the wave" function attributed to consciousness and intention (Dotta and Persinger, 2009).

There is a second implication for this congruence. The spin energy for s=1/2 spin quantum number that reflects normal matter can be calculated as $S = \hbar \cdot 2\pi\sqrt{(s(s+1)}$, where $\hbar$ is modified Planck's constant. The solution is $1.055 \cdot 10^{-34}$ J·s multiplied by 0.866, or $0.914 \cdot 10^{-34}$ J·s. When divided by the energy associated with an average action potential, the frequency is $1.95 \cdot 10^{14}$ Hz. Assuming the velocity of light in a vacuum, the equivalent wavelength would be 1.54 µm.

This solution is quite salient. Bohr (see Lewis, 1921) showed that the quantum for removing or adding a nucleus from a neutral hydrogen molecule (consisting of two similar nuclei each

carrying a unit charge with two electrons rotating in a ring between the nuclei) could be calculated from the equation $f=1.32\cdot\acute{\omega}0\ \sqrt{(m\cdot M^{-1})}$, where m is the mass of the electron and M is the mass of the proton. With the latter ratio of 1835 and $\acute{\omega}0=1.91\cdot10^{14}$ Hz, the equivalent wavelength (λ)=1.57 μm. This width is also within the upper range of the width of a synapse or the width of a node of Ranvier within the human cerebral cortices. Although this convergence does not prove the origin from the synapse or along the axon barrel, the similarities suggest a direction for future exploration.

In fact, if we assume the spin for photons=1, then the quantum energy is $1.492\cdot10^{-34}$ J·s and the equivalent wavelength would be 2.23 μm. The difference between the derived photon spin wavelength and that associated with matter (1.54 μm) is 690 nm, which is within the visible range. For traditional models such differences could reflect phase relationships. If this explanation is accurate, then future experiments that compare photon emissions from the brains of participants through filters for this wavelength should demonstrate the greatest proportion of the effect compared to adjacent wavelengths.

The relevance of 6 mHz is more germane when the contributory role of the earth's free background oscillations is considered. They display a range between 2 and 7 mHz (Nishada et al, 2000). Specific windows, 3.7 mHz and 4.3 mHz, reveal coupling between the Earth's surface vibrations (Raleigh waves) and atmospheric acoustic oscillations. The typical amplitude for this range of oscillations is $0.5\cdot10^{-11}$ $m\cdot s^{-2}$. We (Persinger, 2012) have found that daily power of spectral density in background photon emissions from the ground in our basement laboratory within the 3 mHz range, the one that couples ground and atmospheric oscillations, displays seasonal variations similar to the acoustic oscillations described by Nishada et al (2000).

The product of the 1.5 kg of brain mass and this acceleration is $0.7 \cdot 10^{-11}$ N and when applied over the 0.1 m length of the cerebrum would be $7 \cdot 10^{-13}$ J. For 6 mHz (the coherence peak in our data), the equivalent power would be $4.2 \cdot 10^{-15}$ W. The spectral power density over the cross sectional area of the right temporal lobe ($\sim 2.5 \cdot 10^{-3}$ m^2) would be the equivalent of $\sim 1.7 \cdot 10^{-12}$ $W \cdot m^{-2}$. This quantity is within the error of measurement of the power density increase recorded during the most extreme deviations from random variation recorded by the REG.

There are several interpretations for this complex relationship. At present we are assuming that the greater coherence at ~6 mHz between the photon flux density from the right hemisphere and the deviations for the REG in conjunction with less complexity in the variation of the numbers generated "spontaneously" could reflect the effect of "intention". We are pursuing the idea that the biophotons are affecting the properties, particularly spin, within the REG devices that in term affect "random"; that is, the process exerts a biological signature of some small order. The congruence between the estimated energies that would be available to the cerebral mass from this band of the Earth's free oscillations and those measured during our experiments may be a source of variance that could explain some of the variability between experiments in various laboratories as well as seasonal or daily differences.

Increased standard deviations in the measurements for one group compared to another often reflect the introduction of another source of variance within the former. The appearance of a resonance factor within a spectrum can produce this effect. The increased variability of photon flux density from the right hemisphere during the third minute in conjunction with increased entropy (complexity) score in the REG, the opposite of the 6 mHz relationship, could explain why these processes are "self-limiting". It may be relevant that the occurrence of the greatest increased entropy during the third minute (120 to 180 s) is the equivalent of between 5.5 and 8

mHz. This range encompasses the major extent of the free background oscillations displayed by the Earth.

The photon measurements in the present study were obtained 15 cm from the skull along the right side. Assuming a radius of ~5.5 cm from the center of the brain, then the energy over this surface area of the sphere with a radius of 20.5 cm is $5.23 \cdot 10^{-1}$ m^2 · $3.5 \cdot 10^{-12}$ $W \cdot m^{-2}$ or $1.8 \cdot 10^{-12}$ $J \cdot s^{-1}$ during the extreme deviations in the REG. This assumes no directionality. However, from the cerebral surface ($3.8 \cdot 10^{-2}$ m^{-2}), assuming a reverse inverse square relation, could have been as high as 10^{-10} $J \cdot s^{-1}$. If non-locality rather than locality (some form of influence by propagation of photons to the REG 1 m away) were operating, then a comparable quantity of energy equivalence should emerge within the triggering circuitry.

There were other periodicities shared by variations in the photon flux density from the brains of the participants and the REG data. The 28 mHz peak that was apparent across all sessions is equivalent to a period of about 36 seconds, or about two oscillations per minute. This duration is within the range of short-term memory when the electrical processes associated with representation of memory and the "stream of consciousness" rapidly decline. One would expect the fundamental energies from which intention emerges to utilize the "visual scratchpad" for short-term "storage" of information. The cerebral locus is primarily within the right hemisphere, particularly the right prefrontal region.

This range of periodicities is also the defining feature of the brain's "steady potentials" or infraslow potentials. This largely forgotten legacy from Aladjalova (1964), involves transcerebral electrical variations in the order of 0.3 to 1.5 mV with periods of 7 to 8 s and periods of 0.2 to 2 min. For reference, 0.5 mV is the increment of postsynaptic change over the membrane in

response to the release of molecules from a single pre-synaptic vesicle, i.e., the miniature EPSP (excitatory postsynaptic potential). Rhythmic oscillations between 0.5 and 2 oscillations per second within amplitudes between 0.5 and 1.5 mV can occur for hours to days. They often follow periods of "stress" as well as marked memory consolidation. The role of glial cells, that constitute a syncytium of integrated connection throughout the cerebral volume, cannot be ignored. The resting membrane potential of astrocytes changes within about 4 to 6 sec following the electrical stimulation from neurons. The spectral peak for photon emission during REG outputs that deviated significantly from change compared to those that did not was ~4 s.

To our knowledge this is the first experiment to demonstrate a quantitative relationship between the deviation from random fluctuations in an electronic device and the photon emissions from cerebral function. We (Dotta et al, 2012) had previously demonstrated that "imagining" (a type of intention) compared to mundane (passive or non-intention) thinking was associated with conspicuous and reversible photon emission from the right hemisphere that was strongly correlated with left prefrontal brain activity.

The coupling between electron-photon activity within the neuronal membrane, the presumed bases for the effect, and the electrons within the REG might still be reciprocal. The time required for a photon moving at *c* to traverse a 10 nm membrane is 10^{-16} s. This is the same order of magnitude as the time required for an electron to complete one orbit in a Bohr magneton. Consequently the "information" or some feature of "state" per unit orbit could be reversibly transferred as this dynamic photon traverses the neuronal cell membrane.

3.6 References

Aladjavlova, N.A. (1964). Slow electrical processes in the brain. *Progress in Brain Research, 7*, 1-238

Amoroso, R. L. (1999). An introduction to noetic field theory: The quantization of mind. *Noetic Journal, 2*(1), 28-37.

Apel, K., & Hirt, H. (2004). Reactive oxygen species: Metabolism, oxidative stress, and signal transduction. *Annual Review of Plant Biology, 55*, 373-399.

Bókkon, I. (2005). Dreams and neuroholography: An interdisciplinary interpretation of development of homeotherm state in evolution. *Sleep & Hypnosis, 7*(2), 61-76.

Bokkon, I. (2009). Visual perception and imagery: A new molecular hypothesis. *BioSystems, 96*, 178-184.

Caswell, J. M., Collins, M. W. G., Vares, D. A. E., Juden-Kelly, L. M., & Persinger, M. A. (2013). Gravitational and experimental electromagnetic contributions to cerebral effects upon deviations from random number variations generated by electron tunneling. *International Letters of Chemistry, Physics & Astronomy, 11*, 72-85.

Dotta, B. T., Koren, S. A., & Persinger, M. A. (2013). Demonstration of entanglement of "pure" photon emissions at two locations that share specific configurations of magnetic fields: Implications for translocation of consciousness. *Journal of Consciousness Exploration &*

Research, 4(1).

Dotta, B. T., & Persinger, M. A. (2009). Dreams, time distortion, and the experience of future events: A relativistic, neuroquantal perspective. *Sleep & Hypnosis, 11*(2), 29-39.

Dotta, B. T., & Persinger, M. A. (2011). Increased photon emissions from the right but not the left hemisphere while imagining white light in the dark: The potential connection between consciousness and cerebral light. *Journal of Consciousness Exploration & Research, 2*(10), 1463-1473.

Dotta, B. T., Buckner, C. A., Cameron, D., Lafrenie, R. F., & Persinger, M. A. (2011). Biophoton emissions from cell cultures: Biochemical evidence for the plasma membrane as the primary source. *General Physiology and Biophysics, 30*(3), 301-309.

Dotta, B. T., Saroka, K. S., & Persinger, M. A. (2012). Increased photon emission from the head while imagining light in the dark is correlated with changes in electroencephalographic power: Support for Bokkon's biophoton hypothesis. *Neuroscience Letters, 513*, 151-154.

Gissurarson, L. R. (1992). The psychokinesis effect: Geomagnetic influence, age and sex differences. Journal of Scientific Exploration, 6(2), 157-165.

Gourley, P. L., Hendricks, J. K., McDonald, A. E., Copeland, R. G., Barrett, K. E., Gourley, C. R., Singh, K. K., & Naviaux, R. K. (2005). Mitochondrial correlation microscopy and

nanolaser spectroscopy: New tools for biophotonic detection of cancer in single cells. *Technology in Cancer Research & Treatment, 4*(6), 585-592.

Isojima, Y., Isoshima, T., Negai, K., Kikuchi, K., & Nakagawa, H. (1995). Ultraweak biochemiluminescence detected from rat hippocampal slices. *NeuroReport, 6*, 658-660.

Jahn, R. G., Dunne, B. J., Nelson, R. D., Dobyns, Y. H., & Bradish, G. J. (1997). Correlations of random binary sequences with pre-stated operator intention: A review of a 12-year program. *Journal of Scientific Exploration, 11*(3), 345-367.

Jahn, R., Dunne, B., Bradish, G., Dobyns, Y., Lettieri, A., Nelson, R., Mischo, J., et al. (2000). Mind/machine interaction consortium: PortREG replication experiments. *Journal of Scientific Exploration, 14*(4), 499-555.

Jaynes, E.T. (1957). Information theory and statistical mechanics. *Physics Review, 106*(4), 620-630.

Kobayashi, M., Kikuchi, D., & Okamura, H. (2009). Imaging of ultraweak spontaneous photon emission from human body displaying diurnal rhythm. *PLoS ONE, 4*(7).

Lewis, W. C. (1921). A system of physical chemistry. Vol. 3. Quantum Theory. Sir W. Ramsay and F. G. Donnan (eds). Longmans, Green Co. London.

Li, K. H., Popp, F. A., Nagl, W., & Klima, H. (1983). Indications of optical coherence in

biological systems and its possible significance. In H. Fröhlich & F. Kremer (Eds.), Coherent Excitations in Biological Systems (pp. 117-122).

Nishida, K., Kobayashi, N., & Fukao, Y. (2000). Resonant oscillations between the solid earth and the atmosphere. *Science, 287*, 2244-2246.

Persinger, M. A. (2010). 10^{-20} J as a neuromolecular quantum in medicinal chemistry: An alternative approach to myriad molecular pathways. *Current Medicinal Chemistry, 17*, 3094-3098.

Persinger, M. A., & Lavallee, C. F. (2010). Theoretical and experimental evidence of macroscopic entanglement between human brain activity and photon emissions: Implications for quantum consciousness and future applications. *Journal of Consciousness Exploration & Research, 1*(7), 785-807.

Persinger, M. A., & Saroka, K. S. (2012). Protracted parahippocampal activity associated with Sean Harribance. *International Journal of Yoga, 5*, 145-150.

Persinger, M. A., Dotta, B. T., & Saroka, K. S. (2013). Bright light transmits through the brain: Measurement of photon emissions and frequency-dependent modulation of spectral electroencephalographic power. *World Journal of Neuroscience, 3*, 10-16.

Radin, D. I., & Nelson, R. D. (2003). Meta-analysis of mind-matter interaction experiments:

1959-2000. In Healing, Intention, and Energy Medicine (pp. 39-48). London: Harcourt Health Sciences.

Shannon, C. E. A mathematical theory of communication. *Bell Systems Technical Journal, 27,* 379-423, 623-656.

Sun, Y., Wang, C., & Dai, J. (2010). Biophotons as neural communication signals demonstrated in situ biophoton autography. *Photochemical & Photobiological Sciences, 9*(3), 315-322.

Tu, L. C., Luo, J., & Gillies, G. T. (2005). The mass of the photon. *Reports on Progress in Physics, 68*(1).

Chapter 4 – Simulated Effects of Sudden Increases in Electromagnetic Activity on Deviations in Random Electron Tunnelling Behaviour Associated with Cognitive Intention

Published in *Journal of Consciousness Exploration & Research*

4.1 Abstract

Reliable evidence from the Jahn-Dunne studies conducted over several decades indicated that human proximity can affect the dynamics of certain processes that strongly depend upon "random" processes. Random Event Generators (REG) operate through "random" electron tunneling through spaces that are within the same order of magnitude as synapses. If the mechanisms by which these human-machine interactions occur involve electromagnetic processes, then application of specific temporally patterned magnetic fields to the human volume should affect the strength of the deviation from "random" variations. Whole-body exposure to ~400 nT, complex-patterned magnetic fields based upon 3 ms point durations reversed the effects of normal "intention" upon the operation of REGs. The energies generated within the cerebral volume by that field if emitted as irradiative power were within the range of the mass equivalent of an electron at the level of p-n junction of the semiconductor. These results support the hypothesis that "intention" can be affected experimentally and the energies within the vicinity of the actual dynamic space (~1 μm^2) of the p-n junction of the REG match the extended power of the magnetic energy contained within the cerebrum.

4.2 Introduction

As a species, our dependence on technology can no longer be understated. This reliance can cause the machine of society to grind to a halt as a result of power failures or other electrical disturbances. The study of space weather, particularly the geomagnetic field, has elucidated one mechanism by which both electrical and biological systems are affected on Earth by even small environmental electromagnetic variations. The convergence of a number of scientific disciplines, including geophysics, biology, environmental science, and engineering, have led to a number of discoveries regarding the effects of space weather on terrestrial systems, from human physiology and health to navigation and communications systems.

The same progression of discovery due to the integration of previously disparate fields of study has also proven fortuitous for the study of consciousness, parapsychology, and physical anomalies research. By extending the focus of investigation in these areas from theoretical models of psychology and philosophy to the search for biophysical relationships, mechanistic explanations based on physical principles have begun to emerge. These areas have recently flourished with new models involving physical quantification and interdisciplinary investigation bolstered by new technologies. This increasingly transdisciplinary engagement has encouraged the search for physical relationships which might reveal potential mechanisms by which anomalous or non-local interactions occur in association with psychobiological systems.

The inner core of the Earth, composed of iron-alloy and other lighter elements, rotates within the liquid iron outer core, and this rotation produces a magnetic field through a dynamo effect. This magnetic field extends outwards around the planet to reach solar winds and form the geomagnetic field. It may behave as a filter or transducer of extraterrestrial stimuli such as cosmic rays or protons. Geomagnetic activity and subsequent conditions within the planetary atmosphere affect

terrestrial biology, including a number of species of birds (Mouritsen et al., 2004), fish (Klimley, 1993), and terrestrial mammals (Kimchi et al., 2004). In the context of human studies, effects of geomagnetic activity have been identified for cardiovascular functioning (Dimitrova et al., 2009), bioelectrical activity in the brain (Mulligan et al., 2010), and emotional state (Babayev & Allahverdiyeva, 2007). Geomagnetic storms typically occur in relation to solar activity including variations in solar wind velocity (Snyder et al., 1963), dynamic pressure changes (Persinger, 2009), and coronal mass ejections (Richardson et al., 2001).

It has also been demonstrated that the random output of an external physical system is correlated with the conscious "intention" of a human operator (e.g., Jahn et al., 1997; Radin & Nelson, 2003); decades of research have consistently documented the apparent phenomenon of consciousness-correlated collapse (3C), which suggests that the behaviour of non-deterministic systems may be affected by human consciousness. Given that the relationship between brain activity and variations in the Earth's geomagnetic field is well documented, and there have been potential associations revealed between the 3C phenomenon and cerebral effects (Giroldini, 1991; Caswell et al., 2013; Caswell et al., 2014), it is hypothesized that any potential temporal contiguity between the electromagnetic interactions associated with cognitive intention may be reflected in a relationship between a measure of 3C performance and environmental variations in electromagnetic activity.

The state of geomagnetic activity in particular has previously been studied in the specific context of anomalous physical phenomena associated with consciousness. For example, passive anomalous processes, such as remote viewing, were shown to exhibit a negative correlation between task accuracy and geomagnetic activity (GMA) (Makarec & Persinger, 1987). The most powerful effects for both spontaneous and experimental forms of accessing information at a

distance through non-conventional means occur when the global variations are within the 5 to 8 nT range. Slightly higher intensities are more likely to occur during precognitive dreams (Krippner & Persinger, 1996; Dotta & Persinger, 2009). Alterations of the local geomagnetic field occur when an exceptional individual engaged in intuitive states similar to remote viewing phenomena (Hunter et al., 2010; Persinger et al., 2013). The magnetic energy associated with decrease in geomagnetic intensity within the volume surrounding the person's cerebrum was the same order of magnitude as the increased photon power density recorded within this boundary.

Although studies have previously investigated the relationship between GMA and active anomalous physical processes, such as consciousness-correlated collapse (3C) of external random systems, these tend to be relatively restricted in scope and subsequent analyses have failed to determine a potential effect of geomagnetism on external effects of conscious intention (e.g., Gissurarson, 1992; Radin, 1993). For example, it has been successfully determined that recurrent-spontaneous effects of consciousness on the local environment at the macro-scale tend to occur during periods of increased GMA (Gearhart & Persinger, 1986; Roll et al., 2012). Although a number of these experiences may be subject to relative interpretation, there is contemporary quantitative evidence suggesting the potential for thought to affect matter (Persinger et al., 2008), as well as the relevant quantitative convergence which supports a link between micro- and macro-quantum processes associated with cortical activity (Persinger, 2012).

That even small perturbations of ~20-40 nT have been shown to affect human neurophysiology (Saroka et al., 2014) suggests that weak intensity electromagnetic fields (EMF) have the potential capacity to disrupt normal functioning of cognitive processes. While we have previously demonstrated that transcerebral application of a specific physiologically-patterned EMF shows a potential to increase the capacity to engage external effects of consciousness (Caswell et al.,

2013), we hypothesized that full-body exposure to a relatively 'noisy' signal not patterned after any specific physiological process would potentially disrupt the occurrence of the 3C phenomenon. We designed an experiment in which sudden increases in patterned, weak-intensity electromagnetic activity were simulated using a variation on protocols employed in our laboratory for previous experiments (Mulligan & Persinger, 2012; Murugan et al., 2013). Participants attempted to influence the output of a random event generator (REG) device during both control and EMF conditions.

4.3 Methods

Subjects

Participant age ranged from 22-30 years for N = 8 (N = 3 females, N = 5 males). All were recruited from Laurentian University campus.

Equipment

Simulated EMF increases were produced using two large custom-built rectangular coils (1.15 x 1.15 m) placed 1 m apart on either side of the participant seating area, ~36 cm away from their bodies. The random event generator (REG) device was also placed within the area of the coils ~25 cm in front of the participant on his or her right side. The magnetic field was produced by a DOS PC system using custom software designed by Professor Stan Koren. The original waveform designed to imitate increased GMA consists of 5071 individual points. To simulate a sudden impulse the point durations were designed to be 69 ms. However, during the following experiment the same field pattern was presented with point durations of 3 msec each, and a 3 msec delay between each point, a significantly faster duration and presentation compared to simulation of natural geomagnetic increases (Mulligan & Persinger, 2012). The 3 ms point

durations were selected on the bases of the enhanced physiological effectiveness. The value of each point in the waveform ranged between 0-256 and was converted to a voltage equivalent (-5 to +5 V) using a custom-built digital-to-analogue converter device which delivered the associated current through the coils. The overall intensity of the subsequent electromagnetic field produced by the system had a peak intensity of ~400 to 500 nT as measured by power meters. The actual waveform image is displayed in *Figure 20*.

Figure 20 - Waveform image of GMA patterned field repeated over the course of each exposure; the y-axis is waveform point value (equivalent to voltage value between -5 to +5 V), the x-axis is time

Actual geomagnetic activity before, during, and after testing was examined using estimated 3-hour Kp-indices obtained from the Solen database (www.solen.info/solar/).

Random data was produced using a Psyleron REG-1 random event generator (*Figure 7*; www.psyleron.com). The device produced a random output which was generated by electron tunneling effects within two field effect transistors. The varying voltage levels which result from this process were converted into digital data through a gated sampling procedure which allowed

for regularly spaced bit sequences. The output of both transistors was internally compared through an alternating (0, 1) XOR masking process in order to reduce any potential influence of physical artifacts or other external environmental variables. The device itself was further protected from static electromagnetic factors by an aluminum outer shielding and a Permalloy mu-metal inner shield. Furthermore, the device was rigorously calibrated prior to shipment in order to ensure output conformed to statistical expectations.

The random event generator (REG) was also tested in control experiments within our laboratory to confirm these expectations. The resulting data stream is collected through USB-port using Psyleron FieldREG and Reflector software packages on a laptop computer. Individual events were produced at a rate of either 4/sec for larger samples, or 1/sec for shorter samples in order to accommodate participant availability (~5 and 2 minutes per condition respectively). However, internal consistency was maintained across all conditions; for a given participant, each condition was run using the same event rates and test time. There were no significant differences noted between event rates in this experiment or others ($p > .05$). Values for each event refer to the number of 1's out of 200 bits with binary probabilities, represented by a value of 0-200. The theoretical (chance) mean for each event is 100 with a standard deviation of $\sqrt{50}$.

Measures of entropy (HX) were obtained using Matlab 2011a software. All other statistical procedures were conducted using SPSS software v.17.

Procedure

Each participant was seated in a comfortable chair located within an acoustic chamber which was also a Faraday cage. The large coils were placed on either side of the participant at a distance of ~36 cm (*Figure 21*). The REG device, also within the coils, was placed ~25 cm from the right

side of the participant (*Figure 22*). Each individual was asked to intend for a specific outcome in the REG data (e.g., *Figure 8*). All participants completed four conditions, presented in a rotating A-B-C-D order (e.g., presentation order for the first participant was A-B-C-D, second participant was B-C-D-A, etc.). The REG continuously collected data throughout the experiment. The first condition consisted of a relaxed state with no current from the coils (Baseline-No Field). The second condition maintained the relaxation state while the EMF was applied (Baseline-Field). The third consisted of the participant intending on the REG output with the coils again producing no current (Intention-No Field), while the final condition involved another intention task during simulation of EMF increase (Intention-Field).

Figure 21 - Custom-built coils placed 1 m apart on either side of participant

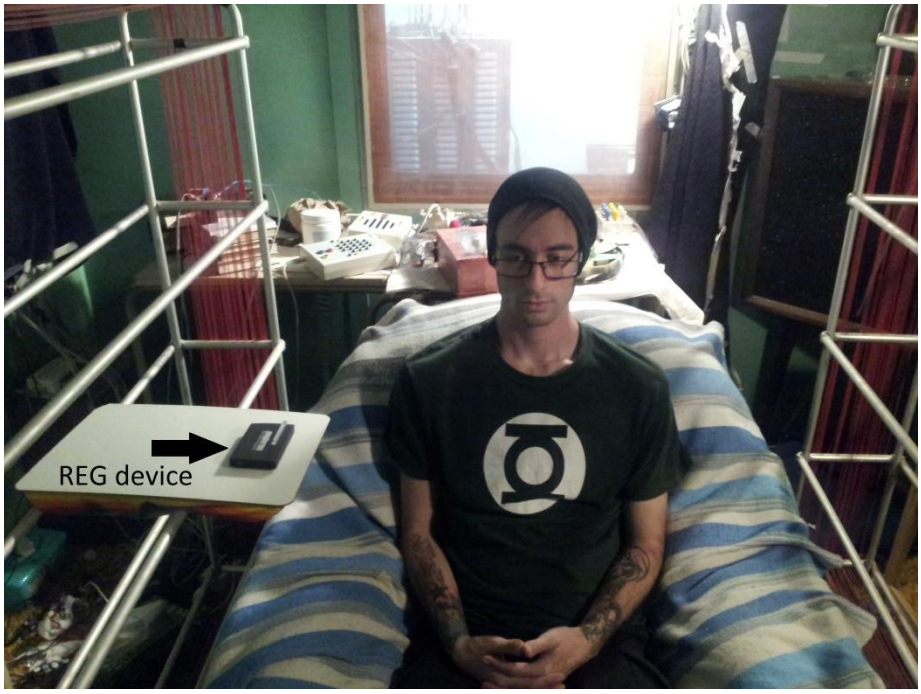

Figure 22 - EMF coils on either side of participant, REG device placed on right side within field

4.4 Results

Data Transformation

REG data was converted where operator intention was present so that the data were maintained, but the overall deviation was reversed in order to represent the direction of intention. If the participant intended for the data to deviate negatively and the overall score was positive, then the session was left unaltered in order to represent a deviation against intention (negative value). However, if the intent was to obtain a negative value in this case, then the overall REG event data would be converted to the polar opposite values in order to represent a deviation in the intended direction (positive value). The reverse would be true of participants who intended for a positive deviation. Where necessary, data reversal was accomplished by obtaining the absolute deviation of each event (x-100) and multiplying the product by -1 before re-adding 100 (e.g., 105 = 105-

100 = 5, 5 · -1 = -5, -5+100 = 95). Following relevant transformation, event data were standardized according to 0.5 chance expectations ([x-100] / √50).

Simulated Electromagnetic Increases and Operator Performance

In order to account for varied event samples, z-scores for each condition were obtained (*Table 8*) by computing the deviation from the chance value mean ($\delta\mu = \mu_{\text{event scores}} - 100$), as well as the measurement uncertainty associated with $\delta\mu$ ($\sigma\mu = \sigma / \sqrt{N}$, where $\sigma = \sqrt{50}$). Dividing these values resulted in a combined z-score for each condition used to obtain subsequent probabilities ($z_c = \delta\mu / \sigma\mu$). It was determined that none of the conditions presented with statistically significant overall deviations ($p > .05$), with the possible exception of the Intention-No Field condition, which was marginally significant given one-tailed probabilities ($z_c = 1.84$, $p = .033$). However, the Baseline-Field condition revealed somewhat suggestive results, approaching statistical significance ($z_c = -1.755$, $p = .08$), particularly given the two-tailed probability typically assigned to REG experiments where no specifically intended outcome is present. Furthermore, the Intention-Field condition showed low numbers of overall deviations in the direction intended by the operator (~17%; *Figure 23*), particularly compared to previous experiments where this ratio tended towards ~50-90% or greater. Similar values were computed for all relevant condition pairings (*Table 9*) in order to determine which conditions were significantly different from one another. Combined z-scores indicated the only difference which was marginally significant was between Intention-No Field and Intention-Field conditions ($z_c = 1.827$, $p = .034$), suggesting that sudden increases in EMF may inhibit initiation of a non-local 3C interaction. Furthermore, increased EMF may actually distort the effects of 3C by encouraging deviations opposite to those intended.

Parameter	BL (No Field)	BL (Field)	Int (No Field)	Int (Field)
N	5565	5669	5657	5641
$\boldsymbol{\mu}$	100.043	99.835	100.173	99.93
sd	6.951	7.109	7.148	7.161
$\boldsymbol{\sigma_{sd}}$	.067	.066	.066	.067
$\boldsymbol{\delta_{\mu}}$	.043	-.165	.173	-.07
$\boldsymbol{\sigma_{\mu}}$	.095	.094	.094	.094
$\boldsymbol{z_c}$	.453	-1.755	1.84	-.745
p	.65 **	.08 **	.033 *	.228 *
%ID	.75 †	.125 †	.5	.167

Table 8 – Detailed REG results for overall conditions (Baseline-No Field, Baseline-Field, Intention-No Field, Intention-Field, data converted to directional measures (e.g., accounting for intended direction of deviations)

Parameter Key:

N: Number of events (200 bits/event)

$\boldsymbol{\mu}$: Mean event score (0-200)

sd: Standard deviation of REG event scores

$\boldsymbol{\sigma_{sd}}$: Measurement uncertainty in value of sd; $\sigma_{sd} = \sigma / \sqrt{2N}$, where $\sigma = \sqrt{50}$

$\boldsymbol{\delta_{\mu}}$: Absolute deviation from theoretical chance expectations (μ-100)

$\boldsymbol{\sigma_{\mu}}$: Measurement uncertainty in value of δ_{μ}; $\sigma_{\mu} = \sigma / \sqrt{N}$, where $\sigma = \sqrt{50}$

$\boldsymbol{z_c}$: Overall condition z-score adjusted for measurement uncertainty; $z_c = \delta_{\mu} / \sigma_{\mu}$

p: Probability of z_c * & **

%ID: Proportion of sessions with deviation in the intended direction; *%ID* = $Ns_{\text{with intention}}$ / Ns, where Ns = number of test sessions †

†For directionality of baseline sessions, positive values are considered to be with intention.

*One-tailed probability (e.g., intention involved).

**Two-tailed probability (e.g., no intention).

Parameter	Int (No Field)-BL	Int (Field)-BL	Int No Field-Field
N	11222	11310	11298
$\boldsymbol{\delta_\mu}$	.13	.095	.243
$\boldsymbol{\sigma_\mu}$	.134	.133	.133
$\boldsymbol{z_c}$	.97	.714	1.827
p	.166 *	.238 *	.034 *****

Table 9 - Detailed REG results comparing overall Intention (Int) conditions with respective Baseline (BL) conditions and each other, data converted to directional measures (e.g., accounting for intended direction of deviations)

Parameter Key:

N: Combined number of events (200 bits/event)

$\boldsymbol{\delta_\mu}$: Absolute deviation; e.g., $= \mu_{\text{intention}} - \mu_{\text{baseline}}$

$\boldsymbol{\sigma_\mu}$: Measurement uncertainty in δ_μ; e.g., $\sigma \cdot \sqrt{([1 / N_{\text{intention}}] + [1 / N_{\text{baseline}}])}$, where $\sigma = \sqrt{50}$

$\boldsymbol{z_c}$: z-score of overall difference adjusted for measurement uncertainty; $z_c = \delta_\mu / \sigma_\mu$

p: Probability of z_c (one-tailed)

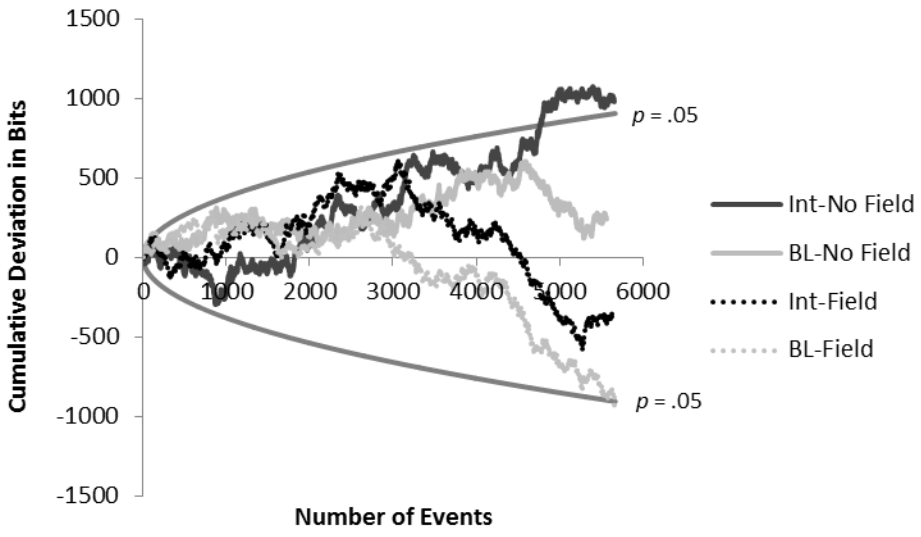

Figure 23 - Cumulative deviations from the mean for REG data combined from each condition (Intention-No Field, Baseline-No Field, Intention-Field, Baseline-Field); parabolas indicate threshold for statistical significance (p = .05, one-tailed)

Although the traditional method for presenting deviations in REG experiments have been to cumulate the deviations over successive subjects (*Figure 23*), this approach does not reveal the actual change in time. To reveal this effect, the mean variations in bits per 10 s increment were completed for the subjects in the four conditions as a function of 10 s increments. The means and standard errors are shown in *Figure 24*. Two way analysis of variance with one between (treatment) and one within (10 s increments) revealed statistically significant interactions between the four treatments and the temporal increments ($F_{(3, 31)} = 4.333$, $p = .013$, $\eta^2 = .317$). *Post-hoc* analyses indicated that the major significant effect was due to the significant difference between the group intending while the field was being presented compared to the period of no intention with field presentation ($p = .008$) during the second increment (10 to 20 s) after the intention began. In other words, intending during the presence of the magnetic field resulted in

numbers of REG events comparable to periods of no intention. This could be interpreted as this field pattern "cancelled" or "nullified" the effect of intention upon the random process.

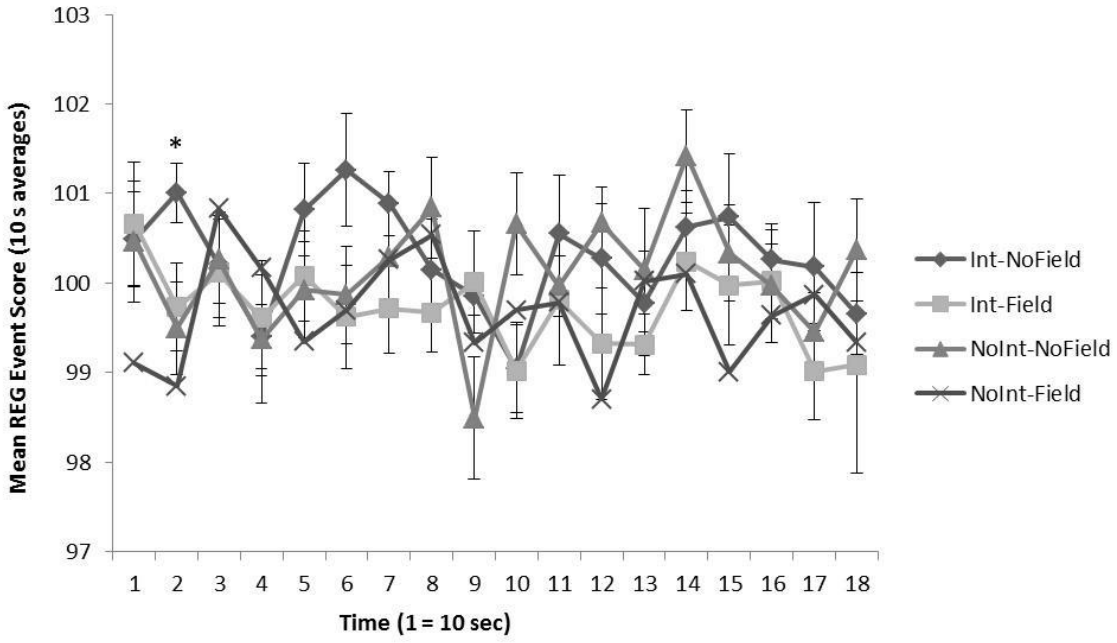

*Figure 24 - Averaged REG event scores for 10 s increments within each condition; * significant difference between Intention-No Field and Intention-Field conditions (Time 2)*

Electromagnetic Field Increases and REG Complexity

Measures of statistical entropy (HX) were computed for REG data using Matlab software. The measure of entropy computed by this method is similar to Shannon entropy of a random variable (Shannon, 1948), $H(X) = -\sum x\ P(x)\log_2 P(x)$, where x = the random variable, X = the number of possible values within x, and P = the probability mass function. Entropy values (HX) represent the level of uncertainty within the data, where higher values indicate greater complexity and less predictability. Signals with greater complexity possess a greater number of distinct values, and these values are more evenly distributed.

A one-way ANOVA was used to demonstrate a statistically significant difference in REG complexity between conditions (*Figure 25*; $F_{(3, 31)} = 5.308$, $p = .005$, $\eta^2 = .362$). *Post-hoc* tests (Tukey) revealed a difference closely approaching statistical significance between Baseline-No Field and Baseline-Field conditions ($p = .05$). Similar results were also obtained for the difference between Intention-No Field and Intention-Field conditions ($p = .05$). However, a significant difference was much more apparent for that observed between Baseline-No Field and Intention-Field conditions ($p = .009$). These results might suggest that sudden electromagnetic increases may tend to decrease the overall complexity of subsequent REG output, regardless of any apparent 3C interaction.

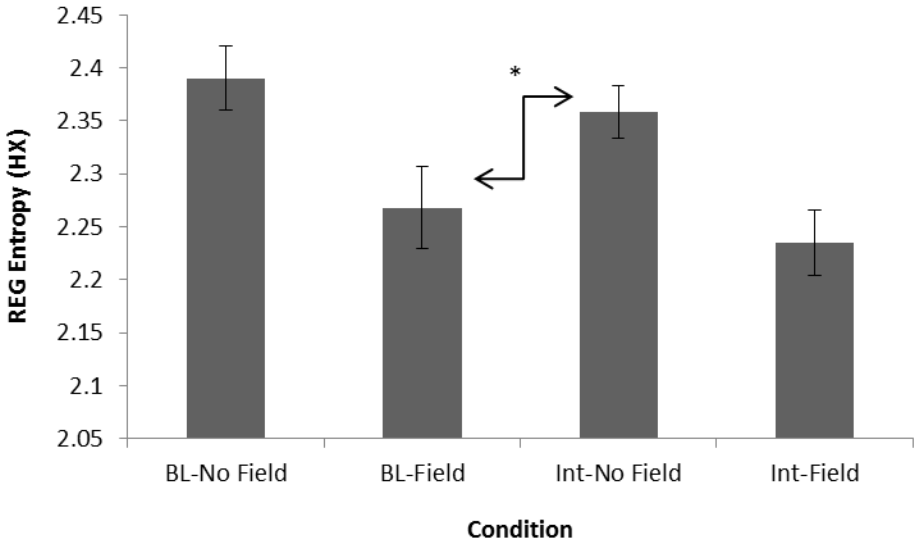

*Figure 25 - Mean REG entropy (HX) for each condition (Baseline-No Field, Baseline-Field, Intention-No Field, Intention-Field); vertical bars represent SEM; * indicates difference is non-significant (p > .05)*

Controlling for Actual Geomagnetic Activity

In order to determine if any potential interaction was present between the use of simulated EMF increases and actual GMA, estimated K_p-indices were obtained for the two 3-hour periods prior to each test session, as well as the K_p-index during testing. A series of ANCOVAs were performed to investigate any potential differences in both REG z-score (Stouffer's method = $\sum z / \sqrt{n}$) and REG entropy (HX) between conditions while controlling for the effects of the actual geomagnetic field. Statistically significant differences between conditions were observed for both REG variables (HX and overall z-score) when covarying for all K_p values (*Figure 26*; $p < .05$). Furthermore, the effect sizes remained within the same range as that found in the original analysis (η^2s = ~36%).

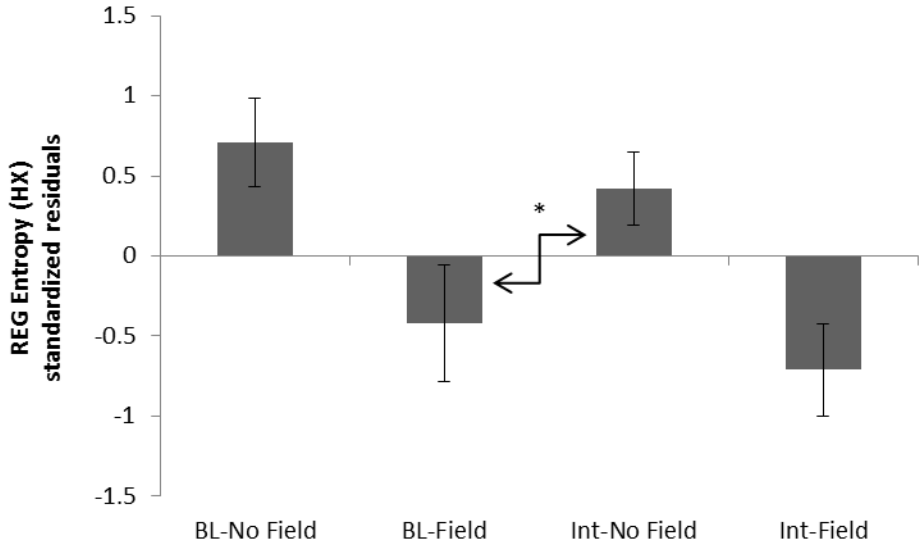

*Figure 26 - Mean REG entropy (HX) residuals (covarying for Kp-index) for each condition (Baseline-No Field, Baseline-Field, Intention-No Field, Intention-Field); vertical bars represent SEM; * indicates difference is non-significant (p > .05)*

4.5 Discussion

The results of these experiments suggest that random variations produced by electron tunneling through commercial devices (Random Event Generators) can be affected by intention. The traditional critique of these reliable although weak effects is that simply the proximity of the human mass, associated within the order of 100 $W \cdot m^{-2}$ of power output, might be mediating these subtle effects. In the present experiments (*Figure 23*) intention was associated with a significant deviation from "random variation". However application of this patterned magnetic field to the whole body cancelled this effect and evoked changes in the opposite direction. Without intention, that is when the person was still sitting in the same place in order to control for body mass (presence) effects and not intending, the random variations during both the presence and absence of the field was remarkably similar.

"Cancellation" or "reversal" of effects from a competitive agonist in neuropharmacology is well known. Usually this is associated with the remarkably similar molecular structure of the competitive structure with the natural agonist. Mach and Persinger (2009) reported similar effects following whole body exposure of rats to a pulsed magnetic field. It was the same temporal structure that when applied as electric currents to hippocampal slices produced Long Term Potentiation (LTP) which is the electromagnetic-chemical substrate for the representation of experience (memory) within the mammalian brain. Mach and Persinger (2009) found that the LTP pattern presented as a magnetic field to the animal before periods of repeated training in a spatial memory task markedly inhibited the learning. The same pattern presented after the hourly learning trials did not affect learning. The powerful effect from these weak (1 μT, 1000 nT) magnetic fields applied to the whole body, were comparable to that of complete saturation of the hippocampal fields by direct current induction.

In the present study the "reversal" of the intention effect which is clearly seen in Figure 6 occurred when the subjects were exposed to 400 to 500 nT (peak) intensity magnetic fields generated through a series of 3 ms point durations. Because simply the presence of the person without intention did not affect the random variations nor did the application of the magnetic fields significantly affect the changes, we assumed that cerebral processes were the mediating factor. The amount of energy from the applied field within the human cerebrum can be calculated by $E=[B^2\cdot(2\mu)^{-1}] \cdot m^3$, where B is the field strength, μ is magnetic permeability and m is the volume. Assume a volume of the cerebral cortices to be ~$0.57\ 10^{-3}\ m^3$ (570 cc) the energy would be $0.5\cdot10^{-11}$ J. If the intrinsic frequency associated with the repeated pattern (~16 s) or $6.3\cdot10^{-2}$ Hz is considered the power is $3.2\cdot10^{-13}$ J per s.

For comparison the energy-mass equivalence of an electron is $9.1\cdot10^{-31}$ kg $\cdot 9\cdot10^{16}\ m^2s^{-2}$ or $0.8\cdot10^{-13}$ J. These two quantities of energy are within the same order of magnitude and would converge when the lower end of the applied magnetic field strengths was involved. Although the concept that magnetic energy within a cerebral volume from an applied field could be converted to and equivalent mass may not be conventional, there are theoretical arguments. First one of the assumptions of the Casimir effect is that virtual particles within the Zero Point Potential Vacuum can be converted to actual particles by electromagnetic fields with changing boundaries. The spatial variations in our time-varying magnetic fields could meet this criterion.

In addition, as calculated by Persinger et al (2008) the discrepancy in velocity to produce the differential width of a classical electron (~10^{-15} m) and that calculated as the Compton wavelength based upon energy (~10^{-12} m) would also produce a differential energy-equivalence for an electron mass moving at these two velocities. The discrepancy is 10^{-20} J which is the amount of energy associated with a single action potential. Stated alternatively, the "collapse" of

the wave to produce a particle would be associated with an increment of energy associated with the act of thinking. Hence there is both a theoretical basis and quantitative convergence to support the possibility that magnetic energy within cerebral mass could result in the "formation" of an electron or at least its virtual manifestation for a brief period.

At the distance of the REG unit, about 25 cm or 30 cm from the center of the cerebrum, the area of the sphere produced by this radius is ~1.1 m^2. Hence the power density from the energy induced by the applied magnetic field in the cerebral volume if radiated equally in all directions would be ~$3 \cdot 10^{-13}$ $W \cdot m^{-2}$. Assuming the width of the p-n junction was similar to other semiconductor devices, or 10^{-12} m^2, the energy per second would be $3 \cdot 10^{-25}$ J. Although possibly spurious we suggest that the resulting frequency, obtained by dividing by Planck's constant of $6.626 \cdot 10^{-34}$ J·s, which is within range of the neutral hydrogen line (1.42 GHz, 21.1 cm) could be relevant to the phenomena. One could argue that access to this line, given its prominence throughout the known universe, allows access to the most intrinsic properties of the entire universe within a specific location.

The origin of the neutral hydrogen line becomes relevant to the quantities we measured. According to quantum interpretations, when the spins of the proton and electron are in the same direction the magnetic interactions exhibit more energy than if the two particles are spinning in opposite directions. The transition between these two states is associated with the hydrogen line. Although the transition is infrequent, that is only about 10^{-15} per s for one atom or a transition once every 10 million years, the large numbers of this elementary pair (a proton and electron) minimizes this constraint. For example, assuming a brain mass of 1.5 kg and the mass of a proton, there would be ~10^{27} proton equivalents within the human cerebrum. Because of the

approaching neutrality of this mass, there would be a comparable number of electrons but these masses would be, in comparison, negligible.

This would allow 10^{12} of those "hypothetical pairs" to generate the transition energy per second. Given the quantum energy of 1.42 GHz (multiplied by Planck's constant) is $9.41 \cdot 10^{-25}$ J, this number of shifts per second within the brain volume would result in available energy of $\sim 10^{-12}$ J per s or 10^{-12} W. With a total cortical surface area in the order of 10^{-1} m^2 the approximate power density would be $\sim 10^{-11}$ $W \cdot m^{-2}$. This value is within the order of magnitude of measured photon emissions from the cerebrum during periods of focused cognition, such as imagining white light (Dotta et al., 2012). However all of the proton-electron pairs within the brain mass are not arranged as neutral hydrogen so this convergence may be coincidental unless there is some recondite geometry or structure that maintains the functional equivalence of this effect.

The absolute differences in the numbers of bits that deviated during intention and when the magnetic field was present during intention were about 3000. Adjusting for the total duration of the exposures for the subjects (about 1440 s), this would be associated with the energy of about 2 electron mass equivalents per second. This number is within the order of magnitude predicted by the energy produced within the brain per second. Even if we accommodated the variability of the intensity of the applied field and the individual differences for the time required to produce the significant deviations from chance, the similarity of values indicate a potential quantitative support for this process.

Why a quantum of energy within the cerebrum would affect specifically the quantum of energy that simulates the movement of an electron across a p-n junction, in our opinion, is by far a more important question. If non-locality is operative, then the conditions within the cerebrum and the

REG should be similar. The geometry may not be identical to the conditions by which photon "entanglement" has been shown experimentally by Dotta and Persinger (2013) and may involve a fundamental form of entanglement that originated from primordial spin processes with direct relevance to consciousness (Hu & Wu, 2004). In the Dotta et al. studies (2013) simultaneous injection of hydrogen peroxide into sodium hypochlorite in two separated localities produced a doubling of the photon emissions (measured by photomultiplier tubes), as if the two localities were the "same space", at least transiently, or that had been a transposition of three-dimensional spatial axes. However, this only occurred if both localities shared the same space-time structural features of the rotating magnetic fields with specific changes in angular velocities.

We suggest that the capacity for "excess correlation" between intention of the participant and the shift in random variations of electron tunnelling within the REG is related to the shared similarities of their geometries and spaces within which the dynamics occur. In general, the widths of the p-region and n-region in a semiconductor are about $1.5 \cdot 10^{-7}$ m and $2.9 \cdot 10^{-7}$ m, respectively. The total depletion width is about $0.4 \cdot 10^{-6}$ m. This width is within the range of the synapse (contact diameter = 0.5 to $2 \cdot 10^{-6}$ m). The tunnelling of electrons occurs within barriers of thickness around 1 to 3 nm (or smaller) while the typical separation of the pre- and post-synaptic cleft or distance for (chemical synapses) is about 20 to 40 nm and electrical "synapses" or gap junctions are about 2 to 3.5 nm. The ratio of the gap for electron tunnelling to the width through a semiconductor medium would be $2 \cdot 10^{-9}$ m divided by $4.4 \cdot 10^{-7}$ m or $0.45 \cdot 10^{-2}$. The ratio of the gap to width for the chemical synapse would be $3 \cdot 10^{-8}$ m divided by $1.3 \cdot 10^{-6}$ m or $2.3 \cdot 10^{-2}$. In comparison, the ratio of the gap to width of the gap junction involves $3 \cdot 10^{-9}$ dived by $1.3 \cdot 10^{-6}$ m or $0.24 \cdot 10^{-2}$. Considering the range involved for both p-n junctions and electrical (gap junction) synapses, the ratios of gap to width values for both of these conditions are remarkably similar.

Electrical interfaces within the brain are as numerous as chemical synapses within the cerebral cortices, thalamus, and hippocampus. Gap junctions are actual physical connections that couple neighbouring neurons by large macromolecules that traverse the membranes of both adjacent neurons. Direct exchange of ions and smaller molecules occur between the two cells. Gap junctions are known for their capacities to rectify (facilitate current in one direction rather than another) movements of charges as well as to coordinate electrical changes within large populations of neurons. They couple with GABAergic interneurons within cerebral cortices and thalamus, particularly in young animals. Spike transients from action potentials can penetrate the gap junction and synchronize multiple neurons that share these interfaces including distributed neuronal circuits (Traub et al., 2001).

This results in the synchronization of the "40 Hz" cortical rhythms which is minimized if the expression of the chemical substrates for the gap junction is prevented because of an absent gene. Gap junctions are also likely to be responsible for the revealing 40 Hz cortical patterns that are commonly seen superimposed upon the theta (4 to 8 Hz) synchronous patterns generated by the hippocampal formation. Such electrical coupling over large area and volumes of cerebral cortical space may be the "cohesive" factor that has been considered essential for producing a "cognitive field" as well as increasing the total power output by summating the very small quantities that would otherwise be cancelled into an integrated value of substantial magnitude.

There may be quantitative suggestions for the potential entanglement of energy and mass between the gap junctions within the participants' cerebral cortices and hippocampal formations and the p-n junctions of the REG at approximately 0.25 m distance. If we assume a classic Casimir effect described by:

$$[\pi^2 (240)^{-1} \hbar c a^{-4}] \cdot S,$$

where ħ is the modified Planck's constant, *c* is the velocity of light and a is the distance between the two planes (2 nm) with surface area S of 0.16 μm^2 , the force would be $0.13 \cdot 10^{-4}$ N and when applied across the 2 nm interface would involve an energy of $0.26 \cdot 10^{-13}$ J. The mass equivalent of that energy is within range, given the variation in width and separation distances for both gap and p-n junctions to that of the classical electron ($\sim 10^{-31}$ kg). One of the basic assumptions for the Casimir force is that virtual particles can become actual particles when the appropriately time-varying magnetic field is applied to a changing boundary. The time-varying magnetic field employed in our present study could meet the criteria for that condition.

On the other hand, the complexity of the digital sequences generated by the REG was not affected by intention. There was a general decrease in complexity when the experimental field was applied, regardless if intention was present or absent. A decrease in complexity could be associated with the consequence of repeating the same field pattern which by definition would have deviated from the greater degrees of freedom that would constitute complexity. The etiology of this effect is not clear. It is not likely to be related to crude current induction because other experiments in which the field strengths were altered did not change the degree of complexity. From another perspective, the fact that the actual deviation of the REG output was affected by intention and attenuated by the simultaneous application of the magnetic field, whereas complexity was not affected by intention, indicates that the two phenomena are quite separate. In addition this differential indicates that the effects of intention involved processes other than non-specific (generalized or artifactual) factors.

4.6 References

Babayev, E.S., & Allahverdiyeva, A. A. (2007). Effects of geomagnetic activity variations on the physiological and psychological state of functionally healthy humans: Some results of Azerbaijani studies. *Advances in Space Research, 40*(12), 1941-1951.

Caswell, J. M., Collins, M. W. G., Vares, D. A. E., Juden-Kelly, L. M., & Persinger, M. A. (2013). Gravitational and experimental electromagnetic contributions to cerebral effects upon deviations from random number variations generated by electron tunneling. *International Letters of Chemistry, Physics and Astronomy, 11*, 72-85.

Caswell, J. M., Dotta, B. T., & Persinger, M. A. (2014). Cerebral biophoton emission as a potential factor in non-local human-machine interaction. *NeuroQuantology, in submission*.

Dimitrova, S., Mustafa, F. R., Stoilova, I., Babayev, E. S., & Kazimov, E. A. (2009). Possible influence of solar extreme events and related geomagnetic disturbances on human cardio-vascular state: Results of collaborative Bulgarian-Azerbaijani studies. *Advances in Space Research, 43*(4), 641-648.

Dotta, B. T., & Persinger, M. A. (2009). Dreams, time distortion, and the experience of future events: A relativistic, neuroquantal perspective. *Sleep and Hypnosis, 11*(2), 29-39.

Dotta, B. T., Saroka, K. S., & Persinger, M. A. (2012). Increased photon emission from the head

while imagining light in the dark is correlated with changes in electroencephalographic power: Support for Bokkon's hypothesis. *Neuroscience Letters, 513*(2), 151-154.

Dotta, B. T., Koren, S. A., & Persinger, M. A. (2013). Demonstration of entanglement of "pure" photon emissions at two locations that share specific configurations of magnetic fields: Implications for translocation of consciousness. *Journal of Consciousness Exploration & Research, 4*(1).

Gearhart, L., & Persinger, M. A. (1986). Geophysical variables and behavior: XXXIII. Onsets of historical and contemporary poltergeist episodes occurred with sudden increases in geomagnetic activity. *Perceptual and Motor Skills, 62*, 463-466.

Giroldini, W. (1991). Eccles's model of mind-brain interaction and psychokinesis: A preliminary study. *Journal of Scientific Exploration, 5*(2), 145-161.

Gissurarson, L. R. (1992). The psychokinesis effect: Geomagnetic influence, age and sex differences. *Journal of Scientific Exploration, 6*(2), 157-165.

Hu, H., & Wu, M. (2004). Spin as primordial self-referential process driving quantum mechanics, spacetime dynamics and consciousness. *NeuroQuantology, 2*(1), 41-49.

Hunter, M. D., Mulligan, B. P., Dotta, B. T., Saroka, K. S., Lavallee, C. F., Koren, S. A., & Persinger, M. A. (2010). Cerebral dynamics and discrete energy changes in the personal

environment during intuitive-like states and perceptions. *Journal of Consciousness Exploration & Research, 1*(9), 1179-1197.

Jahn, R. G., Dunne, B. J., Nelson, R. D., Dobyns, Y. H., & Bradish, G. J. (1997). Correlations of random binary sequences with pre-stated operator intention: A review of a 12-year program. *Journal of Scientific Exploration, 11*(3), 345-367.

Kimchi, T., Etienne, A. S., & Terkel, J. (2004). A subterranean mammal uses the magnetic compass for path integration. *Proceedings of the National Academy of Sciences of the United States of America, 101*(4), 1105-1109.

Klimley, A. P. (1993). Highly directional swimming by scalloped hammerhead sharks, *Sphyrna lewini*, and subsurface irradiance, temperature, bathymetry, and geomagnetic field. *Marine Biology, 117*, 1-22.

Krippner, S., & Persinger, M. A. (1996). Evidence for enhanced congruence between dreams and distant target material during periods of decreased geomagnetic activity. *Journal of Scientific Exploration, 10*(4), 487-493.

Mach, Q. H., & Persinger, M. A. (2009). Behavioral changes with brief exposures to weak magnetic fields patterned to simulate long-term potentiation. *Brain Research, 1261*, 45-53.

Makarec, K., & Persinger, M. A. (1987). Geophysical variables and behavior: XLIII. Negative correlation between accuracy of card-guessing and geomagnetic activity: A case study. *Perceptual and Motor Skills, 65*, 105-106.

Mouritsen, H., Feenders, G., Liedvogel, M., & Kropp, W. (2004). Migratory birds use head scans to detect the direction of the Earth's magnetic field. *Current Biology, 14*(21), 1946-1949.

Mulligan, B. P., & Persinger, M. A. (2012). Experimental simulation of the effects of sudden increases in geomagnetic activity upon quantitative measures of human brain activity: Validation of correlational studies. *Neuroscience Letters, 516*(1), 54-56.

Mulligan, B. P., Hunter, M. D., & Persinger, M. A. (2010). Effects of geomagnetic activity and atmospheric power variations on quantitative measures of brain activity: Replication of the Azerbaijani studies. *Advances in Space Research, 45*(7), 940-948.

Murugan, N. J., Karbowski, L. M., Lafrenie, R. M., & Persinger, M. A. (2013). Temporally-patterned magnetic fields induce complete fragmentation in planaria. *PLoS ONE, 8*(4).

Persinger, M. A. (2009). The possible role of dynamic pressure from the interplanetary magnetic field on global warming. *International Journal of Physical Sciences, 4*(1), 44-46.

Persinger, M. A. (2012). Solutions for real values of Minkowski four-dimensional space may link macro- and micro-quantum processes in the brain. *Neuroscience and Biobehavioral*

Reviews, *36*, 2334-2338.

Persinger, M. A., Koren, S. A., & Lafreniere, G. F. (2008). A neuroquantologic approach to how human though might affect the universe. *NeuroQuantology, 6*(3), 262-271.

Persinger, M. A., Dotta, B. T., Saroka, K. S., & Scott, M. A. (2013). Congruence of energies for cerebral photon emissions, quantitative EEG activities and ~5 nT changes in the proximal geomagnetic field support spin-based hypothesis of consciousness. *Journal of Consciousness Exploration & Research, 4*(1), 1-24.

Radin, D. I. (1993). Environmental modulation and statistical equilibrium in mind-matter interaction. *Subtle Energies, 4*(1), 1-30.

Radin, D. I., & Nelson, R. D. (2003). Meta-analysis of mind-matter interaction experiments: 1959-2000. In *Healing, Intention, and Energy Medicine* (pp. 39-48). London: Harcourt Health Sciences.

Richardson, I. G., Cliver, E. W., & Cane, H. V. (2001). Sources of geomagnetic storms for solar minimum and maximum conditions during 1972-2000. *Geophysical Research Letters, 28*(13), 2569-2572.

Roll, W. G., Saroka, K. S., Mulligan, B. P., Hunter, M. D., Dotta, B. T., & Gang, N. (2012). Case report: A prototypical experience of 'poltergeist' activity, conspicuous quantitative

electroencephalographic patterns, and sLORETA profiles: Suggestions for intervention. *Neurocase: The Neural Basis of Cognition, 18*(6), 527-536.

Saroka, K. S., Caswell, J. M., Lapointe, A., & Persinger, M. A. (2014). Greater electroencephalographic coherence between left and right temporal lobe structures during increased geomagnetic activity. *Neuroscience Letters, 560*, 126-130.

Shannon, C. E. (1948). A mathematical theory of communication. *The Bell System Technical Journal, 27*, 379-423 & 623-656.

Snyder, C. W., Neugebauer, M., & Rao, U. R. (1963). The solar wind velocity and its correlation with cosmic-ray variations and with solar and geomagnetic activity. *Journal of Geophysical Research, 68*(24), 6361-6370.

Traub, R. D., Kopell, N., Bibbig, A., Buhl, E. H., LeBeau, F. E. N., & Whittington, M. A. (2001). Gap junctions between interneuron dendrites can enhance synchrony of gamma oscillations in distributed networks. *Journal of Neuroscience, 21*(23), 9478-9486.

Chapter 5 – An Investigation of Solar Features, Test Environment, and Gender Related to Consciousness-Correlated Deviations in a Random Physical System

Submitted to *Journal of Scientific Exploration*

5.1 Abstract

Whereas a multitude of solar and geomagnetic variables were not correlated with significant deviations in continuous measurements from random physical systems (Random Event Generators), these variables were moderately correlated with REG output during periods of intention. The scalar components (2-10 nT) of the Interplanetary Magnetic Field (r = ~0.50) and global geomagnetic activity (r = ~0.55) were significantly correlated with the REG deviations during the second minute of intention. Significant compared to non-successful deviations occurred during periods of intention when the Solar Radio Flux was about 20 units ($2 \cdot 10^{-21}$ $W \cdot m^{-2}$ Hz^{-1}). The polarity of the deviation was different within a Faraday (echoic) chamber than in normal environment as well as between genders. The amount of energy associated with the increase in geomagnetic activity within the volume of human cerebrum is remarkably similar to the gravitational energy within this mass due to minute variations in G (the Gravitational Constant). These results indicate a subset of variance shared across several components of the ambient heliogeophysical environment may be a significant mediator of intention-coupled changes in random variations in p-n junction devices and that discrete energies associated with intrinsic variations in G may be relevant.

5.2 Introduction

The integration of biological sciences and the study of space weather were largely initiated by the original and insightful work of biophysicist Alexander Chizhevsky, who examined relationships between these areas within the interdisciplinary framework of heliobiology. His investigations into the effects of solar activity on terrestrial systems were wide-ranging and included human health and epidemiology, psychological well-being, electrical systems, and the behaviour of entire societies (Chizhevsky, 1936). Many of these correlations were supported, rediscovered, or advanced through later research using both historiometry and laboratory experiments (e.g., Persinger, 1999; Halberg et al., 2001; Gumarova et al., 2012). That solar activity has been shown to relate to both organic and other physical systems has potential implications for the little-understood area of anomalous cognition and apparently non-local physical interactions involving human consciousness.

The sun, a main-sequence star at the center of our solar system, affects the entire heliosphere, including local planetary conditions on Earth. There are a number of specific measurements associated with various types of solar activity. One particular measure is the sunspot number. Sunspots are seemingly isolated regions of the sun caused by powerful magnetic activity within the solar photosphere, observations of which have been recorded since before the Common Era (Schove, 1955). One reason for examining this phenomenon in the context of solar radiation is because many coronal mass ejections (CMEs) originate from areas surrounding sunspots (e.g., Hundhausen et al., 1984).

One measure of sunspots is the Wolf number (R). This is a daily value used to denote the number of sunspots observed in a given day, and has been in use since 1848 (Clette et al., 2007). The formula used to obtain R is $k(10g + s)$, where k = the personal reduction coefficient, g = number

of sunspot groups, and *s* = number of sunspots (Herrman, 2012). Another measure associated with overall solar activity is the solar radio flux. This refers to radio emissions often produced when plasma within highly active regions of the sun becomes trapped beneath magnetic fields (Donnelly et al., 1983), and as such are also related to sunspots. Significant correlations have been observed between daily values for these measures of solar activity (*r*s = ~0.6-0.7).

These emissions are measured around 2800 MHz at the 10.7 cm wavelength (Tapping, 1987). The background x-ray flux is another similar measure often used which is also related to the occurrence of solar flares (e.g., Neupert, 1968; Sheeley et al., 1983). Emissions in the x-ray wavelength are measured as background flux within the ionosphere (e.g., Thomson et al., 2004). This variable is typically denoted in coefficients of flux ($W \cdot m^{-2}$) ranging from low background ($< 10^{-8}$) to extreme flares ($> 10^{-3}$; Thompson, 2013).

Aside from measures directly associated with overall solar activity, there are also a number of solar wind features which are often examined in the context of space weather. The heliosphere itself is a direct product of solar winds which pervade the solar system (Holzer, 1989). This phenomenon is actually a result of particle streams released from the sun's atmosphere, largely consisting of charged electrons and protons (McComas et al., 1998). Solar proton events, or proton storms, refer to large numbers of these particles being released from the sun, usually associated with solar flares or CMEs (Kahler et al., 1978). These particles can enter the local magnetosphere and release their energy within the ionosphere through the process of ionization (Shea & Smart, 1990).

The phenomenon of solar wind is also responsible for the interplanetary magnetic field (IMF). This refers to the magnetic field of the sun which has been distributed amongst the planets of the

heliosphere (Levine et al., 1977). Because solar winds are a plasma they have sufficient electrical conductivity to carry magnetic field lines from the sun throughout the solar system produced by a magnetohydrodynamic effect with both electric and magnetic components (e.g., Pogorelov et al., 2004). However, as the solar magnetic field extends into interplanetary space, the sun continues to rotate on its axis, while the forces of both plasma and magnetic pressure oppose one another. As a consequence of these two factors, the IMF forms a "Parker spiral" and produces local variations throughout the heliosphere (*Figure 27*; Thomas & Smith, 1980). This field affects not only the outer planets, but also the magnetic field of our own planet (e.g., Friis-Christensen et al., 1972).

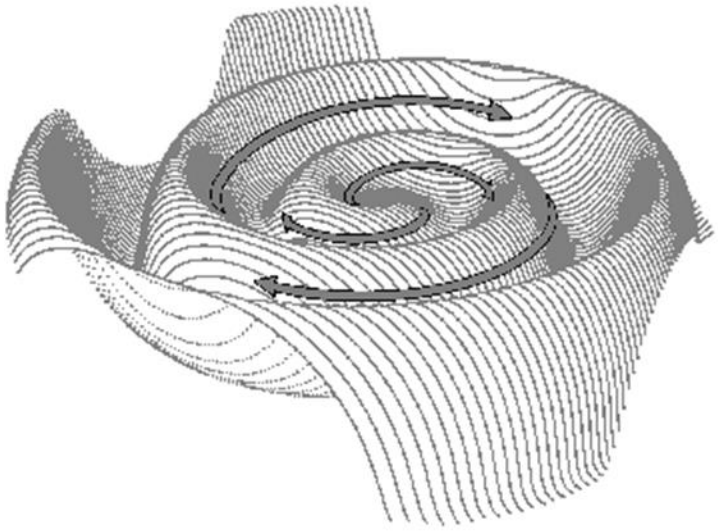

Figure 27 – Representation of a "Parker spiral"

Image source: NASA Cosmicopia (helios.gsfc.nasa.gov/solarmag.html)

The phenomenon of significant deviations in random systems associated with cognitive "intention" has been noted in a number of experiments. Apparent non-local interactions between human "intention" and non-deterministic external systems have been observed in many

laboratories (e.g., Jahn et al., 1997; Radin & Nelson, 2003). Previous research has also suggested that neurophysiological effects may mediate this apparent phenomenon of consciousness-correlated collapse (3C) or presumably random motions. This term, 3C, is preferred to traditional and now pejorative terms concerning "mind-matter" relationships. As an example, electroencephalograph (EEG) activity in the alpha and beta frequencies has been shown to widen during control measures compared to periods when participants successfully achieved significant deviations in a random event generator (REG) device (Giroldini, 1991). Furthermore, a relationship has been identified between the effects of cognitive "intention" and cerebral biophoton emission (Dotta & Persinger, 2011; Caswell et al., 2014a) and both gravitational and electromagnetic mediated effects on the cerebral volume (Caswell et al., 2013).

Given that solar activity has been implicated as a potential factor which may affect human physiology (e.g., Cherry, 2002), it was hypothesized that more subtle effects of the environment on statistically significant deviations in a random physical system correlated with consciousness may be found with factors external to the immediate geosphere. If variations of solar activity exert an influence on neurophysiological functioning, and cerebral effects are involved in the process of the 3C phenomenon, then relationships between this form of non-local interaction and solar variable measures should be observed. Furthermore, it was hypothesized that some form of seasonal variation in successful REG operation associated with the position of the Earth relative to the sun would be revealed.

The obvious variable of participant gender has been previously examined in the context of 3C phenomena, specifically with apparent non-local human-machine interactions. However, results are relatively conflicting depending on the study. This ranges from overall performance gender differences (Gissurarson, 1992), differences between genders within specific modes of target data

analysis (Dunne, 1998), and no apparent gender differences (Nelson et al., 2000). Due to this disparity, it was hypothesized that there might be an environmental covariate which may mediate any 3C performance differences between males and females.

5.3 Methods

Subjects

Participant age ranged from 22-52 years for N = 26 (N = 13 females, N = 13 males). All were recruited from Laurentian University campus or the immediate community.

Data & Equipment

Daily average values were obtained from the GSFC (Goddard Space Flight Center) / SPDF (Space Physics Data Facility) OMNIWeb interface (omniweb.gsfc.nasa.gov) for the scalar component of the interplanetary magnetic field (IMF; nT) and proton density of solar winds ($N \cdot cm^{-3}$). Daily sunspot number (R; Wolf numbers), average daily background x-ray flux (peak flux in coefficients of 10^{-6} $W \cdot m^{-2}$), and average daily solar radio flux (SFU; $1 = 10^{-22}$ $W \cdot m^{-2} \cdot Hz^{-1}$) were obtained from the NOAA (National Oceanic and Atmospheric Administration) / NGDC (National Geophysical Data Center) database (www.ngdc.noaa.gov). Values for the equation of time (apparent solar time) were calculated using the Local Sidereal Time Clock maintained by Jürgen Giesen (www.jgiesen.de/astro/astroJS/siderealClock/). Finally, cosmic ray data (average impulses/min/day) was obtained from the Moscow Neutron Monitor (cr0.izmiran.rssi.ru/mosc/main.htm).

Random data was produced using a Psyleron REG-1 random event generator (*Figure 7*; www.psyleron.com). The device produced a random output which was generated by electron tunneling effects within two field effect transistors. The varying voltage levels which result from

this process were converted into digital data through a gated sampling procedure which allowed for regularly spaced bit sequences. The output of both transistors was internally compared through an alternating (0, 1) XOR masking process in order to reduce any potential influence of physical artifacts or other external environmental variables. The device itself was further protected from static electromagnetic factors by an aluminum outer shielding and a Permalloy mu-metal inner shield.

The device was rigorously calibrated prior to shipment in order to ensure output conformed to statistical expectations. The random event generator (REG) was also tested in control experiments within our laboratory to confirm these expectations. The resulting data were collected through USB-port using Psyleron FieldREG and Reflector software packages on a laptop computer. Data were produced at a rate of either 1 or 2 events (200 0,1 bits/event) per second (experiment dependent), with each event referring to the number of 1's out of 200 bits with binary probabilities, represented by a value of 0-200. The theoretical (chance) mean for each event is 100 with a standard deviation of $\sqrt{50}$. Pilot testing and the following experiment indicated no significant differences between event rates ($p > .05$). Measures of entropy (HX) were obtained using Matlab 2011a software. All other statistical procedures were conducted using SPSS software v.17.

Procedure

In all experiments participants were seated in a dark, comfortable environment approximately 1 m from the REG device, and asked to intend for the data output to deviate either up or down (positive or negative). The device was placed on the right side of each individual. For N = 8 participants, the test location was an ordinary room, where the REG was placed at shoulder

height. For the other N = 18, the test location was an acoustic chamber which was also a Faraday cage. The background average resultant fields within the cage near the REG was about 20,000 nT compared to the typical average of 47,000 nT outside of the chamber. The REG was placed at ground level approximately 45° from the plane of the forward line of sight. Prior to testing, participants viewed a short demonstration with the REG software (e.g., *Figure 8*) in order to understand what they would be focusing their intention on. No feedback was provided during testing. REG data collection was kept hidden from the experimenter until analysis. No significant differences were identified between varying bit rates, and averages were computed accordingly. All environmental measures were obtained following testing.

Data Analyses

Random Event Generator (REG) data were obtained from N = 26 participants within two separate experiments. Individual event scores were standardized according to .5 chance expectations ([*x*-100] / √50). One experiment contributed N = 15 sessions, each lasting approximately 5 minutes. The second experiment consisted of N = 11 participants with data collection lasting about 8 minutes. Minute averages, absolute means, and standard deviations were computed. In order to maintain sample consistency for statistical analysis the first 5 minutes of testing from each participant were used for minute averages. Overall session scores were computed using Stouffer's method ($\sum z / \sqrt{n}$), where z = individual event z-scores, with n = the number of events. Various planetary and solar variables were entered into the database. Significant ($p < .05$) correlations of $r \geq .5$ were reported.

5.4 Results

REG Output without Intention

Daily averaged REG output was gathered for a period of two months. All space weather variables of interest were entered into the database and examined for potential correlations. Subsequent analyses revealed no apparent relationships between output of a random event generator (REG) and various measures of space weather ($p > .05$). It is therefore hypothesized that any potential correlations revealed could potentially be attributed to relationships between space weather and biological/physical processes involved in consciousness-correlated collapse (3C) of an external random process.

Solar Activity and REG Operation

Pearson and Spearman correlations revealed a statistically significant relationship between the best overall REG session score from each participant (e.g., greatest overall deviation obtained) taking direction into account (e.g., positive value = deviation in intended direction), and both sunspot number (*Figure 28*; $r = .57$, $p = .002$; *rho* = .601, $p = .001$) and solar radio flux (*Figure 29*; $r = .541$, $p = .004$; *rho* = .558, $p = .003$). Subsequent partial correlations showed that both solar variables related to REG score independently. Their correlations vanished ($p > .05$) when controlling for the effects of the other. This suggested they shared the same source of variance with respect to the REG data.

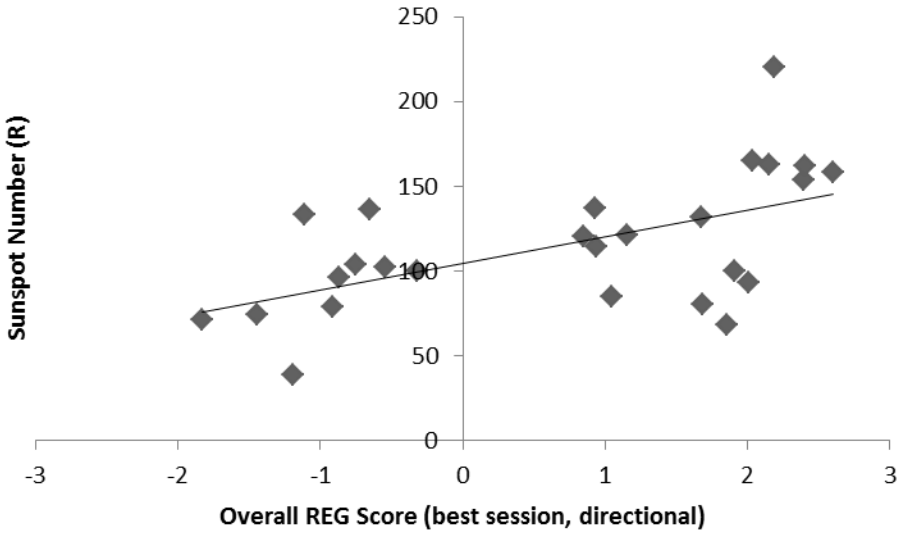

Figure 28 - Correlation between sunspot number and participants' best REG score

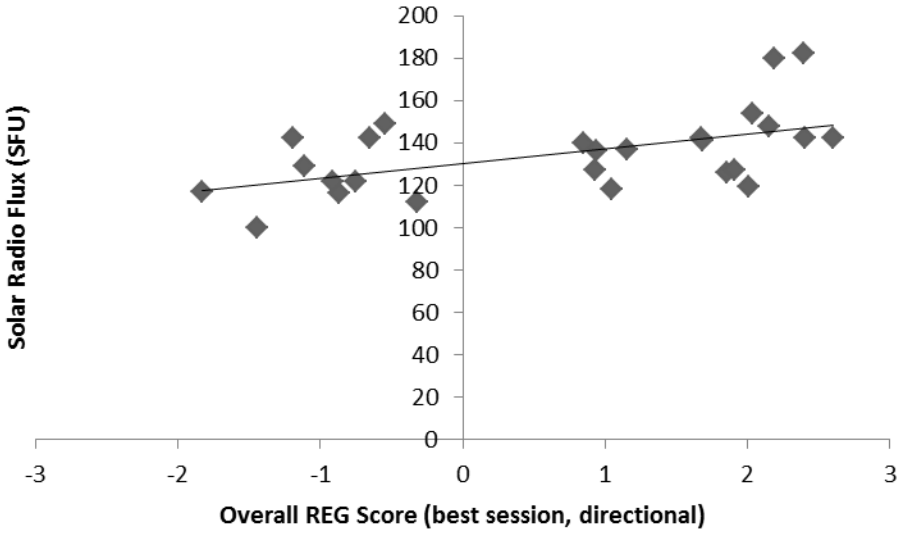

Figure 29 - Correlation between solar radio flux and participants' best REG score

Given the directional REG measures employed in the previous correlations (e.g., accounting for direction of intention) it appears that overall solar activity may be associated with a greater tendency for deviations correlated with operator intention. To further pursue this hypothesis

participants were split into groups determined by whether or not they had successfully achieved at least one significant REG score at the $p \leq .025$ level ($z \leq 1.96$, one-tailed). Independent t-tests revealed a significant difference in both sunspot number (*Figure 30*; $t_{(24)} = 3.865$, $p = .001$, $r = .619$) and average solar radio flux (*Figure 31*; $t_{(24)} = 2.924$, $p = .007$, $r = .513$) on the day of testing between successful and non-successful operators (*Table 10*). A significant difference was also found for the average background x-ray flux (*Figure 32*; $t_{(24)} = 2.885$, $p = .008$, $r = .507$).

REG Score	Sunspot # - μ (sd)	Radio flux - μ (sd)	X-ray flux - μ (sd)
Significant	151.88 (40.07)	149.25 (22.54)	6.6 (1.41)
Non-Significant	99.5 (27.84)	128.78 (13.19)	4.32 (2.01)

Table 10 - Mean (μ) and standard deviation (sd) values of sunspot numbers, solar radio flux, and solar x-ray flux for each operator group

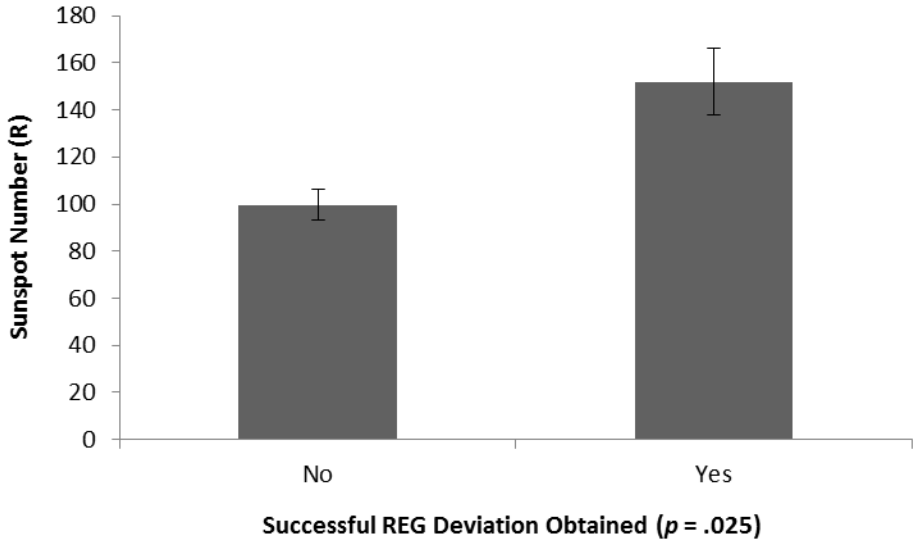

Figure 30 - Difference in daily sunspot number between successful and non-successful REG operators; vertical bars represent standard error of the mean (SEM)

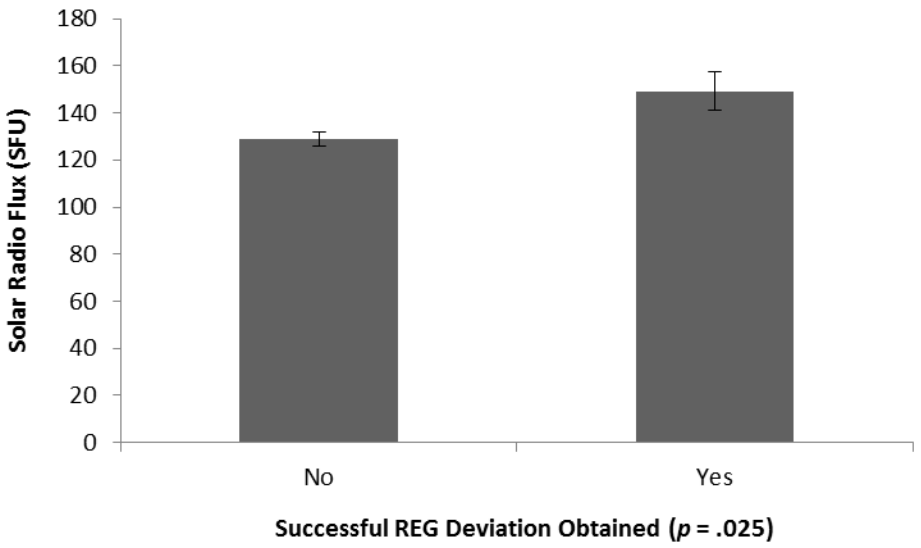

Figure 31 - Difference in daily solar radio flux between successful and non-successful REG operators; vertical bars represent SEM

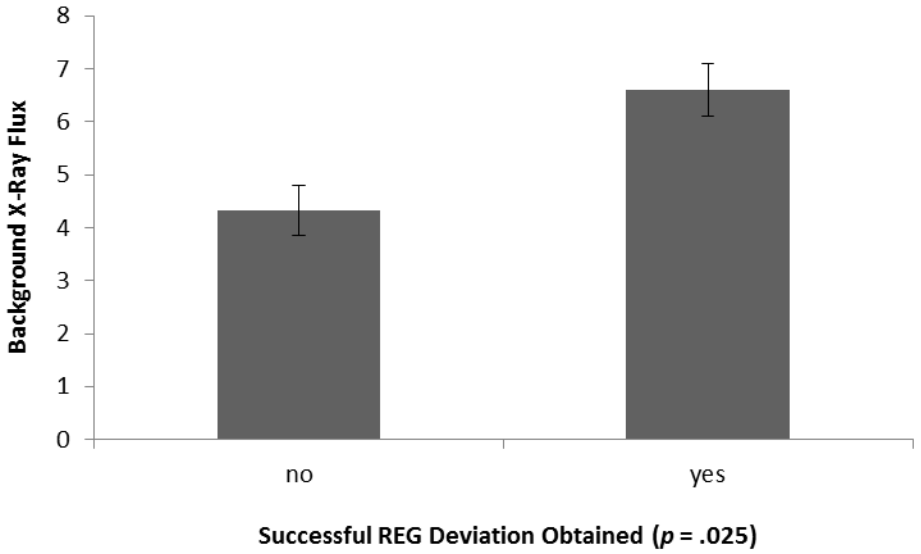

Figure 32 - Difference in average daily background x-ray flux between successful and non-successful REG operators; vertical bars represent SEM

Interplanetary Magnetic Field Correlations

Minute-to-minute averages and standard deviations were examined for potential correlations with measures of space weather employing both parametric and non-parametric testing. A statistically significant relationship was found between average REG score during minute 2 of testing and the scalar component of the IMF (*Figure 33*; r = .51, p = .008; *rho* = .483, p = .013). This relationship was slightly increased when controlling for the variance associated with cosmic ray impulses (r = .526, p = .007; *rho* = .513, p = .007). Average REG score (minute 2) and scalar IMF measures were each entered into separate linear regressions with daily averages of cosmic ray impulses as the independent variable. The subsequent standardized residuals were obtained. The partial correlation is shown in *Figure 34*. We have previously found that this temporal component (2 min) appears to be particularly critical with regard to apparent human-REG interaction (Caswell et al., 2013; Caswell et al., 2014a).

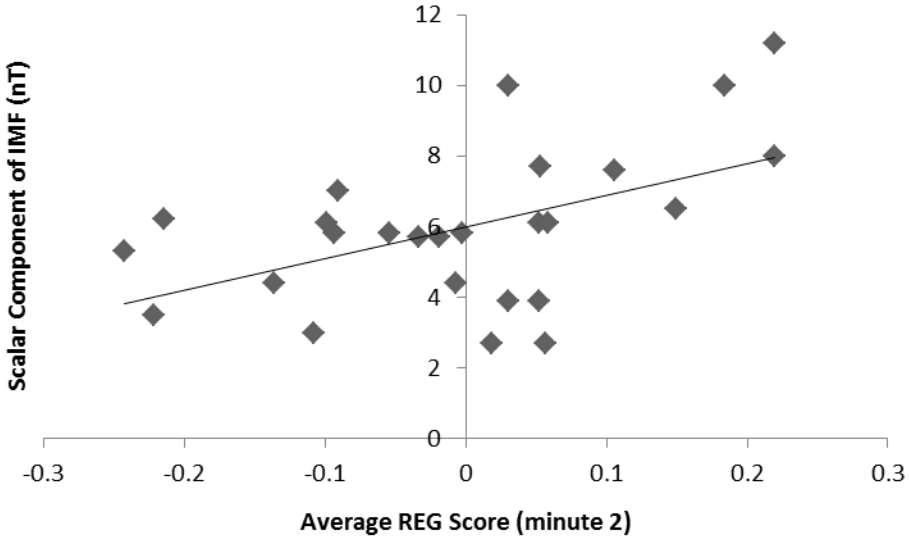

Figure 33 - Correlation between the scalar IMF component and average REG score during minute 2

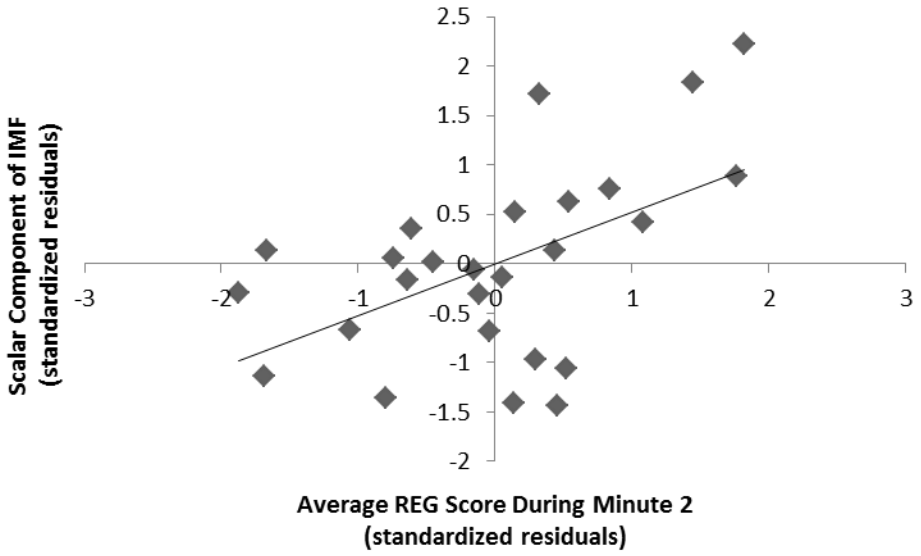

Figure 34 - Partial correlation between the scalar IMF component and average REG score during minute 2, controlling for effects of cosmic ray impulses

Ambient Geomagnetic Conditions

The systematic correlations of similar magnitudes between REG scores and numbers of sunspots, solar flux unit output and interplanetary magnetic field strengths indicated the association with a locality would require some representation of these changes in the vicinity of the measurements. The most obvious local representation would be global geomagnetic activity. Consequently the daily A_p indices as well as the three hour K_p values for the interval of the experiment and each of the three-hour increments before and after the increment were obtained from the Solen online database (www.solen.info/solar/). There was a significant correlation (r = 0.54, p < .01; *rho* = 0.41, p < .05) between the global geomagnetic activity at the time of the intention experiments and the REG deviations. These results are shown in *Figure 35*.

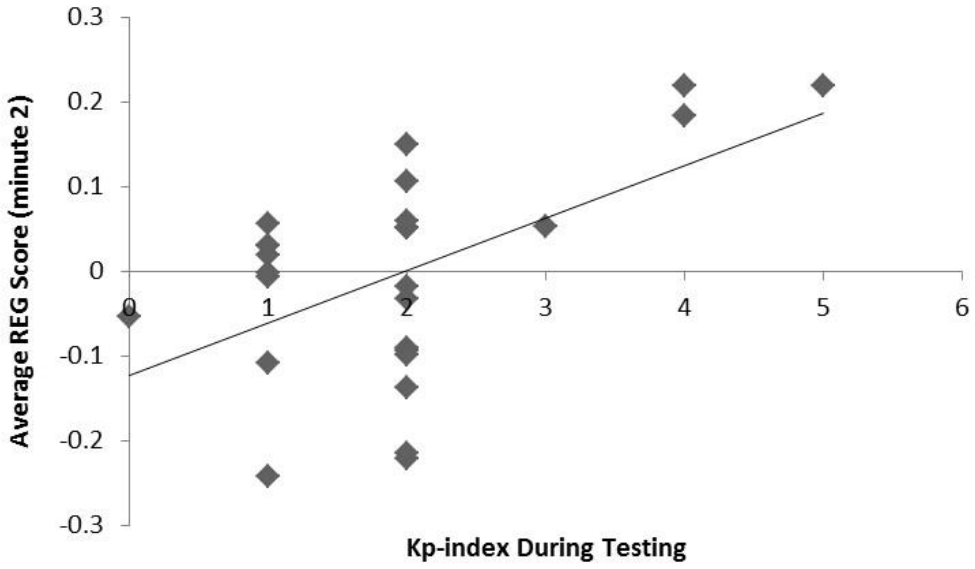

Figure 35 - Averaged deviation from random (vertical axis) during the second minute of testing and the global geomagnetic index during that period

Isolating Shared Sources of Variance

In order to discern the potential sources of shared variance, a factor analysis was completed for the magnitude of the REG variation during the second minute, sunspot numbers for the day, IMF values for the day, solar flux units for the day, and the K_p indices (ambient, but global geomagnetic activity) for the interval in which the measurements were obtained. In order to accommodate the small sample size, loading coefficients of > 0.70 were considered significant. The first factor (eigenvalue = 2.38) which accommodated almost half of the variance was loaded significantly by the K_p values (0.85), IMF (0.85) and the REG variation during the second minute (0.83). The second factor (eigenvalue = 1.53), which explained 31% of the variance was loaded significantly by numbers of daily sunspots and solar flux units. Together the two factors accommodated 78% of the variance. These results indicated that the proximal geophysical

(interplanetary magnetic field and geomagnetic field variations) variables share a source of variance with the REG variations.

Time and REG Performance

Although standard time measures noon with regard to the position of the sun relative to the local meridian, the actual time of this crossing varies throughout the year. The equation of time represents the difference between mean solar time and apparent solar time. The difference between these two times varies by up to 16 minutes in either direction (*Figure 36*). Values for the equation of time (in minutes) were obtained for each test session (*Table 11*). Independent t-test analysis determined that there was a significant difference in the values associated with the equation of time and the occurrence of REG session scores of $p \leq .025$ (*Figure 37*; $t_{(24)} = 2.429$, $p = .023$, $r = .444$). This may suggest some form of seasonal variation associated with the occurrence of various "psi" processes, which may also provide an explanation for why some experiments have been unsuccessful in the past.

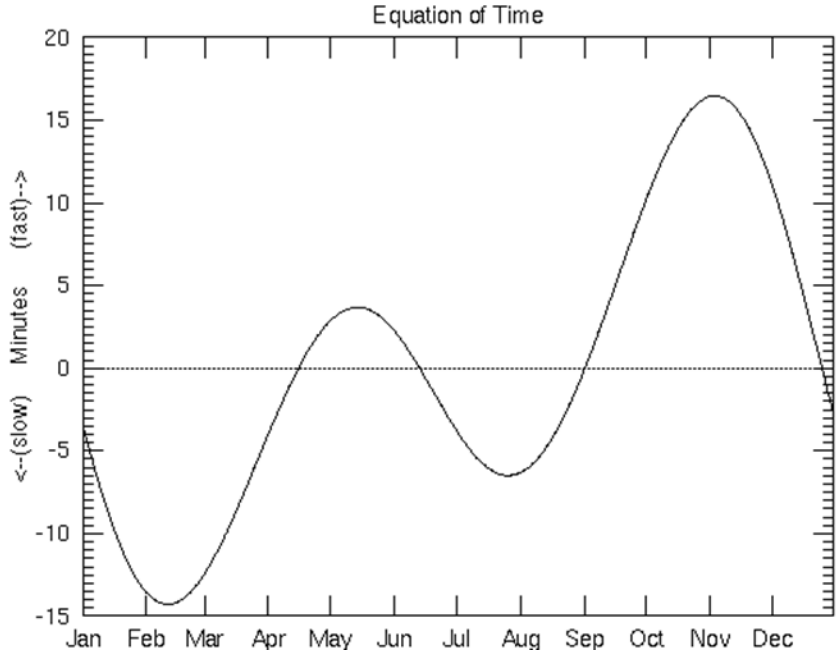

Figure 36 - Equation of time; difference between mean solar time and apparent solar time throughout the year

Image source: Nick Strobel (www.astronomynotes.com/nakedeye/s9.htm)

Equ (min)	Significant	Non-Significant
μ	5.219	-2.648
Sd	(6.909)	(7.897)

Table 11 - Mean (μ) and standard deviation (sd) values for the equation of time values (in minutes) between REG operator groups

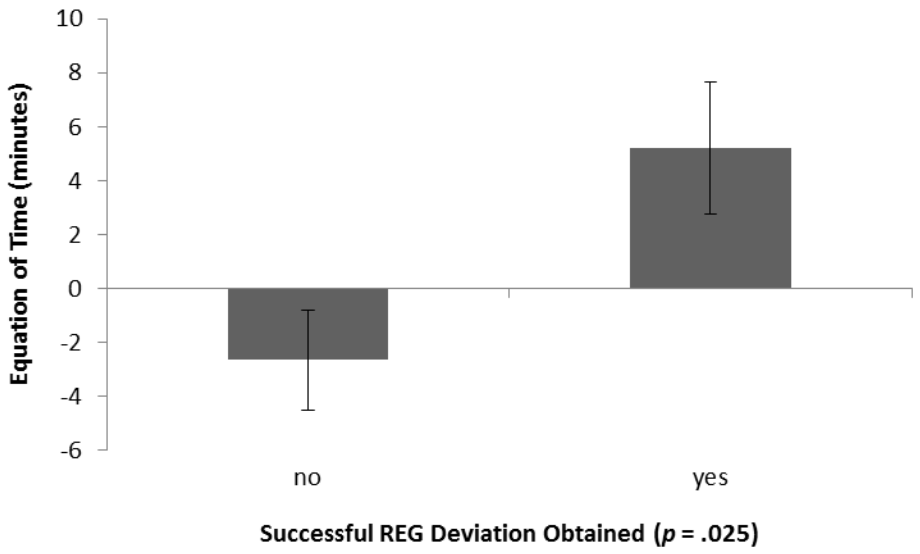

Figure 37 - Difference in equation of time (minutes) between successful and non-successful REG operators; vertical bars represent SEM

Test Location and REG Outcome

Finally, N = 8 participants completed testing within a normal room, while N = 18 were tested within an acoustic chamber which was also a Faraday cage. Initially, there were no indications of significantly different REG session scores between locations. However, when entered into an analysis of covariance (ANCOVA) a significant difference was found for the best session score (e.g., greatest deviation obtained) between locations when covarying for the solar wind proton density ($F_{(1, 25)} = 4.808$, $p = .039$, $\eta^2 = .162$). A linear regression was run for REG scores with proton density as the independent variable to obtain standardized residuals for demonstrating this significant difference in *Figure 38*. More specifically, more positive deviations occurred within the standard location ($\mu = .578$, $sd = .955$), while more negative deviations were obtained within the Faraday cage ($\mu = -.257$, $sd = .9$).

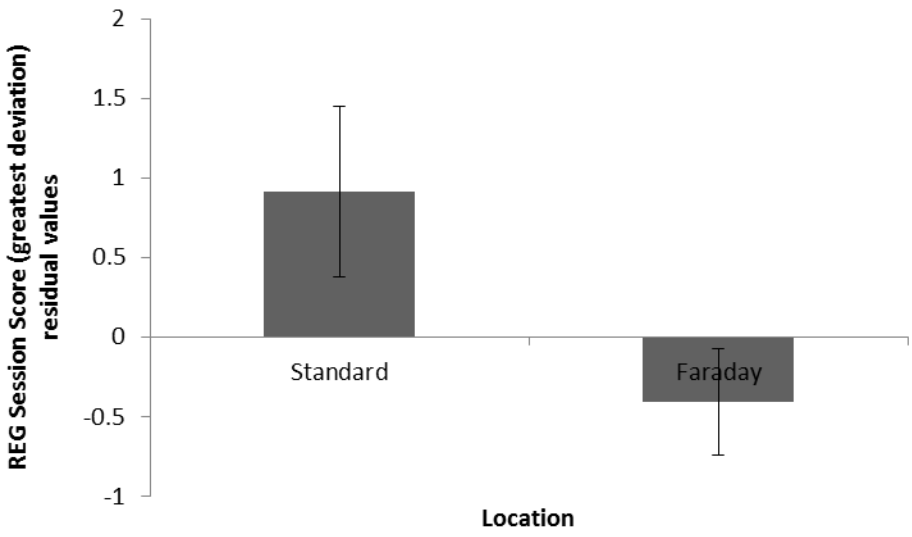

Figure 38 - Difference in best REG session score obtained between locations, covarying for solar wind proton density; vertical bars represent SEM

Gender, REG Performance and Complexity

Signal complexity of REG event data for each session was obtained by using the entropy function in Matlab software. The measure of entropy computed by this method is similar to Shannon entropy of a random variable (e.g., Shannon, 1948), $H(X) = -\sum x\ P(x)\log_2 P(x)$, where x = the random variable, X = the number of possible values within x, and P = the probability mass function. Entropy values (HX) represent the level of uncertainty within the data, where higher values indicate greater complexity and less predictability. Signals with greater complexity possess a greater number of distinct values, and these values are more evenly distributed. Using an independent t-test it was determined that HX values of each participant's best REG session (greatest deviation) were significantly greater for females than males (*Figure 39* & *Table 12*; $t_{(24)} = 2.523$, $p = .019$, $r = .454$).

HX (REG)	Female	Male
μ	2.37	2.27
Sd	(.068)	(.121)

Table 12 - Mean (μ) and standard deviation (sd) values of REG session entropy (HX) for male and female participants

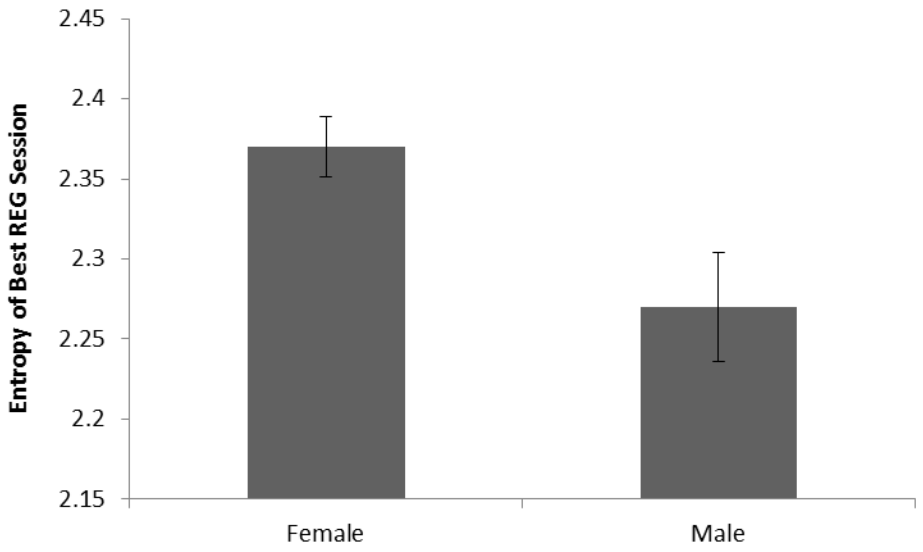

Figure 39 - Entropy (HX) values of REG data (greatest deviation) for males and females

Given the relationship between the reproductive cycle with associated hormonal changes, and the lunar cycle (e.g., Cutler et al., 1987), it was hypothesized that if there were further differences between genders with regard to REG operation the relative position of the moon may be a factor. Subsequently, an ANCOVA was used to compare REG deviations between males and females while covarying for the effects of both lunar apogee and perigee. Distance from the moon was measured by the number of days since the most recent lunar apogee and perigee for each session, as derived from the Lunar Extremes database. The greatest REG session score obtained by each participant (e.g., largest overall deviations) differed significantly between genders, with the greatest effect found when simultaneously controlling for both apogee and perigee (*Figure 40*; *F*

$_{(1, 25)}$ = 5.802, p = .025, η^2 = .186). More specifically, females obtained significantly more positive (μ = .42, sd = .912) scores while male operators resulted in more negative scores (μ = -.42, sd = .232).

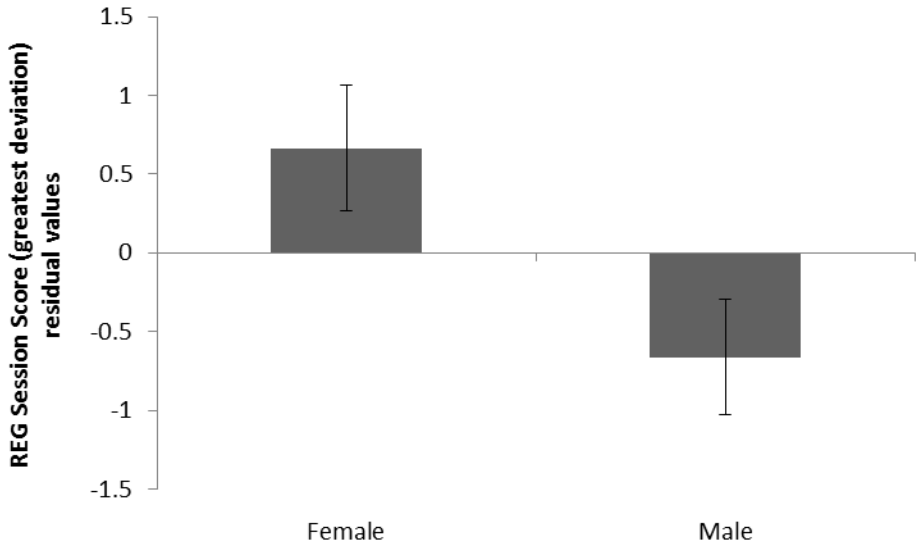

Figure 40 - Difference in overall REG score (best session for each participant) between genders, controlling for the effects of lunar apogee/perigee; vertical bars represent SEM

5.5 Discussion

We measured moderately strong correlations between solar and geomagnetic variables and the deviation from chance from electronic outputs from random event generators when people were intending to alter these outputs. On the other hand, there were no significant correlations between these variables and the output of the REG when there were no subjects in the proximity. These results suggest that an interaction between solar-geomagnetic variables, some physical aspect of human cognition (intent), and random variations from electron tunnelling through p-n junctions at a distance of approximately 1 m may have occurred. We cannot exclude the possibility that simply the mass or presence of the person produced these effects. However, in other experiments

(Caswell et al., 2014b) involving exposure of subjects to experimentally-produced magnetic fields, intention with the presentation of those fields was required to affect the significant deviations. Periods of no-intention, even with the field present, produced changes that did not differ significantly from the no intention, no field condition.

Although the solar and geomagnetic variables we employed in this study are strongly inter-correlated, the energy values associated with the most specific proximity values could be revealing. The mean sfu (solar flux units) during successful REG deviations was about 140 in comparison to deviations that did not differ from chance (120). Because 1 sfu=10^{-22} $W \cdot m^{-2}$ Hz^{-1}, this means that at the level of the typical width of a p-n junction (with an average p and n width around $0.5 \cdot 10^{-6}$ m) and the lower end of the width of a synapse ($0.5 \cdot 10^{-6}$ m), the energy at one unit time at 140 sfu (when there was significant deviation) would be $3.5 \cdot 10^{-33}$ J, while the energy at one unit time around 120 sfu would be $3.0 \cdot 10^{-33}$ J. The difference of 20 sfu between the two is equivalent to $5 \cdot 10^{-34}$ J. When divided by Planck's constant ($6.626 \cdot 10^{-34}$ J·s), this difference is the equivalent shift (increase) of frequency of about 0.5 to 1 Hz. This frequency is within the range of both dc-ac interfaces in cerebral activity as well as hydromagnetic (hm) waves produced by interactions between the geomagnetic magnetic field and variations in the interfacing interplanetary magnetic field.

If we assumed that the entire cerebrum was involved, with approximately ~$6 \cdot 10^{13}$ synapses, the total additional energy output from the $3.0 \cdot 10^{-33}$ J would be ~$3 \cdot 10^{-20}$ J per second. Although more likely to be incidental than real, if the total energy available of this magnitude were integrated per second then the possibility that the state of the entire cerebrum might be shifted by a single neuron affected by these forces becomes feasible. There is experimental evidence that the activity of a single neuron can shift the state of the entire rat cerebral cortices (Cheng-Yu et al., 2009). In

addition a single neuron's state is the initiating condition for a more grossly expressed behaviour, such as the display or not display of an operant response (Houweling and Brecht, 2007), that involves millions of neurons.

The role of gravitational phenomena in REG-related deviations has often been neglected because of the assumption of the low energies and minimal forces for very local space and matter. However, recently Persinger and St-Pierre (2014) showed that the "random variation" in G ($6.67 \cdot 10^{-11}$ $m^3 \cdot kg^{-1} \cdot s^{-2}$), which is about 10^{-14} $m^3 \cdot kg^{-1} s^{-2}$, was moderately and negatively correlated with the strength of the interplanetary magnetic field within the range of ± 8 nT. The gravitational energy from this variation within a mass of 1 L of water (the approximate proportion of water within the volume of the human brain) would be $\sim 3 \cdot 10^{-14}$ J. On the other hand, the energy from 8 nT within the volume of 1 L of water would be $3 \cdot 10^{-14}$ J. The mass-energy equivalence for this quantum of energy is the same order of magnitude as the electron (10^{-31} kg).

Although these correlations would be consistent with a non-locality explanation for the deviations from random exhibited by the REG, the potential local effects cannot be ignored. The correlation between REG scores and geomagnetic activity within which the subject and the equipment would have been immersed was 0.54. This would suggest that the other correlations with solar and IMF variables were significant because they were correlated with the changes in the local geomagnetic field. This inference was supported by the exploratory factor analysis (considering the small sample size) that indicated more than 70% of the variance for the REG deviations during the second minute, global geomagnetic activity at the time of the measurement, and interplanetary magnetic field variations shared a common source. On the other hand, the

direct solar measurements (sunspot number and solar flux units) shared variance on a separate factor.

The actual geomagnetic intensity during the experiments was between 0 and 5. This is equivalent to variations of 0 to 2 nT to 48 to 56 nT. The greatest deviations (*Figure 35*) during intention occurred when the geomagnetic activity was over ~20 nT. This would have been a substantial difference in the magnetic energy stored within the cerebral volume. According to traditional formulae, the value would be $2.4 \cdot 10^{-13}$ J during the greatest deviations and $2 \cdot 10^{-15}$ J during the least deviations. Assuming each action potential is associated with $2 \cdot 10^{-20}$ J, the induced energy during the magnetic field oscillations would be equivalent to the discharge of 10^7 neurons. This is within the order of magnitude of the neurons associated with specific cognitions as inferred by fMRI studies. Assuming an average of 58 neurons per cubic mm, this number of total neurons (if cluster in proximity rather than distributed) could involve a volume of $1.2 \cdot 10^{-4}$ m^3 or less than 10% of the total volume.

Because the significant correlation between geomagnetic variation and REG occurred during the second minute (60 to 120 s) of this measurement, the mean power (assuming and average of 90 s or 0.01 Hz) would have been $2.4 \cdot 10^{-15}$ W. Given the typical cross-sectional area of 10^{-2} m^2 this would be equivalent to about $2.4 \cdot 10^{-13}$ $W \cdot m^{-2}$. Interestingly, this value is within the range of background cosmic ray power density at the earth's surface. Cosmic (proton) ray background has been considered one source of "random variation". If the volume containing the number of estimated neurons (10^7) is considered, the volume of brain mass would extend a length of about 5 cm. With this cross-sectional area ($2.5 \cdot 10^{-3}$ m^2), the power density would be in the order of 10^{-11} $W \cdot m^{-2}$ to 10^{-10} $W \cdot m^{-2}$. This power density is within the range of that associated with photon emission from the cerebrum during cognition (Saroka et al, 2013).

From a traditional heliogeophysical perspective, the ultimate source of the variation that produced the shifts in REG output while the person was intending originated from the sun. The results of the factor analysis indicated that the solar (distal) variables were less related than the proximal (interaction between the interplanetary magnetic field and global geomagnetic field) variables. However, there would be a physical coupling between the two sources. We suggest that a subset of energies originating from the sun and mediated through the interplanetary magnetic field (which is the sun's magnetic field) to the geomagnetic volume within which the person is immersed contributed to the REG changes. Because intention was required, one interpretation is that some component of solar-originating energies interacted with the processes associated with neurocognition.

The difference in polarity between the REG, that is positive or negative deviation, as a function of the location in which the subjects were tested may help reveal the potential source of the negative or positive drift in these studies. The "normal" room within which positive deviations occurred was measured after the experiment by a magnetometer which displayed these parameters: Resultant field: 46,770 nT, inclination: 70.6 deg. On the other hand these values within the Faraday cage (acoustic chamber) were: 19,822 nT and 53.8 deg respectively. The latter value is within the range of magnitude as that found along the equator where the imaginary shift in polarity between north and south pole flux lines would occur. However, because we did not test the REG in multiple sites which displayed similar intensities outside of the acoustic chamber, we cannot conclude if the direction of the REG deviation was due to unique location or the magnetic field discrepancy.

None of the solar-geomagnetic variables were associated with the entropy of the REG scores. The only category that displayed a statistically significant difference involved gender. This is

particularly interesting when compared to differences in statistical complexity for female-male EEG measures. Ahmadi et al. (2013) examined the complexity of EEG profiles using fractal dimensions. Although this method differs from entropy, when mean values of all EEG channels were averaged together within each gender the ratio of female-male complexity (as determined by fractal dimension) was strikingly similar to that obtained for REG entropy measures of female-male complexity (1.02 and 1.04 respectively). The presence of male-female difference in complexity may help explain an interesting historical pattern involved with spontaneous cases of "poltergeists". The ratio of females to males ranges between 2:1 to 20:1 depending upon the study. If the gender differences in electroencephalography and complexity are applicable, then the role of space-time geometry and the information within the matter affected by the proximity of these individuals could be investigated.

5.6 References

Ahmadi, K., Ahmadlou, M., Rezazade, M., Azad-Marzabadi, E., & Sajedi, F. (2013). Brain activity of women is more fractal than men. *Neuroscience Letters, 535*, 7-11.

Caswell, J. M., Collins, M. W. G., Vares, D. A. E., Juden-Kelly, L. M., & Persinger, M. A. (2013). Gravitational and experimental electromagnetic contributions to cerebral effects upon deviations from random number variations generated by electron tunneling. *International Letters of Chemistry, Physics and Astronomy, 11*, 72-85.

Caswell, J. M., Dotta, B. T., & Persinger, M. A. (2014a). Cerebral biophoton emission as a potential factor in non-local human machine interaction. *In Submission*.

Caswell, J. M., Vares, D. A. E., Juden-Kelly, L. M., & Persinger, M. A. (2014b). Simulated effects of sudden increases in electromagnetic activity on deviations in random electron tunneling behaviour associated with cognitive intention. *In Submission*.

Cheng-Yu, T. L., Poo, M. M., & Dan, Y. (2009). Burst spiking of a single cortical neuron modifies global brain state. *Science, 324*(5927), 643-646.

Cherry, N. (2002). Schumann resonances, a plausible biophysical mechanism for the human health effects of solar activity. *Natural Hazards, 26*(3), 279-331.

Chizhevsky, A. (1936). *The Terrestrial Echo of Solar Storms*. Mysl'Press, Moscow.

Clette, F., Berghmans, D., Vanlommel, P., Van der Linden, R. A. M., Koeckelenbergh, A., &

Wauters, L. (2007). From the Wolf number to the International Sunspot Index: 25 years of SIDC. *Advances in Space Research, 40*(7), 919-928.

Cutler, W. B., Schleidt, W. M., Friedmann, E., Preti, G., & Stine, R. (1987). Lunar influences on the reproductive cycle in women. *Human Biology, 59*(6).

Donnelly, R. F., Heath, D. F., Lean, J. L., & Rottman, G. J. (1983). Differences in the temporal variations of solar UV flux, 10.7-cm solar radio flux, sunspot number, and Ca-K plage data caused by solar rotation and active region evolution. *Journal of Geophysical Research: Space Physics, 88*(A12), 9883-9888.

Dotta, B. T., & Persinger, M. A. (2011). Increased photon emissions from the right but not the left hemisphere while imagining white light in the dark: The potential connection between consciousness and cerebral light. *Journal of Consciousness Exploration & Research, 2*(10), 1463-1473.

Dunne, B. J. (1998). Gender differences in human/machine anomalies. *Journal of Scientific Exploration, 12*(1), 3-55.

Friis-Christensen, E., Lassen, K., Wilhjelm, J., Wilcox, J. M., Gonzalez, W., & Colburn, D. S. (1972). Critical component of the interplanetary magnetic field responsible for large geomagnetic effects in the polar cap. *Journal of Geophysical Research, 77*(19), 3371-

3376.

Giroldini, W. (1991). Eccles's model of mind-brain interaction and psychokinesis: A preliminary study. *Journal of Scientific Exploration, 5*(2), 145-161.

Gissurarson, L. R. (1992). The psychokinesis effect: Geomagnetic influence, age and sex differences. *Journal of Scientific Exploration, 6*(2), 157-165.

Gumarova, L., Lissen, G. C., Hillman, D., & Halberg, F. (2012). Geographically selective assortment of cycles in pandemics: Meta-analysis of data collected by Chizhevsky. *America, 12,* 15.

Halberg, F., Cornelissen, G., Otsuka, K., Katinas, G., & Schwartzkopff, O. (2001). Essays on chronomics spawned by transdisciplinary chronobiology. *Neuroendocrinology Letters, 22*(5), 359-384.

Herrman, P. L. (2012). Glossary of terms for the data available in the N0NBH solar banners. Retrieved from http://www.hamqsl.com/Glossary.pdf

Holzer, T. E. (1989). Interaction between the solar wind and the interstellar medium. *Annual Review of Astronomy & Astrophysics, 27*, 199-234.

Houweling, A. R. & Brecht, M. (2007). Behavioural report of single neuron stimulation in somatosensory cortex. *Nature, 451*(7174), 65-68.

Hundhausen, A. J., Sawyer, C. B., House, L., Illing, R. M. E., & Wagner, W. J. (1984). Coronal mass ejections observed during the Solar Maximum Mission: Latitude distribution and rate of occurrence. *Journal of Geophysical Research: Space Physics, 89*(A5), 2639-2646.

Jahn, R. G., Dunne, B. J., Nelson, R. D., Dobyns, Y. H., & Bradish, G. J. (1997). Correlations of random binary sequences with pre-stated operator intention: A review of a 12-year program. *Journal of Scientific Exploration, 11*(3), 345-367.

Kahler, S. W., Hildner, E., & Van Hollebeke, M. A. I. (1978). Prompt solar proton events and coronal mass ejections. *Solar Physics, 57*(2), 429-443.

Levine, R. H., Altschuler, M. D., & Harvey, J. W. (1977). Solar sources of the interplanetary magnetic field and solar wind. *Journal of Geophysical Research, 82*(7), 1061-1065.

McComas, D. J., Bame, S. J., Barker, P., Feldman, W. C., Phillips, J. L., Riley, P., & Griffee, J. W. (1998). Solar wind electron proton alpha monitor (SWEPAM) for the Advanced Composition Explorer. In C. Russell, R. Mewaldt & T. Von Rosenvinge (Eds.), *The Advanced Composition Explorer Mission* (pp. 563-612). Netherlands: Springer Netherlands.

Nelson, R. D., Jahn, R. G., Dobyns, Y. H., & Dunne, B. J. (2000). Contributions to variance in REG experiments: ANOVA models and specialized subsidiary analyses. *Journal of*

Scientific Exploration, 14(1), 73-89.

Neupert, W. M. (1968). Comparison of solar x-ray line emission with microwave emission during flares. *The Astrophysical Journal, 153*, 59-64.

Persinger, M. A. (1999). Wars and increased solar-geomagnetic activity: Aggression or change in intraspecies dominance?. *Perceptual and Motor Skills, 88*, 1351-1355.

Persinger, M. A., & St-Pierre, L. (2014). Is there a geomagnetic component to variation in G?. *In submission*.

Pogorelov, N. V., Zank, G. P., & Ogino, T. (2004). Three-dimensional features of the outer heliosphere due to coupling between the interstellar and interplanetary magnetic fields: I. Magnetohydrodynamic model: Interstellar Perspective. *The Astrophysical Journal, 614*(2), 1007.

Radin, D. I., & Nelson, R. D. (2003). Meta-analysis of mind-matter interaction experiments: 1959-2000. In *Healing, Intention, and Energy Medicine* (pp. 39-48). London: Harcourt Health Sciences.

Saroka, K. S., Dotta, B. T., & Persinger, M. A. (2013). Concurrent photon emission, changes in quantitative brain activity over the right hemisphere, and alterations in the proximal geomagnetic field while imagining white light. *International Journal of Neuroscience,*

3(1), 30-34.

Schove, D. J. (1955). The sunspot cycle, 649 B.C. to A.D. 2000. *Journal of Geophysical Research, 60*(2), 127-146.

Shannon, C. E. (1948). A mathematical theory of communication. *The Bell System Technical Journal, 27*, 379-423, 623-656.

Shea, M. A., & Smart, D. F. (1990). A summary of major solar proton events. *Solar Physics, 127*(2), 297-320.

Sheeley, N. R., Howard, R. A., Koomen, M. J., & Michels, D. J. (1983). Associations between coronal mass ejections and soft x-ray events. *The Astrophysical Journal, 272*, 349-354.

Tapping, K. F. (1987). Recent solar radio astronomy at centimeter wavelengths: The temporal variability of the 10.7-cm flux. *Journal of Geophysical Research: Atmospheres, 92*(D1), 829-838.

Thomas, B. T., & Smith, E. J. (1980). The Parker spiral configuration of the interplanetary magnetic field between 1 and 8.5 AU. *Journal of Geophysical Research: Space Physics, 85*(A12), 6861-6867.

Thompson, R. (2013). Meaning of x-ray fluxes from the sun. Retrieved from http://www.ips.gov.au/Educational/2/1/3

Thomson, N. R., Rodger, C. J., & Dowden, R. L. (2004). Ionosphere gives size of greatest solar flare. *Geophysical Research Letters, 31*(6).

Chapter 6 - A Nonlinear Autoregressive Approach to Statistical Prediction of Disturbance Storm Time Geomagnetic Fluctuations Using Solar Data

Published in *Journal of Signal and Information Processing*

6.1 Abstract

A nonlinear autoregressive approach with exogenous input is used as a novel method for statistical forecasting of the disturbance storm time index, a measure of space weather related to the ring current which surrounds the Earth, and fluctuations in disturbance storm time field strength as a result of incoming solar particles. This ring current produces a magnetic field which opposes the planetary geomagnetic field. Given the occurrence of solar activity hours or days before subsequent geomagnetic fluctuations and the potential effects geomagnetic storms have on terrestrial systems, it would be useful to be able to predict geophysical parameters in advance using both historical disturbance storm time indices and external input of solar winds and the interplanetary magnetic field. By assessing various statistical techniques it is determined that artificial neural networks may be ideal for the prediction of disturbance storm time index values which may in turn be used to forecast geomagnetic storms. Furthermore, it is found that a Bayesian regularization neural network algorithm may be the most accurate model compared to both other forms of artificial neural network used and linear models employing regression analyses.

6.2 Introduction

Artificial Neural Networks

Many complex system interactions are present throughout the disciplines of geophysics and associated solar dynamics. A number of these processes remain outside the capability of standard statistical procedures, requiring equally complex computational models in order to more accurately reflect physical relationships. Artificial neural networks (ANN) form the basis for a number of computational models based on the mammalian brain. Instead of relying on linear correlative relationships among a particular dataset, ANNs are a form of machine learning in which the system learns to recognize an output variable based on an input variable series (Erguo & JinShou, 2002). Data is processed through a number of interconnected 'neurons' which form 'synaptic connections' from the input nodes through a hidden layer before converging on the output neurons (e.g., *Figure 41*). Each input and hidden neuron consists of statistical weights which are capable of adaptation (Mehrotra et al., 1997), the exact parameters of which are modified by an algorithm over the course of network training procedures. These weights essentially form the synaptic connections between neurons which activate during network construction. This form of computation is capable of operating in parallel units, much like the human nervous system. Because neural networks do not rely on linear correlations for learning, ANNs are capable of nonlinear modelling and may therefore provide a useful alternative approach to a number of both theoretical and real world problems. This includes geo and solar physics (Boynton et al., 2013), medical diagnosis (Khan et al., 2001), pattern recognition (Looney, 1997), and many other areas. The nonlinear approach used in ANN computations is particularly useful in the context of highly complex or 'noisy' datasets.

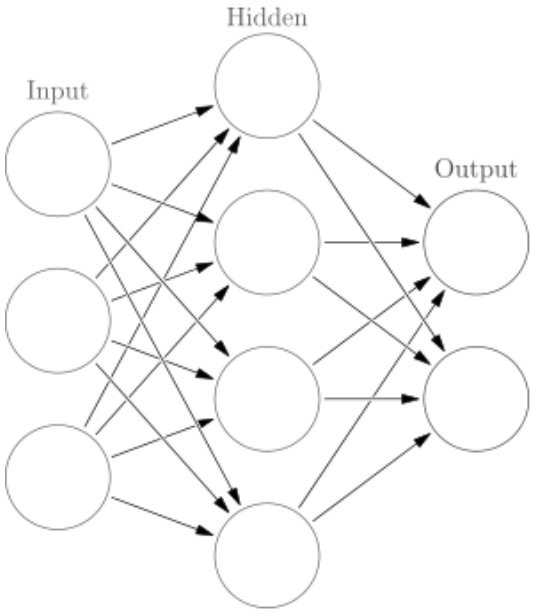

Figure 41 - Feedforward artificial neural network diagram; input layer neurons, hidden layer neurons, output neuron(s), lines indicate data weights ('synaptic connections')

Image source: Glosser.ca

Backpropagation algorithms constitute a primary basis for the construction of ANNs (Widrow & Lehr, 1990). In general backpropagation, the delta rule is employed for updating the statistical weights of each neuron in the network using a gradient descent (Leonard & Kramer, 1990). An activation function is applied to artificial neurons in both the input and hidden layers, which in this case was a sigmoid function (e.g., *Figure 42*):

$$\phi(t) = (1 + e(-t))^{-t}$$

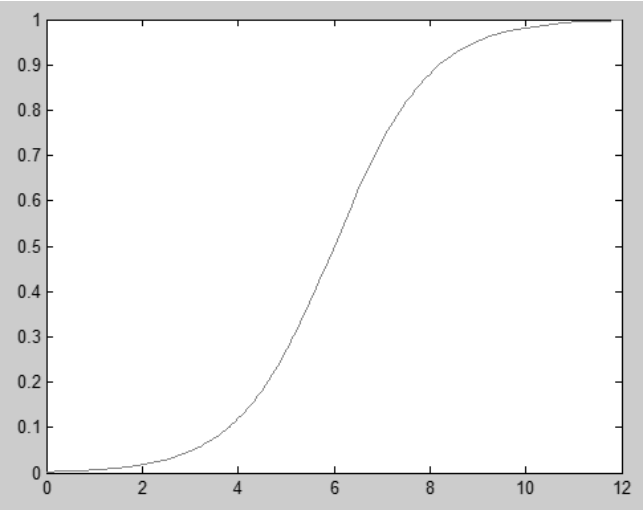

Figure 42 - Plotted sigmoid function (logistic curve)

One of the primary training algorithms employed in ANN modelling is the Levenberg Marquadt algorithm (LMANN). This particular method is a standard backpropagation curve fitting algorithm typically employed to solve generic problems using a damped least squares process (Levenberg, 1944). While the LMANN option is a popular choice, it is capable of obtaining a local minimum only, and is therefore not always ideal for greater generalization (Mahintakumar & Sayeed, 2005). However, a neural network trained using a Bayesian regularization algorithm (BRANN) has been shown to possess greater generalization than other ANNs and have demonstrated more robust results overall compared to standard backpropagation networks (Burden & Winkler, 2008). There are a number of other benefits associated with this particular learning algorithm summarized by Burden & Winkler (2008), including reduced probability of network 'overtraining' or overfitting, reduced difficulty in cross validation, and more effective stopping procedures. Overfitting refers to a resultant model which describes random noise as opposed to the intended output, which will subsequently have poor overall predictive performance by overemphasizing minute data fluctuations. By integrating Bayesian probabilities,

this also allows for greater accuracy in network learning; probabilities associated with artificial neuron weights are updated according to newly observed data using a likelihood function which compares a standard Gaussian function with the updated observations:

$$L(\theta \mid x)=P(x|\theta), \text{ where } \theta=\text{set of parameters, } x=\text{observed parameter outcomes}$$

In the following analyses, two training algorithms were employed using a nonlinear autoregressive exogenous network (NARX). This particular form of ANN is used in time series modelling (Menezes Jr. & Barreto, 2008) in order to predict an outcome variable [$y(t)$] based on both d past values of the outcome variable and current and d past values of an external source of influence [$x(t)$], as illustrated by

$$y(t)=f(x(t\text{-}1),\ldots,x(t\text{-}d),y(t\text{-}1),\ldots,y(t\text{-}d))$$

The fit of predicted output values can be compared to the original target values using simple correlation coefficients (Oliveira et al., 2013), while an error term is also employed in order to further gauge predictive accuracy, typically presented as some form of mean or summed squared error term (target-output).

ANNs and Space Weather

A number of novel approaches to space weather dynamics have been examined using ANN models. Many of these models possess useful real world applications which enable researchers to predict future values associated with various geo and solar physical systems. The NARX form of network used in this study was previously employed by Oliveira et al. (2013) in order to simulate conditions of the interplanetary magnetic field (IMF) using ground observations associated with cosmic rays as the exogenous input. Furthermore, the disturbance storm time (DST) index, which

was also the focus of this study, was recently examined using various measures of solar winds and the IMF (Boynton et al., 2013). The present study focuses on daily averages of simple, untransformed values obtained from a freely available online source (omniweb.gsfc.nasa.gov).

Solar Geomagnetic Activity

The Earth's magnetic field has an average static background intensity of ~50,000 nT (Saroka et al., 2014). Despite this relatively weak value, variations in geomagnetic activity have been shown to affect terrestrial systems including electronics and power systems (Boteler, 2001), and human health (Mulligan et al., 2010), while even small perturbations of ~20 to 40 nT have been related to alterations in brain activity associated with altered states of consciousness (Saroka et al., 2014). One of many measures associated with geomagnetic activity, the DST index refers to the varying power of the ring current which surrounds the geosphere. The subsequent DST magnetic field opposes the geomagnetic field such that decreases in DST index accompany increases in geomagnetic activity. This specific measure is particularly useful in studying solar geophysical interactions given that the DST ring current is produced as a result of solar particle streams (Leske et al., 1995), and also has direct correlations with the geomagnetic field. Furthermore, there are a number of complex relationships previously noted between various sources of solar activity and geomagnetic fluctuations (Zhang et al., 2007). Given the large number of solar factors found to have potential relationships with geomagnetic activity, it would be beneficial to identify an optimal statistical model for forecasting geomagnetic storms based on a simple subset of input variables. This would allow for potential early warning systems to be placed in effect at relevant institutions regarding future geomagnetic perturbations.

6.3 Methods

Geomagnetic and Solar Data

A number of predictive models were constructed using varying statistical methods of both linear and nonlinear processes. In each, the disturbance storm time (DST) index was used as the target variable to be predicted, while a number of solar wind and interplanetary magnetic field (IMF) measures were employed as independent variables (*Bx*, *By*, and *Bz* components of the IMF in nT, solar wind proton density in $N \cdot cm^{-3}$, solar wind plasma speed in $km \cdot s^{-1}$, and plasma flow pressure in nPa). A total of N = 1460 daily averages were obtained from January 1, 2009 to December 31, 2012. All data was obtained from the GSFC (Goddard Space Flight Center) / SPDF (Space Physics Data Facility) OMNIWeb interface (omniweb.gsfc.nasa.gov).

Statistical Methods

Five separate models were computed with varying forms of artificial neural network (ANN) and regression analyses using both Matlab 2011a and SPSS 17 software.

An ANN was constructed using Matlab in order to produce a nonlinear autoregressive network with exogenous input (NARX). DST index was entered as the target variable with 6 feedback delays specified for the autoregressive function, and 6 input delays also specified for the exogenous input. A single hidden layer was deemed adequate for this particular problem with 10 hidden neurons (HN) specified (*Figure 43*). Data was segmented into three sets using the *divideblock* function in order to maintain temporal characteristics of the time series. A total of 70% was allocated for training, with 15% of cases used in both validation and testing trials. Neural network learning was limited to a maximum of 1000 epochs a priori. Initial neural

weights were randomized. Two training algorithms were employed for comparison; Bayesian regularization (BRANN) and Levenberg Marquadt (LMANN).

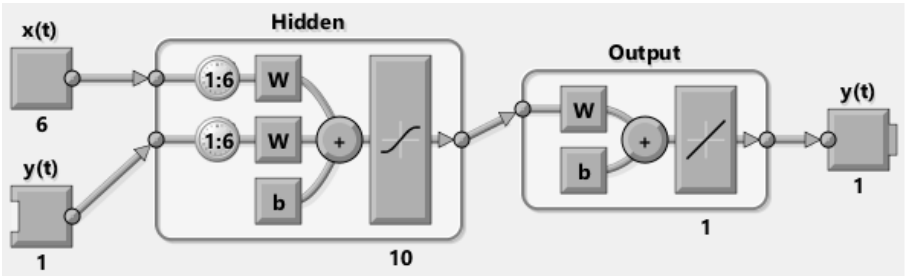

Figure 43 - NARX network architecture; input layer consisting of x (6 variable exogenous input time series) and y (single variable autoregressive time series), 6 exogenous input delays and 6 feedback delays, 10 hidden layer neurons with single bias node and sigmoid activation function, single target (output) time series y

A third variation of nonautoregressive ANN was constructed using SPSS Multilayer Perceptron (MLPANN) module with sigmoid hidden and output layer activation functions. Network hidden layer architecture was constructed according to previous specifications obtained in Matlab (single hidden layer, 10 HN), with 70% of cases allocated to training and the remaining 30% used for testing.

For linear comparison, regression analyses were conducted using both full variable and stepwise variable entry.

6.4 Results

NARX: Bayesian Regularization

A NARX neural network constructed with Matlab software using a BRANN algorithm converged upon a solution after the maximum allowed number of iterations (1000). There were no

significant error crosscorrelation or autocorrelation issues identified (e.g., *Figure 44*). The Bayesian method obtained highly significant ($p < .001$) correlations between output and target data (*Figure 45*; $r = .918$, *rho* = .84).

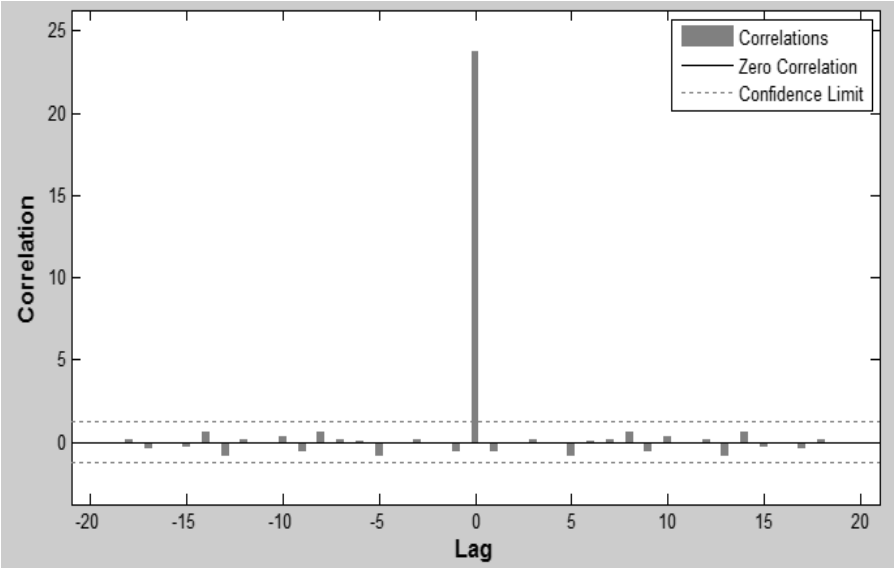

Figure 44 - BRANN error (target-output) autocorrelation

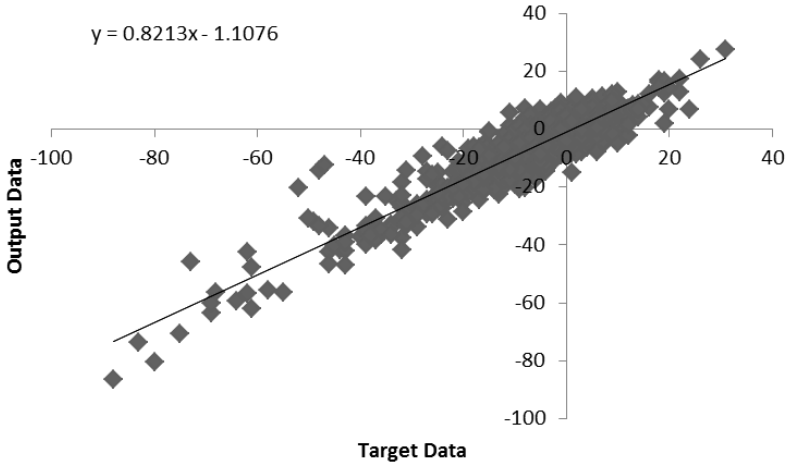

Figure 45 - Correlation between original (target) and predicted (output) DST index values obtained with BRANN

NARX: Levenberg Marquadt

Matlab was again utilized and a secondary NARX network was constructed by substituting the previous training with an LMANN algorithm. Again, there were no error crosscorrelation or autocorrelation issues identified. This particular network revealed significant ($p < .001$) correlations between target and output data (*Figure 46*; $r = .732$, $rho = .747$), although not as strong as that obtained using BRANN.

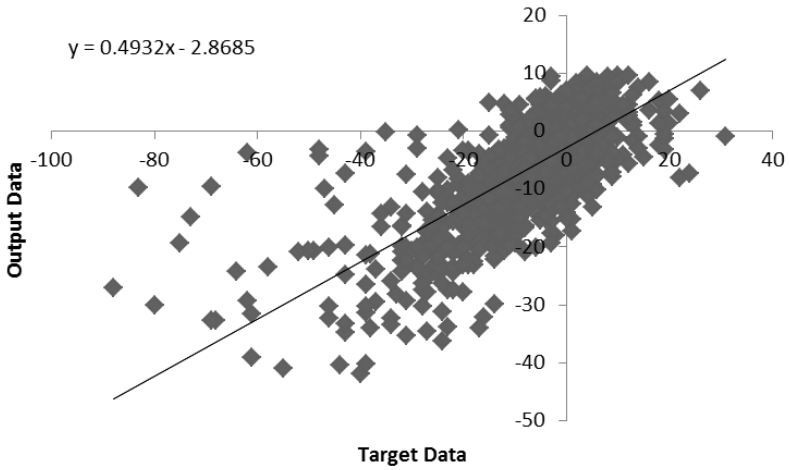

Figure 46 - Correlation between original (target) and predicted (output) DST index values obtained with LMANN

Non-Autoregressive: Multilayer Perceptron

Using a nonautoregressive neural network, MLPANN was used to predict DST indices based solely on the input and hidden layers. This particular method revealed a significant correlation ($p < .001$) closer to that found with the LMANN analysis (*Figure 47*; $r = .706$, $rho = .663$). Additional independent importance analysis revealed that the *Bz* component of the IMF and solar wind proton density had the greatest connection to the output layer (*Figure 48*).

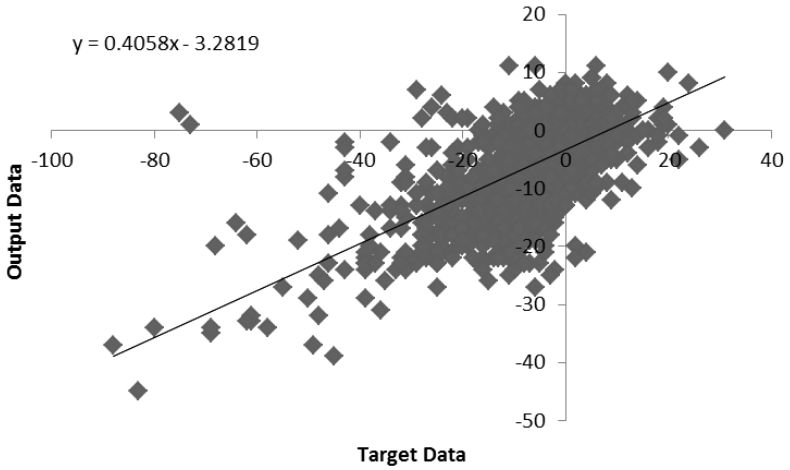

Figure 47 - Correlation between original (target) and predicted (output) DST index values obtained with MLPANN

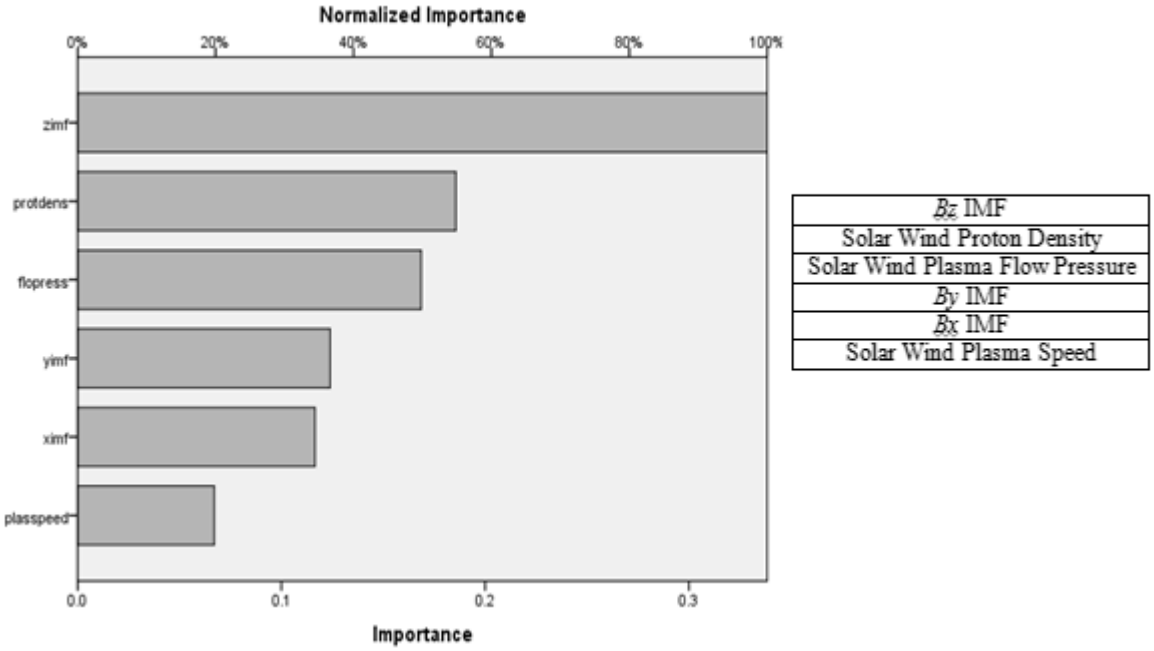

Figure 48 - Independent importance of each input variable as related to the connection with DST index

LR Enter

A linear regression (LR) was performed for further comparison of statistical predictive power. The first model was obtained by entering all predictor variables. A significant regression was revealed ($F_{(6,\ 1459)} = 165.295$, $p < .001$, adj. $R^2 = .403$). The Durbin Watson statistic (.935) indicated minute potential autocorrelations in the data (*Figure 49*). All variance inflation factors were < 10 suggesting no issues of multicollinearity. Significant correlations ($p < .001$) were obtained between target and predicted values (*Figure 50*; $r = .637$, *rho* = .634), but the relationship identified was reduced in power compared to ANN methods.

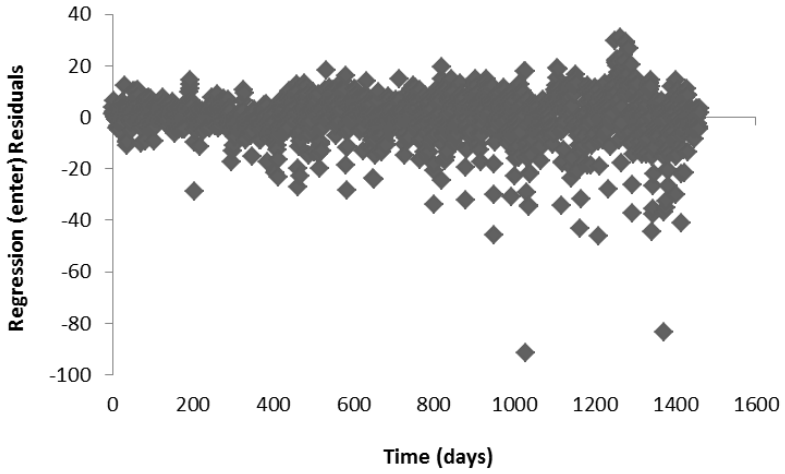

Figure 49 - Potential weak autocorrelation in regression model (LR enter)

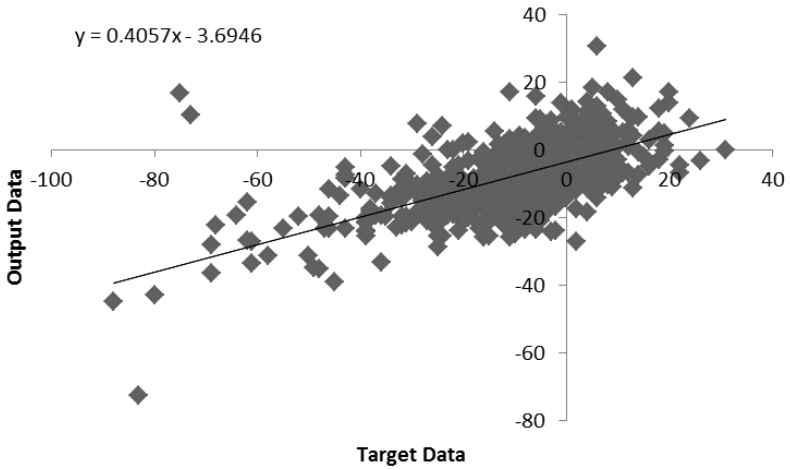

Figure 50 - Correlation between original (target) and predicted (output) DST index values obtained with LR enter

LR Stepwise

A secondary LR analysis was conducted using a stepwise method of variable entry for theoretically improved accuracy of results. The only predictor variables to enter the equation were plasma speed and the *Bz* component of the IMF. A significant regression was identified ($F_{(2, 1459)} = 458.729$, $p < .001$, adj. $R^2 = .386$), although the Durbin Watson statistic (.933) again suggested potential data autocorrelations (*Figure 51*). There were no issues of multicollinearity according to the variance inflation factor statistics (all VIF < 10). Again, significant correlations ($p < .001$) were obtained between target and predicted data (*Figure 52*; $r = .622$, *rho* = .622), which were also reduced in coefficient strength compared to ANN methods.

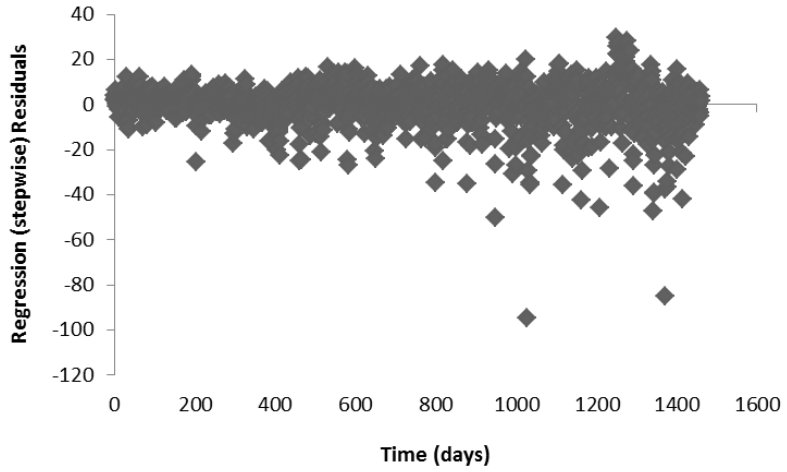

Figure 51 - Potential autocorrelation in regression model (LR stepwise)

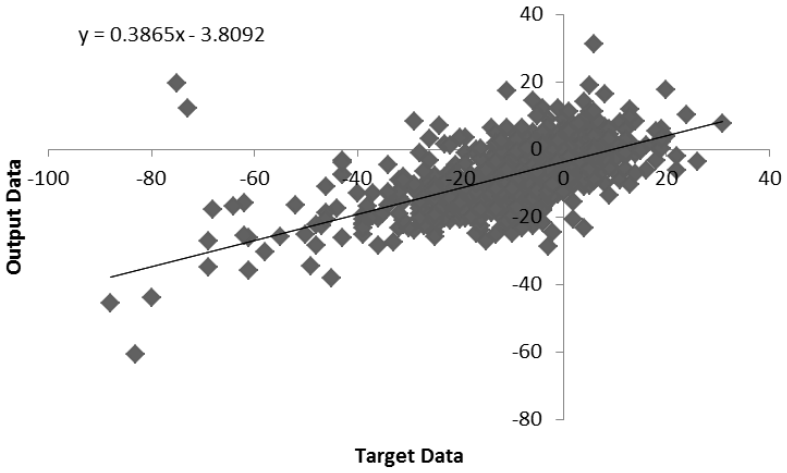

Figure 52 - Correlation between original (target) and predicted (output) DST index values obtained with LR stepwise

Fit Comparisons

A Fisher *r* to *z* transformation ($z = .5[\ln(1 + r) - \ln(1 - r)]$) was applied to pairings of correlation coefficients and compared using a simple z-test ($[z_1 - z_2]/\sqrt{[(\sigma_1 / n_1) + (\sigma_2 / n_2)]}$) in order to determine significant differences in final output of each model.

The BRANN model prediction correlation was significantly greater ($p < .0001$) than LMANN ($z = 17.35$), MLPANN ($z = 18.81$), LR enter ($z = 22.21$), and LR stepwise ($z = 22.88$). LMANN and MLPANN methods did not differ significantly ($z = 1.45$, $p > .05$). However, the LMANN algorithm prediction coefficients were significantly greater ($p < .0001$) than both LR enter ($z = 4.85$) and LR stepwise ($z = 5.52$). MLPANN method also revealed predictive coefficients which were greater ($p < .0001$) than both LR enter ($z = 3.4$) and LR stepwise ($z = 4.07$).

Average Accuracy

Overall measures of performance error (target-output) were obtained as the root mean squared error (RMSE) of each model and were similarly reflective of a clear hierarchy in model accuracy, the values of which are summarized in *Table 13*. These results suggest that neural network methods produce a greater predictive capacity for both fit and accuracy in the context of DST index and solar winds compared to more traditional regression methods, while the Bayesian regularization (BRANN) algorithm was superior to other variations of ANN (*Figure 53*). This method was far more accurate regarding both the direction and magnitude of target values as demonstrated by the clear distinctive features shown in *Figure 54* and *Figure 55*.

Model	Pearson *r*	RMSE
BRANN	.918	3.784
LMANN	.732	8.371
MLPANN	.706	9.482
LR enter	.637	9.418
LR stepwise	.622	9.569

Table 13 - Fit (r) and performance error (RMSE) of each statistical model

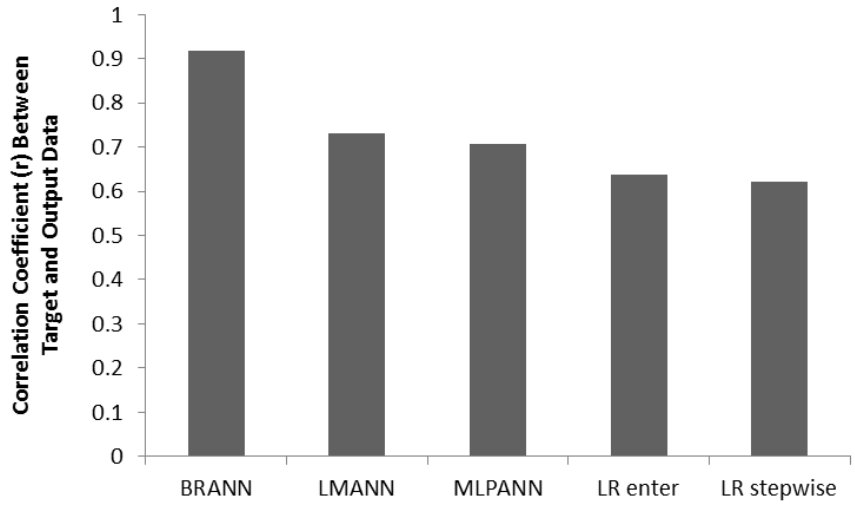

Figure 53 - Correlation coefficients (r) for predictive fit of each model

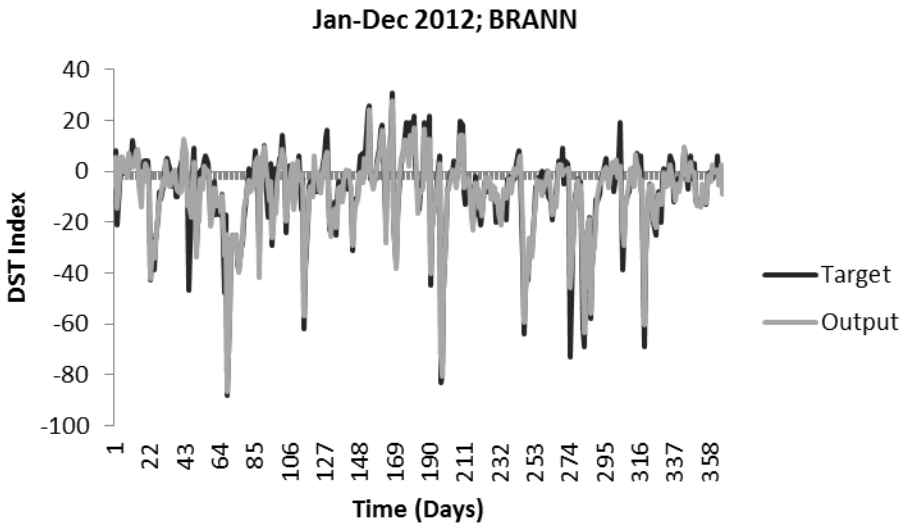

Figure 54 - Target (original) and output (predicted) DST index values for 2012 using the BRANN algorithm

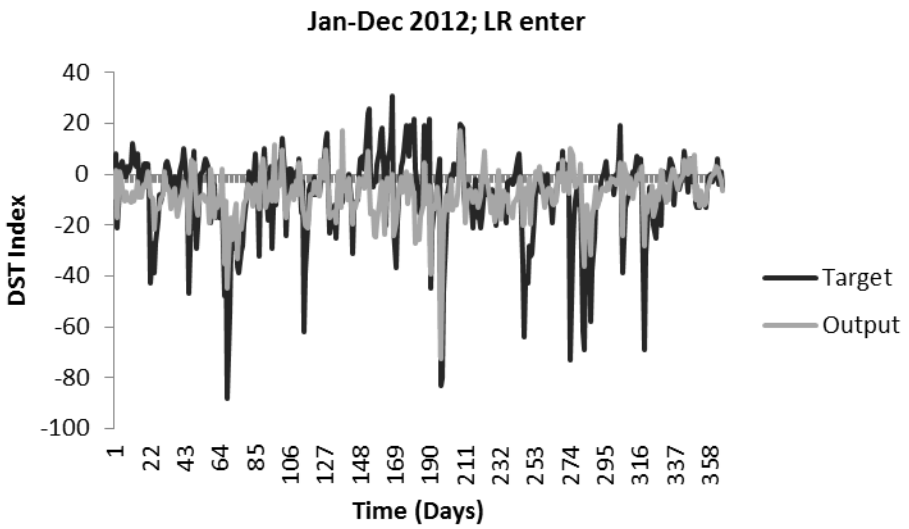

Figure 55 - Target (original) and output (predicted) DST index values for 2012 using linear regression (enter all variables)

6.5 Discussion

The results of this analysis appear to confirm those from a number of previous studies which have suggested that ANN models are more accurate compared to simple regressions for many applications (e.g., Jefferson et al., 1997; Eftkhar et al., 2005). While the NARX models used relied on past values of the DST index, there was a significantly greater target to output fit apparent for the MLPANN network compared to regression analyses, which did not utilize DST feedback. There was a clear hierarchy of statistical models in the present analyses indicated by both fit (*r*) and overall accuracy (RMSE); models from greatest to least relative fit/accuracy were BRANN, LMANN, MLPANN, LR enter, LR stepwise.

The Bayesian regularization algorithm for neural network training has previously been implicated as a superior model compared to other network algorithms (Burden & Winkler, 2008). This appears to be the case in the context of DST autoregressive prediction with solar wind input. It is

clear that Bayesian probabilities are well suited to neural network learning for DST forecasting given the adaptive neural weights updated over the course of network construction based on new probabilities. Furthermore, regression models typically require *a priori* knowledge of variable interactions for accurate forecast implementation, while neural networks are capable of learning from an array of related measures and producing a highly accurate model. Standard regression models also tend to ignore non-linear effects which may be present, particularly in noisy datasets, or time series data with no clear linear relationship. It may also be important to note that the NARX model is capable of both open and closed loop performance and can be used to predict a step beyond an available dataset with associated performance measures. However, there are clear benefits to employing a range of statistical methods when interpreting complex interactions in order to gain a fuller picture of the system in question.

It is also interesting to note that the *Bz* component of the IMF was consistently identified as the greatest shared source of variance with geomagnetic disturbances, along with the speed and proton density of solar winds. This assemblage of contributing factors has previously been identified in the context of geomagnetic activity including *Bz*, particle density, and velocity of solar winds with DST index (Lundstedt et al., 2002). Modelling of DST variations was later examined using more complex methods of data transformation and analysis on a wider array of input measures (Boynton et al., 2013).

In the present study, the effects of solar wind variations are demonstrated using a range of input measures and statistical methods, which clearly demonstrate the enhanced potential for ANN models compared to more traditional statistical methods. Prior analyses also suggested that network performance improved with the addition of a greater range of IMF variables (e.g., *Bx*, *By*, *Bz*), which was also previously suggested by Boynton et al. (2013). However, network

performance was reduced in magnitude with the addition of solar wind temperature in the input layer. The NARX networks still managed to outperform other models using untransformed variables of simple daily averages. Additionally, all data is freely available from an online source (omniweb.gsfc.nasa.gov) open to any researcher interested in constructing models relevant to their own location.

Similarly, local forecasting with ANNs has proven effective in a number of areas and may be useful for predicting a range of events. Accurate modelling of solar and geomagnetic interactions is a particularly useful endeavor when considering the increasing reliance on technology civilization has reached. Given the known effects of geomagnetic storms on electrical systems, and even the significant effects of small geomagnetic perturbations on neurophysiology (e.g., Saroka et al., 2014), monitoring and forecasting of this phenomenon is increasingly vital. This is particularly prominent for satellite systems outside of the planetary atmosphere which may be quite sensitive to variations in ring current activity.

That powerful statistical software is widely available is also a tremendous boon to statistical modelling and related research endeavors; the complicated computations required for ANN methods are now easily employed in standard mathematical software, making relatively intimidating methods more accessible to the average researcher. Neural network predictions can be very powerful tools for both local and global predictions and can potentially be used to improve traditional models. ANN methods should be further investigated for potential applicability in better prediction of geomagnetic variations and storm level events, as well as to further elucidate the complex interconnections between solar and geophysical parameters.

6.6 References

Boteler, D. H. (2001). Assessment of geomagnetic hazard to power systems in Canada. *Natural Hazards, 23*(1-2), 101-120.

Boynton, R. J., Balikhin, M. A., Billings, S. A., & Amariutei, O. A. (2013). Application of nonlinear autoregressive moving average exogenous input models to geospace: Advances in understanding and space weather forecasts. *Annales Geophysicae, 31*, 1579-1589.

Burden, F., & Winkler, D. (2008). An empirical relationship between interplanetary conditions and DST. *Methods in Molecular Biology*, 458, 25-44.

Eftekhar, B., Mohammad, K., Eftekhar Ardebili, H., Ghodsi, M., & Ketabchi, E. (2005). Comparison of artificial neural network and logistic regression models for prediction of mortality in head trauma based on initial clinical data. *BMC Bioinformatics and Decision Making, 5*(3).

Erguo, L., & JinShou, Y. (2002). An input-training neural network based nonlinear principal component analysis approach for fault diagnosis. *Proceedings of the 4th World Congress on Intelligent Control and Automation, 4*, 2755, 2759.

Jefferson, M. F., Pendleton, N., Lucas, S. B., & Horan, M. A. (1997). Comparison of a genetic algorithm neural network with logistic regression for predicting outcome after surgery for patients with non-small cell lung carcinoma. *Cancer, 79*, 1338-1342.

Khan, J., Wei, J. S., Ringner, M., Saal, L. H., Ladanyi, M., Westermann, F., Berthold, F., Schwab, M., Antonescu, C. R., Peterson, C., & Meltzer, P. S. (2001). Classification and diagnostic prediction of cancers using gene expression profiling and artificial neural networks. *Nature Medicine, 7*, 673-679.

Leonard, J., & Kramer, M. A. (1990). Improvement of the backpropagation algorithm for training neural networks. *Computers & Chemical Engineering, 14*(3), 337-341.

Leske, R. A., Cummings, J. R., Mewaldt, R. A., Stone, E. C., & von Rosenvinge, T. T. (1995). Measurements of the ionic charge states of solar energetic particles using the geomagnetic field. *The Astrophysical Journal Letters, 452*(2).

Levenberg, K. (1944). A method for the solution of certain non-linear problems in least squares. *Quarterly of Applied Mathematics, 2*, 164-168.

Looney, C. G. (1997). *Pattern Recognition Using Neural Networks: Theory and Algorithms for Engineers and Scientists*. Oxford University Press.

Lundstedt, H., Gleisner, H., & Wintoft, P. (2002). Operational forecasts of the geomagnetic DST index. *Geophysical Research Letters, 29*(24), 2181.

Mahintakumar, G., & Sayeed, M. (2005). Hybrid genetic algorithm: Local search methods for solving groundwater source identification inverse problems. *Journal of Water Resources*

Planning and Management, 131(1), 45-47.

Mehrotra, K., Mohan, C. K., & Ranka, S. (1997). *Elements of Artificial Neural Networks*. MIT Press.

Menezes Jr., J. M. P., & Barreto, G. A. (2008). Long-term time series prediction with the NARX network: An empirical evaluation. *Neurocomputing, 71*(16-18), 3335-3343.

Mulligan, B. P., Hunter, M. D., & Persinger, M. A. (2010). Effects of geomagnetic activity and atmospheric power variations on quantitative measures of brain activity: Replication of Azerbaijani studies. *Advances in Space Research, 45*(7), 940-948.

Oliveira, A. G., Silva, M. R., Echer, E., Dal Lago, A., Braga, C. R., Mendonca, R. R. S., Schuck, N. J., Munakata, K., & Kuwabara, T. (2013). Simulations of the interplanetary magnetic field conditions with NARX networks. *33rd International Cosmic Ray Conference, The Astroparticle Physics Conference Proceedings*.

Saroka, K. S., Caswell, J. M., Lapointe, A., & Persinger, M. A. (2014). Greater electroencephalographic coherence between left and right temporal lobe structures during increased geomagnetic activity. *Neuroscience Letters, 560*, 126-130.

Widrow, B., & Lehr, M. A. (1990). 30 years of adaptive neural networks: Perceptron, Madaline, and backpropagation. *Proceedings of the IEEE, 78*(9), 1415-1442.

Zhang, J., Richardson, I. G., Webb, D. F., Gopalswamy, N., Huttunen, E., Kasper, J. C., Nitta, N. V., Poomvises, W., Thompson, B. J., Wu, C. C., Yashiro, S., & Zhukov, A. N. (2007). Solar and interplanetary sources of major geomagnetic storms (DST<-100 nT) during 1996-2005. *Journal of Geophysical Research – Space Physics, 112*(a10).

Chapter 7 – Discussion

7.1 Conclusions

The preceding series of experiments lends support to the decades of research suggesting that human intention appears capable of influencing the outcome of non-deterministic, random physical systems (e.g., Jahn et al., 1997). As with previous research, the effect sizes are often relatively small but consistently significant. Rather than simply producing further 'proof-of-psi' results, the findings from these studies identify a number of potential correlates of successful performance in the context of the consciousness-correlated collapse (3C) phenomenon.

The current results strongly implicate fundamental forces as factors in the process of apparent 3C interaction, particularly electromagnetism. Previous studies have shown that shamanic states of consciousness may be more conducive to successful psi phenomena, or non-local interactions with consciousness, than traditional parapsychology paradigms (Rock & Storm, 2010). Given the dominant theoretical constructs which currently drive the emerging subdisciplines of both neuroquantology and paranthropology (e.g., Persinger et al., 2010; Miller, 2012), it was initially suggested that transcerebral application of specific physiologically-patterned electromagnetic fields (EMF) associated with altered states of consciousness (ASC) might enhance the occurrence and/or magnitude of the 3C phenomenon. However, further research in the area of neurophysiology also lends support to this theory by implicating specific neural correlates of a psi-process, including the right parahippocampal gyrus (Persinger & Saroka, 2012).

The current research (Chapter 2) revealed significant 3C performance correlated with human intention during periods where participants received EMFs associated with the induction of ASCs (e.g., Cook & Persinger, 1997). This appears to confirm the initial theory underlying this

experiment. Further analysis of specific field parameters revealed support for the previous association of the right hippocampus with non-local consciousness processes by showing a greatly enhanced effect for participants who received an EMF patterned after the hippocampus applied to the right hemisphere compared to an amygdaloid field application over the left hemisphere. While this transcerebral application of specific patterned EMFs lends support to theories of psi related to both cross-cultural contexts (e.g., shamanism) and neurophysiology, further research into the role of EMFs appears to suggest that altering the field parameters away from physiological functions may produce the opposite effect.

Subsequent experiments (Chapter 4) employed full-body exposure of a non-physiological EMF in which the participant and random event generator (REG) device were immersed. Results suggest that application of electromagnetic 'noise' may actually interfere with successful 3C interaction. However, there are at least two potential theories which could explain this effect. The most obvious conclusion is that immersion in electromagnetic noise may simply interfere with whatever fundamental processes underlie the 3C phenomenon; whether this process is driven by a complex EMF configuration or electromagnetic particles (photons), it may be that a non-physiological EMF 'blocks' this form of consciousness-driven non-local signal transmission or distorts it in some way so that REG output remains unaffected by cognitive intention to any obvious extent. Furthermore, constant application of an EMF to the REG device itself appears to potentially affect subsequent results by reducing the overall data complexity produced.

The second hypothesis involves a much more relatively exotic theoretical approach, although this has been supported experimentally. Previous research has indicated that space itself may be capable of conditioning through application of specific EMFs; this anomalous process has been shown to occur in the context of both photon emission (Persinger & Dotta, 2011) and water pH

levels (Dotta et al., 2013). If electromagnetic fields can indeed condition space in order to 'retrieve' a specific pattern of output at a later time, then perhaps consecutive application of the same field parameters may have conditioned the REG test area to produce consistently poor results in this specific experiment only. Given that photons are the quanta of electromagnetic radiation, and biophoton emissions (BPE) have been associated with psi processes (e.g., Hunter et al., 2010), it may be that the majority of participants who achieved non-significant results could have 'conditioned' the proximal space which the EMF then stored. Subsequent testing may have been partially influenced by previous experiments during periods of field application. Although this second possibility is far less likely in this particular scenario, it should not be discarded without further investigation.

Aside from the fundamental force of electromagnetism, the current research (Chapter 2) has also implicated gravitational contributions as a potential factor in the phenomenon of 3C. Given the previous associations between anomalous psi interactions and the brain itself, it was suggested that the fundamental unit of neuroscience (Persinger, 2010), the action potential ($1.9 \cdot 10^{-20}$ J), would be a good candidate for the energy band on which 3C likely operates. Subsequent dimensional analyses identified further sources of this particular energy band which could potentially influence the cerebral volume; the gravitational energy from the Earth applied across the cell membrane (10 μm) is $\sim 10^{-20}$ J. Furthermore, the background free oscillations of the Earth range from 2 to 7 mHz (Nishida et al., 2000), and when the peak-to-peak amplitudes are applied to the human brain to obtain force, and this force is applied across the neuronal membrane, the associated energy value is also within the range of $\sim 10^{-20}$ J. Given these overlapping ranges of energy and that a duration of approximately 2-3 minutes strongly overlaps with the periodicity of Earth oscillations, it was hypothesized that the 2-3 minute period of REG experimentation would

be an integral component for identifying potential physical factors associated with 3C. The most obvious potential sources of gravity which might contribute to this phenomenon included the actual weight of each participant, as well as the moon itself. This latter aspect was derived through further dimensional analysis which show that the lunar gravitational effect on a cell mass applied across the width of a typical cell is also ~10^{-20} J. Even more intriguing, when variations of lunar distance associated with apogee and perigee were accounted for, the gravitational energy on a typical cell during the time when the moon is closest to the Earth (perigee) was $2.01 \cdot 10^{-20}$ J, which is the associated energy value which most closely overlaps with that of the neuronal action potential. It was therefore hypothesized that perigee would be the optimal measure associated with REG performance.

After analyzing minute averages of REG data it was determined that the average score during minute 2 of testing was strongly associated with the number of days since lunar perigee. Although this appeared to confirm initial hypotheses regarding the 2-3 minute period of testing and lunar distance associated with perigee, further analysis showed that this relationship was enhanced when controlling for the variability associated with individual participant weight. This finding seems to support the previous contention that participant mass (as a function of absolute weight) may provide another source of gravitational contribution to the 3C phenomenon. The fact that the second minute of testing also appeared to be the most significantly associated with the final REG outcome suggests that the relationship between temporally varying gravitational sources may partially account for previously unsuccessful experiments examining 3C. Finally, these results may also implicate a form of 'resonance' between the cerebral volume and geophysical parameters which could be involved in successful 3C performance. The fact that specific patterned transcerebral EMF application also appeared to enhance this process may

further suggest that electromagnetic and gravitational energies could be coordinated within cerebral space during this phenomenon.

The temporal unit of 2 minutes into REG testing was again identified as a significant correlate of 3C performance through examination of cerebral biophoton emission (BPE) during an intention task (Chapter 3). Participant BPE significantly differed between three clusters of REG scores (negative and positive deviations, and baseline output) suggesting that photons emitted during cognitive intention are most likely to influence subsequent REG activity during this previously identified timeframe. However, further analyses at the level of individual REG events also suggested that individual temporal units (seconds) of BPE may influence specific ranges of REG output at a smaller time scale. These results seem to support the initial theory that human photon emissions may be related to 3C interactions. This is not entirely surprising given the previous associations observed between electromagnetic forces and REG processes, and the simple fact that photons are essentially the quanta of electromagnetic radiation. Again, previous studies have shown that cerebral BPE may be related to alternate psi processes other than 3C (Hunter et al., 2010). Therefore, this may suggest that *outgoing* psi phenomena (e.g., 3C) may operate in a manner similar to *incoming* psi (e.g., remote viewing).

When further examined within the frequency domain, additional relationships between participant BPE and REG output were obtained. The cross-spectral amplitudes (extreme differences) of photomultiplier tube (PMT) and REG data indicated a significant relationship with overall REG output within a narrow frequency range of 28 mHz. Interestingly, this periodicity is within the range of infraslow electrical potentials in the human brain (Aladjalova, 1964) and may further implicate neuronal functioning in successful 3C. Furthermore, the cross-spectral coherence (covariance) of PMT and REG measures were significantly related to the

overall complexity (entropy) of REG data within the 6 mHz frequency, which is within range of the Earth's background free oscillations (Nishida et al., 2000). Again, this may further validate previous experiments which suggest a form of resonance or overlapping energy bands associated with the Earth itself could be involved in the process of 3C.

Given the reliable associations previously demonstrated between both solar and geomagnetic activity (Richardson et al., 2001), and neurophysiological functioning (Saroka et al., 2014), it was initially hypothesized that various measures of solar activity would be correlated with REG output during periods of human intention (Chapter 5). This should be particularly likely given the relationships observed between space weather and geophysical energies with psi interactions in previous research (Radin, 1993) and the current experiments.

Subsequent analyses confirmed these hypotheses by revealing significant relationships between overall measures of solar activity (e.g., sunspot numbers and solar radio flux) and output of a REG device during participant intention. Furthermore, it was found that these solar measures also significantly differed between days where participants successfully obtained a significant REG deviation and those who did not. It is likely that these apparent differences in 3C performance were simply associated with variations in neuroelectrical activity mediated by solar and subsequent geophysical energies. However, there is also the slight potential that the level of photons emitted by the sun was greater on certain days which could have influenced the REG device in a minute manner. This idea has potential given the previous associations found between ultraweak BPE from participants' heads and REG results.

As noted before, the fact that REG output resulted in deviations either intended for or opposite of intention, and that this relationship (with or against intention) was correlated with overall solar

activity, this could also help explain the phenomenon of 'psi-missing' in which some participants may achieve statistically significant results that are opposite of those which would normally be expected. The earlier hypothesis regarding the 2 minute period of REG testing was again identified as a significant factor. Minute averages of REG event scores were found to be significantly correlated with activity of the interplanetary magnetic field (IMF) produced by the sun only during minute 2 of testing. Aside from further supporting the hypothesis of the 2 minute period, this also suggests an interesting involvement of some form of valence; if the IMF activity was associated with extreme deviations of REG output regardless of bit direction (0 or 1, up or down) then we would expect a 'V' shaped line of best fit. However, the linear relationship currently observed suggests that heliospheric electromagnetic activity may be associated with the direction of REG device electron tunneling behavior, which could in turn influence the results obtained within the context of the 3C anomaly. Finally, the association observed between successful 3C performance and the equation of time (difference between mean and apparent solar time) may again provide an explanation for the occurrence of unsuccessful psi results in some studies (e.g., Jahn et al., 2000) by implicating some form of annual variation associated with significant REG deviations that are correlated with human intention. Specifically, when the equation of time is slow (negative values) participants are typically unsuccessful in achieving significant REG scores. Conversely, an increased value for the equation of time (positive values) was associated with REG deviations which were significant at $p \leq .025$.

While previous research has been relatively ambiguous in determining a potential relationship between actual geomagnetic activity and 3C interactions (e.g., Gissurarson, 1992), the current study had the drawback of too few participants tested during periods of geomagnetic storm-level activity. Having an available method for the accurate prediction of geomagnetic activity (and

other space weather) would be ideal for scheduling this type of experiment and many others. To that end, statistical investigation of disturbance storm time (DST) indices and solar activity was undertaken in order to determine to what degree the prediction of geomagnetic activity could be enhanced using novel computational methodologies compared to more traditional statistical approaches.

Subsequent results (Chapter 6) identified significantly improved predictive performance for three variations of artificial neural network (ANN) models compared to linear regressions (two variable entry methods examined). Furthermore, an ANN employing the Bayesian regularization learning algorithm was shown to be the most accurate model in the analysis. Given these results, and the ability for nonlinear autoregressive (NAR and NARX) networks to easily predict a step ahead of the available data without further detailed analyses, this provides an exciting possibility for the future prediction of geomagnetic activity, which could in turn be used to better schedule particular psi protocols.

Although the previous research regarding the effect of gender on 3C performance has been relatively limited (Dunne, 1998), the often conflicting or overly-specific results have seemingly failed to rationalize the reason for these potential differences. The finding (Chapter 5) that the overall complexity (entropy) of REG data significantly differed between males and females has a potential basis in neurophysiology, particularly when considering the striking similarity of the female:male ratio between complexity of both REG and EEG data, which were 1.04 and 1.02 respectively (Ahmadi et al., 2013), with females showing greater complexity for both measures.

Further biological implications are potentially revealed through analysis of male-female differences in overall REG score when covarying for lunar distance (both apogee and perigee).

Because the reproductive cycle has been related to the lunar cycle (Zimecki, 2006), it may be that individual hormone functioning could be involved in the process of 3C. As a result, males tended to produce significantly more negative REG results, while females typically produced positive results.

One of the more counterintuitive findings of the current research was strictly qualitative in nature. Following testing, participants typically described their subjective mental state during each session of testing. It was subsequently found that a vast majority of participants in all studies had apparently been 'trying less' or 'forcing' their intention less during sessions where the greatest REG deviations were obtained. Some theorists have previously examined the potential role of the 'intensity' of participant intention during a 3C task and the possible effects of reduced or enhanced intensity (Moddel, 2006). Given the qualitative observation in the current research, it is suggested that the 3C phenomenon using REG hardware devices may perform according to the relationship of effect size = p / i_i, where p = probability of occurrence, and i_i = intensity of intention. As an example, a participant with relatively reduced i_i (5) would be better capable of achieving a significant REG result than those with an increased i_i (10), assuming a 50% chance probability (e.g., 0.5/5 = 0.1 or 0.5/10 = 0.05 respectively).

Taken as an aggregate, the preceding experiments strongly implicate some form of resonance or overlapping environmental sources of minute energies with cerebral functioning and subsequent 3C performance. Specifically, the 2 minute period itself appears to be the most strongly affected component of REG output in the context of a 3C experiment. Furthermore, a number of results strongly suggest an important role of electromagnetic forces in affecting this phenomenon. This particular aspect could be used in the future to further enhance the process of 3C interactions in order to better exploit this currently anomalous phenomenon for the eventual development of

novel technologies. The relationships identified between neuronal activity and that of related gravitational sources, along with the subsequent output of a REG device, not only provides an additional mechanistic candidate or correlated factor in 3C processes, but also may partially explain the occurrence of unsuccessful psi experiments. To further this statement, the fact that 3C performance appears to vary with both solar activity and solar time lends additional support to the contention that environmental factors may account for various psi results to some degree, including the phenomenon of 'psi-hitting' and 'psi-missing'. Aside from the more obvious real-world applications which could result from better-harnessing this process, these results may also inform theorists about the nature of consciousness itself as a fundamental process of reality. Additionally, this may provide greater insight into new ideas in physics by better understanding the role which consciousness plays in the physical realm (e.g., Drageset, 2013).

If any number of psi experiments is indeed correct in their interpretation, this area also has a range of potential implications for human development itself; to what degree does 'information at a distance' influence either physical or cognitive development? How does the human brain integrate non-local information during developmental processes? How are some individuals more capable of developing these 'psi' skills compared to others? These are important questions which should be addressed in future research. By better understanding the biophysical nature of anomalous interactions correlated with consciousness, we may also be able to enhance our appreciation and application of various forms of complementary and alternative medicine (e.g., Braud, 1994). By furthering our knowledge of how these apparently non-local processes occur, we may be able to enhance the delivery and efficacy of various forms of alternative healthcare practices within the framework of non-local consciousness effects.

7.2 References

Ahmadi, K., Ahmadlou, M., Rezazade, M., Azad-Marzabadi, E., & Sajedi, F. (2013). Brain activity of women is more fractal than men. *Neuroscience Letters, 535*, 7-11.

Aladjalova, N. A. (1964). Slow electrical processes in the brain. *Progress in Brain Research, 7*, 1-238.

Braud, W. (1994). Empirical explorations of prayer, distant healing, and remote mental influence. *Journal of Religion and Psychical Research, 17.2*, 62-73.

Cook, C. M., & Persinger, M. A. (1997). Experimental induction of the 'sensed presence' in normal subjects and an exceptional subject. *Perceptual and Motor Skills, 85*, 683-693.

Dotta, B. T., Karbowski, L. M., Murugan, N. J., & Persinger, M. A. (2013). Incremental shifts in pH spring water can be stored as “space-memory”: Encoding and retrieval through the application of the same rotating magnetic field. *NeuroQuantology*, *11*(4), 511-518.

Drageset, O. (2013). How physics could explain the mind. *Physics Essays, 26*(1), 7-14.

Dunne, B. J. (1998). Gender differences in human/machine anomalies. *Journal of Scientific Exploration, 12*(1), 3-55.

Gissurarson, L. R. (1992). The psychokinesis effect: Geomagnetic influence, age and sex differences. *Journal of Scientific Exploration, 6*(2), 157-165.

Hunter, M. D., Mulligan, B. P., Dotta, B. T., Saroka, K. S., Lavallee, C. F., Koren, S. A., &

Persinger, M. A. (2010). Cerebral dynamics and discrete energy changes in the personal environment during intuitive-like states and perceptions. *Journal of Consciousness Exploration & Research, 1*(9), 1179-1197.

Jahn, R. G., Dunne, B. J., Nelson, R. D., Dobyns, Y. H., & Bradish, G. J. (1997). Correlations of random binary sequences with pre-stated operator intention: A review of a 12-year program. *Journal of Scientific Exploration, 11*(3), 345-367.

Jahn, R., Dunne, B., Bradish, G., Dobyns, Y., Lettieri, A., Nelson, R., Mischo, J., Boller, E., Bosch, H., Vaitl, D., Houtkooper, J., & Walter, B. (2000). Mind/machine interaction consortium: PortREG replication experiments. *Journal of Scientific Exploration, 14*(4), 499-555.

Miller, I. (2012). A transdisciplinary look at paranthropology: An emerging field of exploration. *Journal of Consciousness Exploration & Research, 3*(8), 1018-1031.

Moddel, G. (2006). *Entropy and information transmission in causation and retrocausation*. In D. Sheehan (Ed.), Frontiers of Time, Retrocausation: Experiment and Theory (pp. 62-74). Melville, NY: American Institute of Physics.

Nishida, K., Kobayashi, N., & Fukao, Y. (2000). Resonant oscillations between the solid Earth and the atmosphere. *Science, 287*(5461), 2244-2246.

Persinger, M. A. (2010). 10^{-20} joules as a neuromolecular quantum in medicinal chemistry: An alternative approach to myriad molecular pathways. *Current Medicinal Chemistry, 17*(27), 3094-3098.

Persinger, M. A., & Dotta, B. T. (2011). Temporal patterns of photon emissions can be stored and retrieved several days later from the "same space": Experimental and quantitative evidence. *NeuroQuantology, 9*(4), 605-613.

Persinger, M. A., & Saroka, K. S. (2012). Protracted parahippocampal activity associated with Sean Harribance. *International Journal of Yoga, 5*, 145-150.

Persinger, M. A., Corradini, P. L., Clement, A. L., Keaney, C. C., MacDonald, M. L., Meltz, L. I., Murugan, N. J., Poirier, M. R., Punkkinen, K. A., Rossini, M. C., & Thompson, S. E. (2010). Neurotheology and its convergence with neuroquantology. *NeuroQuantology, 8*(4), 432-443.

Radin, D. I. (1993). Environmental modulation and statistical equilibrium in mind-matter interaction. *Subtle Energies, 4*(1), 1-30.

Richardson, I. G., Cliver, E. W., & Cane, H. V. (2001). Sources of geomagnetic storms for solar minimum and maximum conditions during 1972-2000. *Geophysical Research Letters, 28*(13), 2569-2572.

Rock, A. J., & Storm, L. (2010). Shamanic-like journeying and psi: II. Mental boundaries, phenomenology, and the picture-identification task. *Australian Journal of Parapsychology, 10*(1), 41-68.

Saroka, K. S., Caswell, J. M., Lapointe, A., & Persinger, M. A. (2014). Greater electroencephalographic coherence between left and right temporal lobe structures during increased geomagnetic activity. *Neuroscience Letters*, in press.

Zimecki, M. (2006). The lunar cycle: Effects on human and animal behavior and physiology. *Postępy Higieny i Medycyny Doświadczalnej, 60*, 1-7.